

# CONFORMAL MAPPING IN LINEAR TIME

CHRISTOPHER J. BISHOP

ABSTRACT. Given any  $\epsilon > 0$  and any planar region  $\Omega$  bounded by a simple  $n$ -gon  $P$  we construct a  $(1 + \epsilon)$ -quasiconformal map between  $\Omega$  and the unit disk in time  $C(\epsilon)n$ . One can take  $C(\epsilon) = C + C \log \frac{1}{\epsilon} \log \log \frac{1}{\epsilon}$ .

---

*Date:* August 13, 2009.

*1991 Mathematics Subject Classification.* Primary: 30C35, Secondary: 30C85, 30C62 .

*Key words and phrases.* numerical conformal mappings, Schwarz-Christoffel formula, hyperbolic 3-manifolds, Sullivan's theorem, convex hulls, quasiconformal mappings, quasisymmetric mappings, medial axis, CRDT algorithm.

The author is partially supported by NSF Grant DMS 04-05578.

## 1. INTRODUCTION

If  $\Omega$  is a proper, simply connected plane domain, then by the Riemann mapping theorem there is a conformal map  $f : \mathbb{D} \rightarrow \Omega$ , but for most domains there is no simple, explicit formula. In this paper we will show that there is “almost” such a formula in the sense that there is a linear time algorithm for computing the conformal map with estimates on time and accuracy that are independent of the geometry of the particular domain. Thus the computational complexity of conformal mapping is linear in the following sense.

**Theorem 1.** *Given a simply connected domain  $\Omega$  bounded by an  $n$ -gon we can compute the conformal map  $f : \mathbb{D} \rightarrow \Omega$  to within quasiconformal error  $\epsilon$  in time  $O(n \cdot p \log p)$  where  $p = O(\log \frac{1}{\epsilon})$ .*

The phrases “can compute” and “quasiconformal error” require some explanation in order to make this a precise mathematical statement. A unit of work consists of an infinite precision arithmetic operation or an evaluation of  $\exp$  or  $\log$ . We will cover the unit disk by  $O(n)$  regions (disks and annuli) and in each region approximate the conformal map using a  $p$ -term power or Laurent series and some elementary functions. Combining these using a partition of unity will give a  $(1+\epsilon)$ -quasiconformal map from  $\mathbb{D}$  to  $\Omega$ . Our series converge geometrically fast on the associated regions, and so each series has  $p \sim \log \frac{1}{\epsilon}$  terms in general. The fastest known methods for multiplication, division, composition or inversion of power series use the fast Fourier transform, and the time to perform an FFT on a  $p$ -term power series is  $\text{FFT}(p) = O(p \log p)$ , so Theorem 1 says we only need  $O(1)$  such operations per vertex.

The Schwarz-Christoffel formula (see Appendix A) provides a formula for the conformal map onto a polygon, but involves unknown parameters (the conformal preimages of the vertices). Thus, it is not really a solution of the mapping problem, but simply reduces it to finding the  $n$  conformal prevertices. Suppose  $\Omega$  is bounded by a simple  $n$ -gon with vertices  $\mathbf{v} = \{v_1, \dots, v_n\}$ , let  $f : \mathbb{D} \rightarrow \Omega$  be conformal and let  $\mathbf{z} = f^{-1}(\mathbf{v})$  be the conformal prevertices. A more concrete version of Theorem 1 is:

**Theorem 2.** *Given any  $\epsilon > 0$  there is a  $C = C(\epsilon) < \infty$  so that if  $\Omega$  is bounded by a simply polygon  $P$  with  $n$  vertices we can find points  $\mathbf{w} = \{w_1, \dots, w_n\} \subset \mathbb{T}$  so that*

- (1) *All  $n$  points in  $\mathbf{w}$  can be computed in at most  $Cn$  steps.*

(2)  $d_{QC}(\mathbf{w}, \mathbf{z}) < \epsilon$  where  $\mathbf{z}$  are the true conformal prevertices.

Here  $d_{QC}(\mathbf{w}, \mathbf{z}) = \inf\{\log K : \exists K\text{-quasiconformal } h : \mathbb{D} \rightarrow \mathbb{D} \text{ such that } h(\mathbf{z}) = \mathbf{w}\}$ . The constant  $C(\epsilon)$  may be taken to be  $C + C \log \frac{1}{\epsilon} \cdot \log \log \frac{1}{\epsilon}$  where  $C$  is independent of  $\epsilon$  or  $n$ .

Note that  $d_{QC}(\mathbf{w}, \mathbf{z}) = 0$  iff the  $n$ -tuples are Möbius images of each other. It is not hard to see that this happens iff the corresponding polygons are linear images of each other, and so this is a natural metric for the problem. Quasiconformal approximation implies uniform approximation but is stronger; not only are the points of  $\mathbf{w}$  within  $O(\epsilon)$  of the corresponding points of  $\mathbf{z}$ , but the relative arrangement of  $\mathbf{w}$  approximates the corresponding arrangement of  $\mathbf{z}$  equally well at every scale (see Lemma 45).

We will define a quadratically convergent iteration on  $n$ -tuples in  $\mathbb{T}$  and provide a starting point from which it is guaranteed to converge with an estimate independent of the domain. Although there are various details to check, each of basic ideas involved is fairly easy to explain and involves a geometric construction. We will discuss these briefly here, leaving the details and difficult cases for the rest of the paper.

The first idea is to consider the so called “iota-map”,  $\iota : P \rightarrow \mathbb{T}$  to obtain an  $n$ -tuple  $\mathbf{w} = \iota(\mathbf{v}) \subset \mathbb{T}$  that is only a bounded  $d_{QC}$ -distance  $K$  from the true prevertices (it is known from [14] that we can take  $K \leq 7.82$ ). The definition of this map and the proof that it has the desired approximation properties are motivated by results from hyperbolic 3-dimensional geometry, but we can give a simple, geometric description in the plane. We approximate our polygon by a finite collection of medial axis disks (these are subdisks of the domain whose boundary hits the boundary of the domain in at least two points). The union of these disks,  $\Omega$ , can be written as a union of a single  $D$  disk and a collection of disjoint crescents. See Figure 1. Each crescent is foliated by circular arcs orthogonal to its two boundary arcs. Following leaves of this foliation gives the desired map  $\iota : \partial\Omega \rightarrow \partial D$ . The initial approximation by a union of disks is unnecessary, but convenient for various reasons (the  $\iota$  map for a polygon can be computed directly, using the medial axis of the polygon e.g., [17]). The construction of  $\iota$  in linear time depends on the fact that the medial axis of a  $n$ -gon can be computed in linear time, a result of Chin, Snoeyink and Wang [33].

The next idea is to decompose polygons into pieces, again following a motivation from hyperbolic geometry. A standard technique in the theory of hyperbolic manifolds

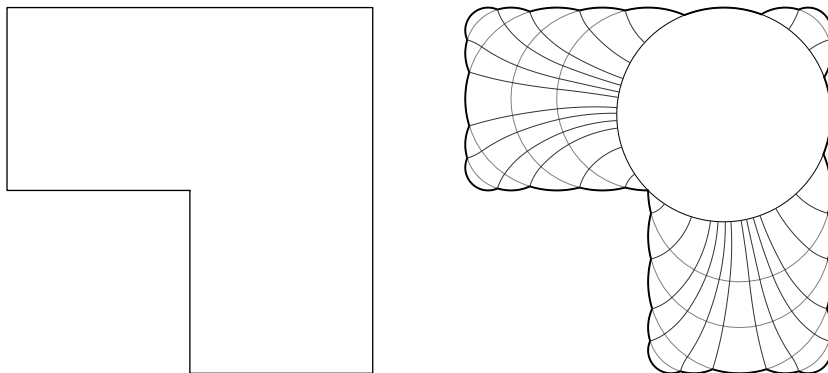


FIGURE 1. An example where we have approximated a domain by a union of disks; written the new domain  $\Omega$  as a disjoint union of one disk  $D$  and several crescents; and used circular arcs orthogonal to the crescents to define a flow from  $\partial\Omega$  to  $\partial D$ . The resulting map is close to the Riemann map with estimates independent of the domain.

is to partition the manifold into its thick and thin parts (based on the length of the shortest non-trivial loop through each point). See Figure 2. Thin parts often cause technical difficulties, but this is partially compensated for by the fact that there are only a few possible types of thin parts and each has a well understood shape. Thus we can think of the manifold as consisting of some “interesting” thick parts attached to some annoying, but explicitly described, thin parts. The manifold is considered especially nice if it is thick, i.e., no thin parts occur.

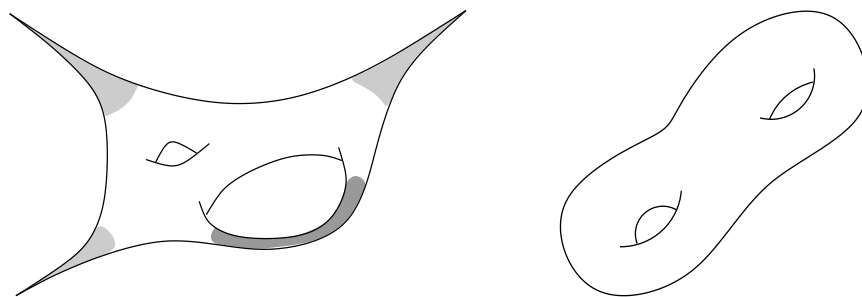


FIGURE 2. On the left is a surface with one hyperbolic thin part (darker) and three parabolic thin parts (lighter). On the right is a “thick” surface with no thin parts.

We will describe an analogous decomposition of a polygon into thick and thin parts. The thin parts occur when the extremal length between two edges is very small

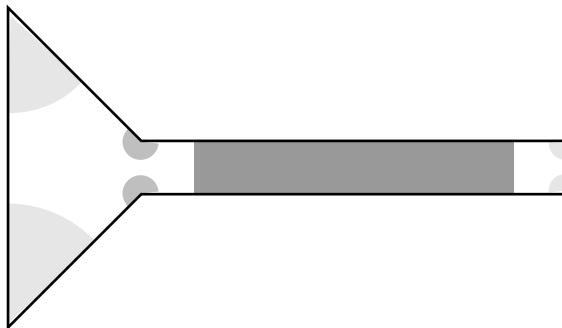


FIGURE 3. A polygon with one hyperbolic thin part (darker) and six parabolic thin parts, which we further divide into two groups corresponding to interior vertex angles  $< \pi$  and  $> \pi$ .

(roughly this means the Euclidean distance inside the domain between the edges is small compared to their Euclidean diameters). This occurs whenever the edges are adjacent, but we shall be mostly interested in thin parts corresponding to non-adjacent edges and we denote the two cases as parabolic and hyperbolic respectively, in analogy to the thin parts of a Riemann surface (in that case, parabolic thin parts are non-compact and have one boundary component attached to the thick part of the surface; hyperbolic thin parts are compact and have two boundary components, both attaching to the thick part of the surface). See Figure 3. The parabolic thin parts look like sectors, and the hyperbolic thin parts look like generalized quadrilaterals (with two sides on the boundary of the given polygon). We say the polygon is thick if no hyperbolic thin parts occur. See Figure 4 for various ways hyperbolic thin parts can arise.

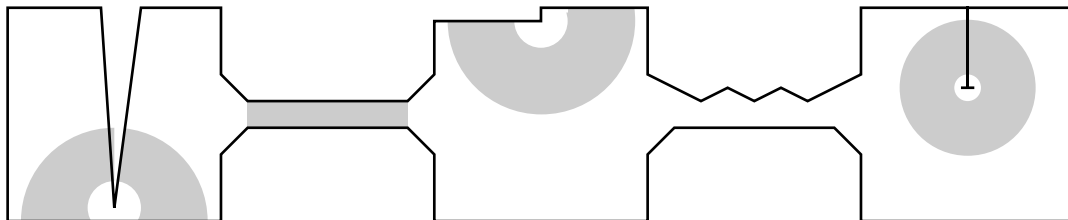


FIGURE 4. The five hyperbolic thin parts of this polygon are shaded gray. The channel on the right is not thin because there are many vertices lining one side of it. The complementary white regions are “thick”; one of our strategies is to compute mappings onto thick domains and “glue” them together across the thin connecting regions.

As with manifolds, the thin parts of polygons cause technical difficulties. However, our thin parts can only have a small number of simple shapes and the conformal maps from the disk into a thin part can be well approximated by explicit formulas. Thus they are “well understood”. Indeed, much of the algorithm described in this paper will only be applied to the remaining thick parts, making them the “interesting” part of the polygon. Thus, as with hyperbolic manifolds, polygons will be divided into interesting thick parts, attached to annoying, but well understood, thin parts.

The next idea concerns how to represent a map onto  $\Omega$ . A conformal map onto a polygon has a convergent power series on  $\mathbb{D}$ , but since  $f'$  is discontinuous at the prevertices, it converges slowly and the number of terms needed for a given accuracy depends on the geometry of the image domain. For convenience we will replace the disk by the upper half-plane  $\mathbb{H}$ , and we will represent a map  $f : \mathbb{H} \rightarrow \Omega$  by breaking  $\mathbb{H}$  into  $O(n)$  simple pieces and using a  $p$ -term power series or Laurent expansion on each piece that represents  $f$  with error  $\leq 2^{-p}$ , independent of the geometry of  $\Omega$ . The series are combined using a partition of unity to give a single quasiconformal map whose dilatation can be computed and corrected for to give an improved approximation. The decomposition  $\mathcal{W}$  of  $\mathbb{H}$  is accomplished by taking the hyperbolic convex hull of the point set  $S$  (our current prevertex approximation) and covering it by  $O(n)$  Whitney boxes, Carleson squares and regions we call arches and then dividing the remaining regions, which all lie outside the convex hull, into  $O(n)$  Carleson boxes. See Figure 5.

More precisely, an  $\epsilon$ -representation of a polygon is a triple  $(S, \mathcal{W}, \mathcal{F})$ , where  $S$  is a  $n$ -tuple in  $\mathbb{R}$  (the prevertices),  $\mathcal{W}$  is a decomposition of  $\mathbb{H}$  into  $O(n)$  simple pieces and  $\mathcal{F}$  is a collection of functions, one for each piece of our decomposition. These functions consist of  $p = O(|\log \epsilon|)$  terms of a series expansion on each piece, and a choice of a certain elementary function for each piece, which is the identity or a power function in most cases. Moreover, we require that functions for adjacent pieces agree to within  $\epsilon$  (in a certain metric) along the common boundary.

We will prove a Newton type iteration for improving  $\epsilon$ -representations. We will show that there is an absolute constant  $\epsilon_0 > 0$  (independent of  $n$  and  $\Omega$ ) so that if  $\epsilon < \epsilon_0$ , then we can quickly improve a  $\epsilon$ -representation to a  $\epsilon^2$ -representation. Thus starting with a  $n$ -tuple at distance  $\epsilon_0$  from the true answer, it only takes  $O(\log \log \frac{1}{\epsilon})$

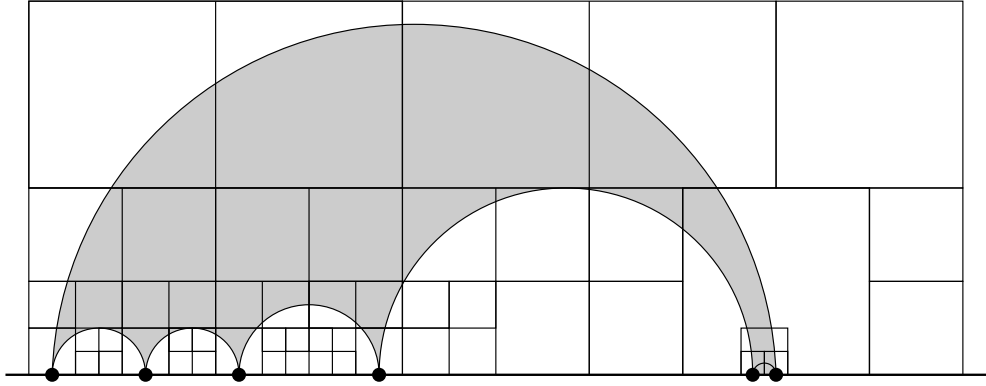


FIGURE 5. Decompose the plane by first covering the convex hull of the prevertices. This picture has one arch on the right hand side. Arches correspond to clusters of two or more prevertices which are isolated in a precise way.

iterations to reach accuracy  $\epsilon$ . The main problem is to estimate the time needed to perform each iteration.

Combining the functions in  $\mathcal{F}$  with a piecewise polynomial partition of unity gives a  $(1 + \epsilon)$ -quasiconformal map from  $F : \mathbb{H} \rightarrow \Omega$ . Let  $\mu = \bar{\partial}F/\partial F$  be the Beltrami dilatation of  $F$ . Then  $\|\mu\|_\infty = O(\epsilon)$  and  $\mu$  can be explicitly computed from the series expansions in  $\mathcal{F}$  and the partition of unity. If we could solve a Beltrami equation to find a mapping  $H$  of the upper half-plane to itself so that  $\mu_H = \mu_F$ , then  $F \circ H^{-1}$  would be the desired conformal map. We can't solve this equation exactly in finite time, but we can solve  $\mu_H = \mu_F + O(\|\mu_F\|_\infty^2)$  in linear time using the fast multipole method of Greengard and Rokhlin. Thus  $F \circ H^{-1}$  will be  $(1 + O(\epsilon^2))$ -quasiconformal, and this is the improved representation. Each iteration consists of approximately solving an equation  $\bar{\partial}H = \mu$  by evaluating  $p = O(\log \frac{1}{\epsilon})$  terms of the power series of a Beurling transform of  $\mu$  on  $n$  disks. Using a fast multipole method and fast manipulation of power series, we can do each iteration in time  $O(np \log p) = O(n \log \frac{1}{\epsilon} \cdot \log \log \frac{1}{\epsilon})$ . Moreover, since  $p = |\log \epsilon|$  increases geometrically with each iteration, the total work is dominated by the final iteration, which gives the desired estimate.

Another basic idea of the paper deals with how to improve our initial  $n$ -tuple (provided by the  $\iota$  map) that is at most distance  $K$  from the correct answer to an  $n$ -tuple that is within the distance  $\epsilon_0$  required by the Newton type iteration. This is accomplished by connecting our domain to the unit disk by a chain of  $N + 1 = O(1/\epsilon_0)$

regions  $\mathbb{D} = \Omega_0, \dots, \Omega_N = \Omega$ . As before, it is convenient to work with a domain that is a finite union of disks (such domains are also called “finitely bent” for reasons that will be clear when we discuss the dome of a domain later).

In this case there is a “normal crescent” decomposition of  $\Omega$ . If  $\Omega = \cup D_k$  is a finite union of disks and  $\partial D_1 \cap \partial D_2 \cap \partial \Omega \neq \emptyset$ , then the corresponding crescent is the subregion of  $\Omega$  bounded by circular arcs perpendicular to  $\partial D_1$  and  $\partial D_2$  at their two intersection points. Removing every such crescent from a finitely bent domain leaves a collection of “gaps”. See Figure 6. This decomposition has a natural interpretation in terms of 3-dimensional hyperbolic geometry. Each planar domain  $\Omega$  is associated to a surface  $S$  (called the dome of  $\Omega$ ) in the upper half space that is the upper envelope of all hemispheres with base disk in  $\Omega$ . If  $\Omega$  is a finite union of disks then the dome is a finite union of geodesic faces that meet along hyperbolic geodesics called the bending lines. There is a map  $R : \Omega \rightarrow S$  (the hyperbolic nearest point projection onto  $S$ ) and the gaps in  $\Omega$  are simply the points that map to faces of  $S$  and the crescents are points that map to bending lines.

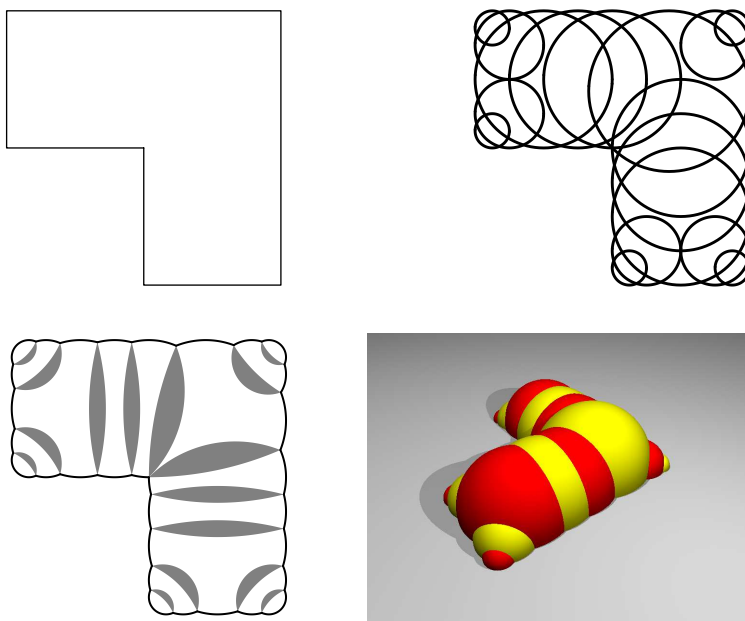


FIGURE 6. A polygon, an approximation by a finite union of disks, its normal crescent decomposition and the corresponding dome.

Given the normal crescent decomposition of the domain, we can build a one parameter family of regions by varying the angles of the crescents (this procedure is



called “angle scaling”). When the angles have all been collapsed to zero, the resulting domain is the disk. See Figure 7 for an example of such a chain. More examples are illustrated in Figures 23 to 26.

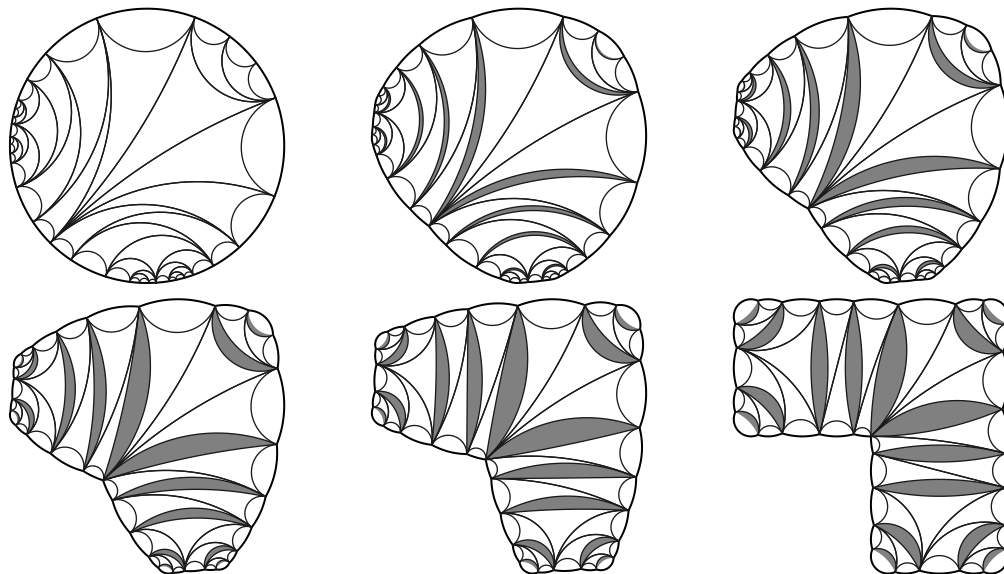


FIGURE 7. Deforming the disk to an approximate polygon. The gaps have been subdivided to make our decomposition into a hyperbolic triangulation of the disk.

We shall see that each domain in the chain is mapped to the next by an explicit map  $g_k : \Omega_k \rightarrow \Omega_{k+1}$  with small quasiconformal constant. This will allow us to convert an  $\epsilon$ -representation for one domain in our chain into a  $2\epsilon$ -representation for the next one. We can then use our improvement iteration to improve  $2\epsilon$  to  $\epsilon$  and repeat the process. In this way we can start with a representation of the disk (which is easy to find) and finish with one for  $\Omega$  (which is what we want), in a uniformly bounded number of steps.

There are (at least) two alternatives for approximating a conformal map  $f : \mathbb{D} \rightarrow \Omega$ : approximate it by conformal maps  $f_n : \mathbb{D} \rightarrow \Omega_n$  where  $\Omega_n$  converges to  $\Omega$ , or approximate by maps  $f_n : \mathbb{D} \rightarrow \Omega$  which are not conformal, but converge to the conformal map. The first approach is natural when dealing with Schwarz-Christoffel maps since a choice of parameters defines a conformal map onto a region with the right angles, but perhaps the wrong side lengths. We then adjust the parameters to

get a better approximation to the target domain. There are various heuristics for doing this that work in practice, but the relation between the parameters and the geometry of the image can be subtle and I have not seen how to prove convergence for any such method. In this paper, I take the second choice above. Information about the geometry of  $\Omega$  is built directly into our approximating functions, and our iteration merely has to force the approximation to be “more conformal”; this can be done without reference to  $\Omega$ , and hence with estimates independent of  $\Omega$ . This choice also leads naturally to the representation of these maps using power series on Whitney-Carleson decompositions to enforce the desired boundary conditions.

The  $\epsilon$ -representations used to approximate conformal maps onto polygons can also approximate maps onto other domains, as long as each boundary point has a neighborhood which is an image of a half-disk by an explicit conformal map. The algorithm is just a way of computing a global conformal map from knowing the local maps around each boundary point; we deal with polygons since the local maps are trivial. The work needed in general is  $O(N)$ , where  $N$  is the number of simple disks needed to cover the boundary (a simple disk is one so that  $2D \cap \Omega$  can be explicitly mapped to a half-disk, with the boundary going to the line segment). In the case of polygons, we can reduce  $O(N)$  to  $O(n)$  by using arches, but this requires “conformally straightening” two boundary arcs simultaneously. For polygons, we do this with 3-parameter Schwarz-Christoffel maps, but it may not be easy to do for curved boundary segments. For example, local boundary maps are also easy to find for circular arc polygons, but I don’t know how to “straighten” pairs of circular arcs (unless they happen to lie on intersecting circles). Thus the method of this paper will compute an  $(1 + \epsilon)$ -quasiconformal map onto a circular arc  $n$ -gon in time  $O(N |\log \epsilon \log \log \epsilon|)$ , but I don’t yet see how to reduce  $N$  to  $n$ . The special case of finitely bent domains (unions of disks) will be discussed later in detail, and conformal maps onto such domains will be computed as part of the proof of Theorems 1 and 2.

This paper is part of a series of papers that have studied hyperbolic geometry and its relation to conformal mappings [11], [13], [14], [17], [16]. Along the way, many people have contributed helpful comments, advice and encouragement including Rapha Coifman, Tobin Driscoll, David Epstein, John Garnett, Peter Jones, Al Marden,

Vlad Markovic, Joe Mitchell, Nick Trefethen, Jack Snoeyink and Steve Vavasis. Many thanks to them and the others who helped me reach the results described here.

Also special thanks to the referees who made a tremendous effort reading and evaluating the manuscript. Their thoughtful and extensive remarks touched on everything from typos to the overall strategy of the proof, and prompted a rewriting which simplified parts of the proof and improved the exposition. The longer the paper, the more important (and more difficult) good writing becomes, and I very much appreciate their help in making this a better paper.

## 2. SUMMARY OF THE PROOF

Now we will summarize our method for computing conformal maps. I hope that even without the precise definitions, this sketch will help motivate what follows and give a “map” for reading the rest of the paper.

Suppose  $\Omega$  is a simply connected domain with a polygonal boundary with  $n$  sides. Let  $\epsilon_0$  be the radius of convergence of our Newton-type iteration for representations (see Lemma 31). Compute the medial axis of  $\Omega$  and use it to break  $\Omega$  into  $O(n)$  thick and thin pieces (see Section 12). Fix a thick piece  $\Omega^{\text{thick}}$  and approximate it by a finitely bent region  $\Omega^{\text{fb}}$  using Lemma 26 with a “flattening map” that is  $(1 + \delta)$ -quasiconformal. Compute the corresponding bending lamination (Section 8), normal crescent decomposition (Section 5) and the chain of finitely bent angle scaling domains  $\Omega_0 = \mathbb{D}, \dots, \Omega_N = \Omega^{\text{fb}}$ . We will prove that if  $\delta$  is small enough and  $N$  is large enough (depending only on  $\epsilon_0$ ), then:

- (1) (Starting point) We can construct an  $\epsilon_0/2$  representation of  $\Omega_0 = \mathbb{D}$  (trivial).
- (2) (Composition step) Given an  $\epsilon_0/2$  representation of  $\Omega_k$  we can construct an  $\epsilon_0$  representation of  $\Omega_{k+1}$  (Lemma 29).
- (3) (Improvement step) Given an  $\epsilon_0$  representation of  $\Omega_k$  we can compute an  $\epsilon_0/2$  representation of  $\Omega_k$  (Lemma 31).
- (4) (Final conversion) Given an  $\epsilon_0/2$ -representation of  $\Omega_N = \Omega^{\text{fb}}$  we can construct a  $\epsilon_0$  representation of  $\Omega$  (Lemma 30).
- (5) (Iterate to desired accuracy) Given any  $\epsilon < \epsilon_0$  and a  $\epsilon_0$ -representation of  $\Omega$ , we can compute an  $\epsilon$ -representation of  $\Omega$  (Lemma 31).

It is important to note that in steps (1)-(4) we only compute maps to a fixed accuracy; just enough to use it as a good starting point for the map onto the next element. Thus the precise timing of these steps is unimportant, as long as it is linear in  $n$  with a constant depending only on  $\epsilon_0, \delta, N$ . All these constants will be chosen independent of  $n$  and the geometry of  $\Omega$ , so the total work to get an  $\epsilon_0$ -representation of  $\Omega$  is  $O(n)$  with an constant independent of  $n$  and  $\Omega$ .

At the final step we use Lemma 31 to iterate until we reach the desired  $\epsilon$ . By Lemma 31, the  $k$ th iteration gives accuracy  $\epsilon_0^{2^k}$  and takes time  $O(n2^k k)$  to perform (with constant depending only on the fixed number  $\epsilon_0$ ). Thus  $O(\log \frac{1}{\epsilon})$  iterations are needed to reach accuracy  $\epsilon$ . Since the time per iteration grows exponentially at each step, the total time is dominated by the final step, which is  $O(n \log \frac{1}{\epsilon} \log \log \frac{1}{\epsilon})$ .

In an earlier version of this paper, the chain of domains consisted of polygons inscribed in the angle scaling family of finitely bent domains. This was awkward, but avoided some complications of extending the idea of  $\epsilon$ -representations from polygons to finitely bent domains. This version deals with these complications, in return for a cleaner presentation of the angle scaling chain and inductive steps.

The paper divides roughly into five parts: (1) an expository introduction to the medial axis,  $\iota$ -map and angle scaling, (2) the construction of the bending lamination, the associated decomposition of  $\mathbb{H}$  and our representation of conformal maps, (3) the thick/thin decomposition of polygons and the special properties of thin polygons, (4) constructing the chain of domains connecting  $\mathbb{D}$  to  $\Omega$  and implementing the composition step on representations, and (5) our iteration for improving representations based on finding approximate solutions of the Beltrami equation by the multipole method. More precisely, the remaining sections are:

**Section 3:** We introduce the medial axis and the hyperbolic dome.

**Section 4:** We discuss Thurston's observation that the dome of a simply connected domain  $\Omega$  is isometric to the hyperbolic disk. We show how this gives a mapping  $\iota$  from  $\partial\Omega$  to  $\mathbb{T}$ .

**Section 5:** We introduce the gap/crescent decomposition of a finitely bent domain, the corresponding bending lamination on the disk and construct the angle scaling chain of domains that connects the disk to  $\Omega$ .

**Section 6:** We show that elements of the angle scaling chain are close in a uniform quasiconformal sense. This is one of the key ideas that makes the whole method work with uniform estimates.

**Section 7:** We prove a technical result used in the Section 6. We introduce the idea of piecewise Möbius maps and  $\epsilon$ -Delaunay triangulations to prove that a map which is close to Möbius transformations locally has a global approximation by a hyperbolic bi-Lipschitz function.

**Section 8:** We show the bending lamination of a finitely bent domain can be computed in linear time.

**Section 9:** We cover the bending lamination by  $O(n)$  “simple” regions.

**Section 10:** We refine this covering and extend it to a decomposition of  $\mathbb{H}$ .

**Section 11:** We define an  $\epsilon$ -representation of a polygonal domain and show such a representation corresponds to a  $1 + O(\epsilon)$ -quasiconformal map onto the domain.

**Section 12:** We define thick and thin polygons and show that any polygon with  $n$  sides can be decomposed into thick and thin pieces with a total of  $O(n)$  sides, and with certain estimates on the overlaps of the pieces. We also record some approximation results for conformal maps onto thin polygons.

**Section 13:** We show how to approximate thick polygons by finitely bent domains and define  $\epsilon$ -representations of conformal maps onto such domains. We use the approximation to define an angle scaling family.

**Section 14:** We show that if a polygon satisfies a strong form of thickness, its finitely bent approximation satisfies a weak form. We use this to show how a representation of one element of the angle scaling family can be used to construct a representation of the next element.

**Section 15:** Assuming we can approximately solve a certain Beltrami equation we show how to update a  $\epsilon$ -representation to a  $\epsilon^2$ -representation.

**Section 16:** We reduce solving the Beltrami problem to solving a  $\bar{\partial}$  problem.

**Section 17:** We show how to quickly solve the  $\bar{\partial}$ -problem by computing the Beurling transform of a function using the fast multipole method.

**Appendix A:** Background on conformal maps, hyperbolic geometry and quasiconformal mappings. Non-analysts may wish to review some of this material before reading the rest of the paper.

**Appendix B:** We review known results about power series and show that  $O(p \log p)$  suffices for all the manipulations needed by the algorithm.

### 3. DOMES AND THE MEDIAL AXIS: AN INTRODUCTION

Here we introduce two closely related geometric objects associated to any planar domain  $\Omega$ : the dome of  $\Omega$  and the medial axis of  $\Omega$ . We start with the dome.

Given a closed set  $E$  in the plane, we let  $C(E)$  denote the convex hull of  $E$  in the hyperbolic upper half-space,  $\mathbb{H}^3 = \mathbb{R}_+^3$ . This is the convex hull in  $\mathbb{H}^3$  of all the infinite hyperbolic geodesics that have both endpoints in  $E$  (recall these are exactly the circular arcs in  $\mathbb{H}^3$  that are orthogonal to  $\mathbb{R}^2 = \partial\mathbb{H}^3$ ). One really needs to take the convex hull of the geodesics ending in  $E$  and not just the union of these geodesics; for example, if  $E$  consists of three points, then there are three such geodesics and these form the “boundary” of an ideal triangle whose interior is also in the convex hull of  $E$ .

The complement of  $C(E)$  is a union of hyperbolic half-spaces. There is one component of  $\mathbb{H}^3 \setminus C(E)$  for each complementary component  $\Omega$  of  $E$  and this component is the union of hemispheres whose bases are disks in  $\Omega$  (also include half-planes and disk complements if  $\Omega$  is unbounded). For example, when  $E$  is the boundary of a square, the lower and upper boundaries of  $C(E)$  are illustrated in Figure 8.

In this paper we will focus exclusively on the case of a single, bounded, simply connected domain  $\Omega$ . In this case, the dome of  $\Omega$  is the unique boundary component of the convex set  $C(\Omega^c)$ . The dome is fairly easy to draw because of the description of  $W$  as a union of Euclidean hemispheres with bases in  $\Omega$ . Moreover,

**Lemma 3.** *Suppose  $S_\Omega$  is the dome of a simply connected, proper plane domain  $\Omega$ . Then for every  $x \in S_\Omega$  there is an open hyperbolic half-space  $H$  disjoint from  $S_\Omega$  so that  $x \in \partial H \cap S_\Omega$ . For any such half-space,  $\partial H \cap S_\Omega$  contains an infinite geodesic, and its base disk (or half-plane) has boundary that hits  $\partial\Omega$  in at least two points.*

*Proof.* Let  $W = C(\Omega^c)$  be the hyperbolic convex hull of  $\Omega^c$ , so  $S_\Omega = \partial W$ . By definition,  $W$  is the intersection of all closed half-spaces that contain it, and from

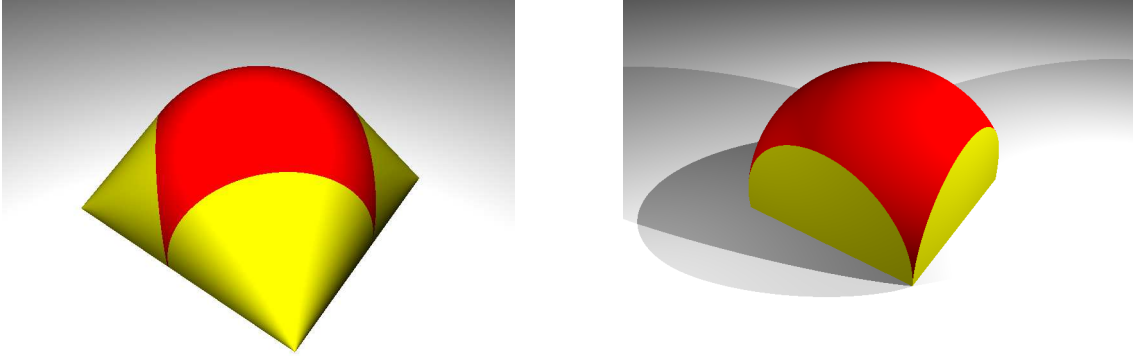


FIGURE 8. The lower and upper boundaries of the hyperbolic convex hull of the boundary of a square (left and right figures respectively). The lower boundary consists of one geodesic face (dark) and four Euclidean cones (lighter). The upper boundary has five geodesic faces (one hemisphere and four vertical). The outside of the square is a finitely bent domain, but the inside is not.

this it is easy to see that any boundary point on  $W$  is on the boundary of some closed half-space that contains  $W$ . Thus  $x$  is also on the boundary of the complementary open half-space  $H$  (which must be disjoint from  $W$ ). The base of  $H$  on  $\mathbb{R}^2$  is a half-plane or a disk and by conjugating by a Möbius transformation, if necessary, we assume it is the unit disk  $D = \mathbb{D}$  and that  $H$  contains the point  $z = (0, 0, 1) \in S_D$ . Clearly  $\partial D$  hits  $\partial\Omega$  in at least one point, for otherwise its closure would be contained in another open disk in  $\Omega$ , whose dome would be strictly higher than  $S_D$ , contradicting that  $z \in S_D \cap S_\Omega$ . In fact,  $\partial D$  must hit  $\partial\Omega$  in at least two points. For suppose it only hit at one point, say  $(1, 0) \in \mathbb{R}^2$ . Then for  $\epsilon > 0$  small enough the disk  $D(-2\epsilon, 1 + \epsilon)$  would also be in  $\Omega$  and its dome would strictly separate  $z$  from  $S_\Omega$ . Thus  $\partial D$  hits  $\partial\Omega$  in at least two points and the geodesic in  $\mathbb{R}_+^3$  between these points lies on the  $\partial H \cap S_D$ , as desired.

□

Thus each point on the dome is also on the dome of a disk in  $\Omega$  whose boundary hits  $\partial\Omega$  in at least two points. Such a disk is called a “medial axis disk” for  $\Omega$  and the set of centers of such disks is called the medial axis of  $\Omega$ , denoted  $\text{MA}(\Omega)$ . (The centers, together with the radii, is usually called the medial axis transform of  $\Omega$ ,

$\text{MAT}(\Omega)$ ). It is easy to see that the  $\Omega$  is the union of its medial axis disks, and so it is determined by  $\text{MAT}(\Omega)$ .

The dome is easiest to visualize when  $\Omega$  is a finite union of disks, e.g., see Figure 9. Such a domain will be called “finitely bent” because the dome consists of a finite union of geodesic faces (each contained on a geodesic plane in  $\mathbb{H}^3$ , i.e., a Euclidean hemisphere or vertical plane) which are joined along infinite geodesics called the bending geodesics.

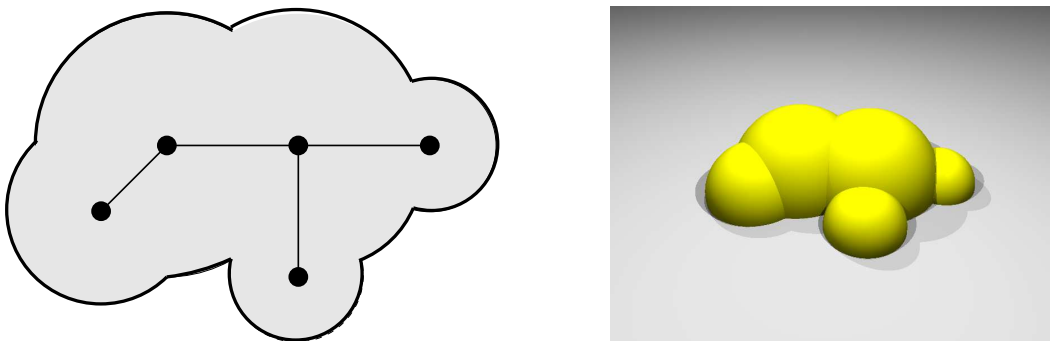


FIGURE 9. A finitely bent domain, its medial axis and its dome

When we are given a finitely bent domain  $\Omega$  we shall always assume we are given a complete list of disks in  $\Omega$  whose boundaries hit  $\partial\Omega$  in at least three points. Then every face of the dome corresponds to a hemisphere that has one of these disks as its base. This is slightly different than just giving a list of disks whose union is  $\Omega$ ; in Figure 10 we show a domain that is a union of four disks  $\Omega = D(1, 1) \cup D(i, 1) \cup D(-1, 1) \cup D(-i, 1)$  but that contains a fifth disk,  $D(0, \sqrt{2})$ , which also corresponds to a face on the dome of  $\Omega$ .

The faces of the dome of a finitely bent domain form the vertices of a finite tree, with adjacency defined by having an infinite geodesic edge in common. This induces a tree structure on the maximal disks in the base domain: disks that hit exactly two boundary points are interior points of edges of the tree and disks that hit three or more points are the vertices.

**Lemma 4.** *For any tree the number of vertices of degree three or greater is less than the number of degree one vertices.*



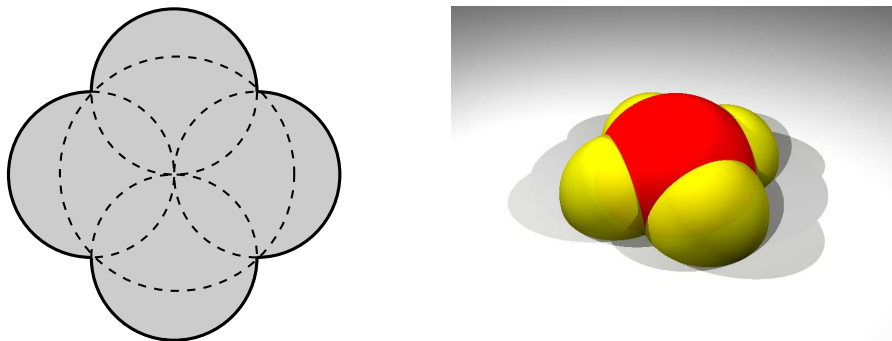


FIGURE 10. A domain that is a union of four disks, but which has five faces on the dome because of a “hidden” maximal disk.

The proof is easy and left to the reader (remove a degree one vertex and use induction). So if  $\Omega$  can be written as a union of  $n$  disks in any way, there are at most  $2n$  vertices of the medial axis.

For polygons the medial axis is also a finite tree, but now there are three types of edges: (1) edge-edge bisectors that are straight line segments equidistant from two edges, (2) point-point bisectors, which are straight line segments equidistant from two vertices, or (3) point-edge bisectors, which are parabolic arcs equidistant from a vertex and an edge. For an  $n$ -gon the medial axis has at most  $O(n)$  vertices (it is not hard to show  $2n + 3$  works).

To illustrate these ideas we show a few polygons, along with their medial axes and their domes. The dome of a polygon is naturally divided into kinds of pieces: (1) a hyperbolic geodesic face corresponding to a vertex of the medial axis of degree three or more (2) a cylinder or cone corresponding to sweeping a hemisphere along a bisector of two edges or (3) sweeping a hemisphere along the parabolic arc of a point-edge bisector. Disks corresponding to the interiors of point-point bisector edges do not contribute to the dome since the union of the two disks at the endpoints of this edge contain all the disks corresponding to the interior points.

In the dome of a convex polygon, only the first two types of pieces can occur. These are illustrated in Figure 11. The third type of medial axis arc can occur in non-convex domains, as illustrated in the polygonal “corner” in Figure 12.

The medial axis also suggests a way of approximating any domain by a finite union of disks; simply take a finite subset of the medial axis so that the corresponding union of medial axis disks is connected. The medial axis of such a union consists

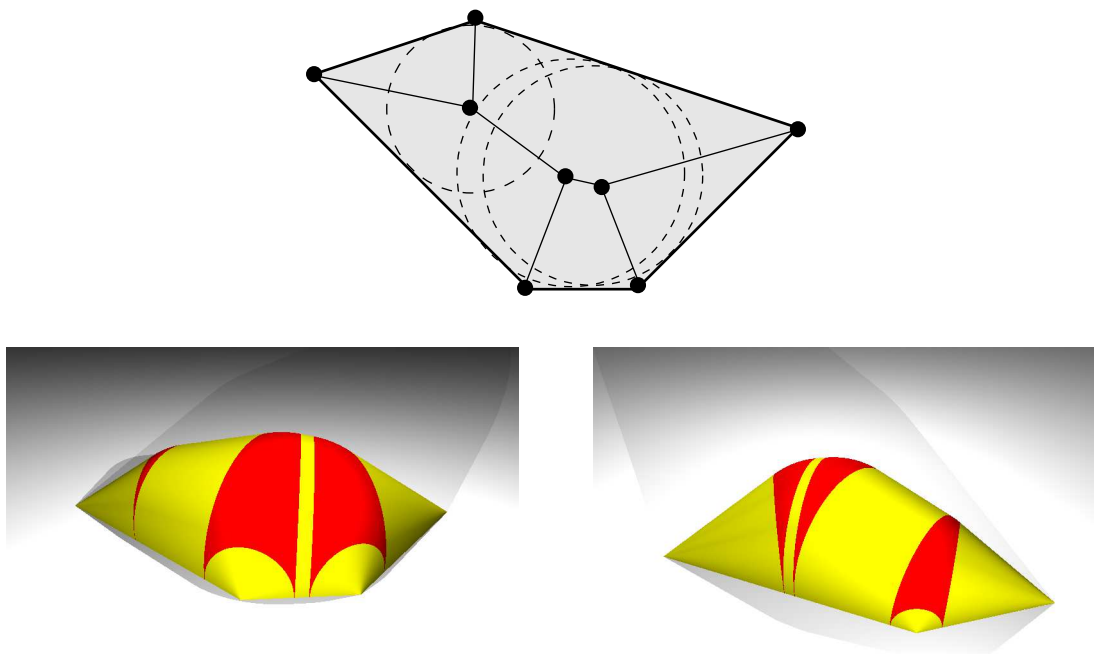


FIGURE 11. The medial axis and dome of a convex region. This dome has three geodesic faces that are shaded darker (these correspond to vertices of the medial axis); the lighter parts of the dome are Euclidean cones that correspond to edges of the medial axis. The dome is shown from two different directions

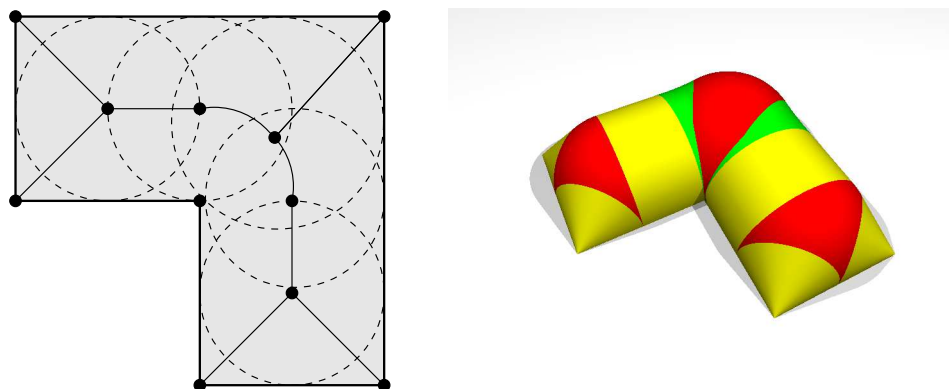


FIGURE 12. The dome of a “corner”. The darkest shading are geodesic faces (vertices of the medial axis); the lightest are Euclidean cones or cylinders (edge-edge bisectors in the medial axis). The medium shading illustrates the third type of medial axis edge that can occur: the parabolic bisector of a point and a line.

of one vertex for each geodesic face in the dome and straight lines connecting the vertices corresponding to adjacent faces. A polygon, its medial axis and a finitely bent approximation are shown in Figure 13. In Figure 14 we show the domes of the polygon and its approximation. The process of approximating a polygon by a finitely bent region will be discussed in greater detail in Section 13. Alternate approximations of polygons by disks coming from circumcircles of a triangulation of the polygon are used in [16], [49].

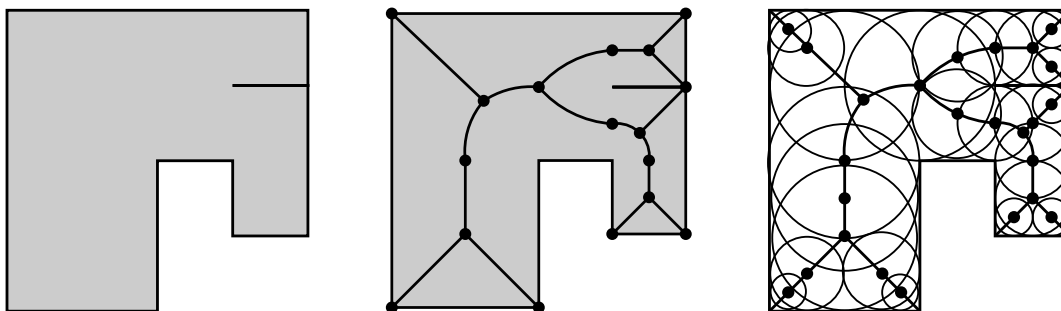


FIGURE 13. A (non-simple) polygon, its medial axis and a finitely bent approximation.

The medial axis is a fundamental concept of geometry that seems to have been rediscovered many times and goes by several names: medial axis, skeleton, symmetry set, cut locus (defined as the closure of the medial axis in [134]), equidistant set, ridge set (think of an island where the elevation is proportional to the distance to the sea), wildfire set (think of a fire started simultaneously along the boundary that burns inward at a constant rate). The earliest reference I am aware of is a 1945 paper of Erdős [57], where he proves the medial axis (he calls it “ $M_2$ ”) of a planar domain has Hausdorff dimension 1.

In some parts of the literature the medial axis is confused with the set of centers of maximal disks in  $\Omega$ , that, following [62], we will call the central set of  $\Omega$ . For polygons the two sets are the same, but in general they are not (e.g., the parabolic region  $\Omega = \{(x, y) : y > x^2\}$  contains a maximal disk that is only tangent at the origin). More dramatically, the medial axis of a planar domain always has  $\sigma$ -finite 1-dimensional measure [62], but the central set can have Hausdorff dimension 2, [15]. Some papers in the mathematical literature that deal with the medial axis include [6], [25], [50], [59], [68], [69], [80], [94], [95], [123].

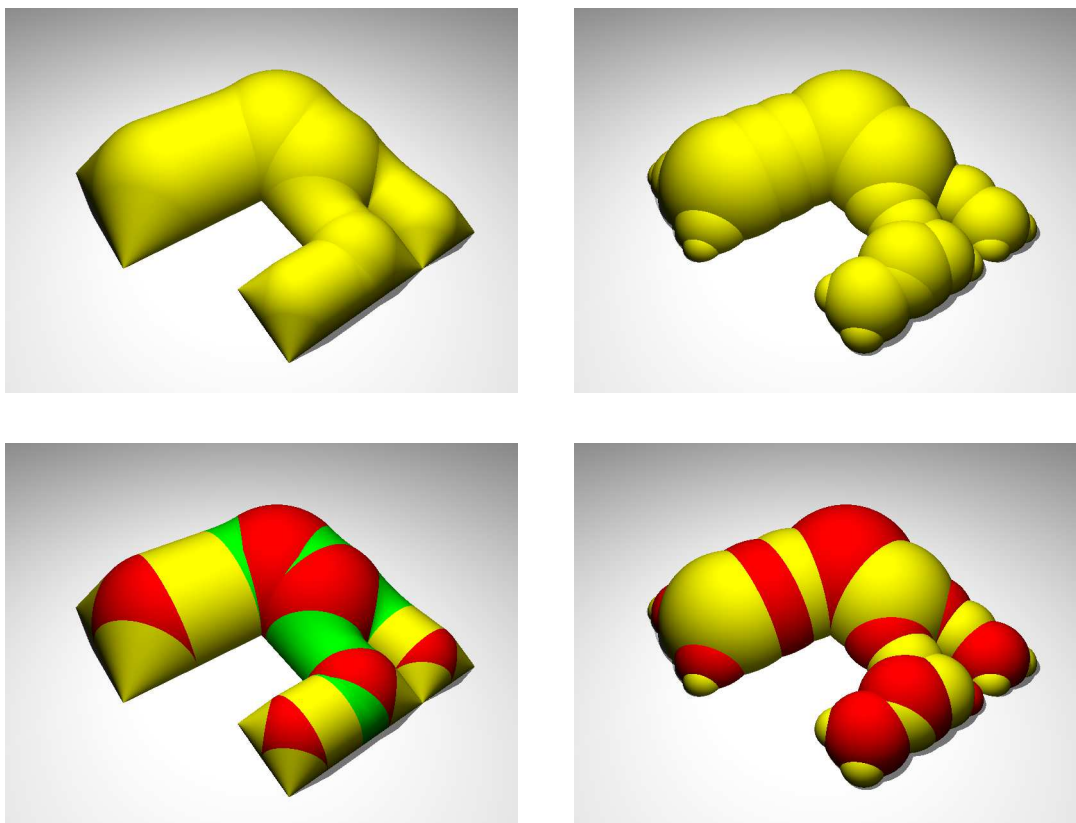


FIGURE 14. On the top left is the dome of the polygon  $P_2$  and on the top right is the dome of the finitely bent approximation  $\Omega_2$ . Below each, we have redrawn the domes, but with different sections shaded differently. For  $P_2$ , regions corresponding to different edges of the medial axis colored differently. For  $\Omega_2$  the dome is a union of geodesic faces (which form the vertices of a tree) and adjacent faces are shaded in alternating colors.

In the computer science literature the medial axis is credited to Blum who introduced it to describe biological shapes [19], [20], [21]. A few papers consider the theory of the medial axis (e.g., [34], [35], [36], [37], [114], [134]), but most deal with algorithms for computing it and with applications to areas like pattern recognition, robotic motion, control of cutting tools, sphere packing and mesh generation. A sample of such papers includes: [28], [29], [32], [41], [58], [65], [71], [77], [78], [84], [88], [89], [90], [91], [92], [102], [103], [104], [112], [113], [131], [135], [137].

Given a finite collection of disjoint sets (called sites), the corresponding Voronoi diagram divides the plane according to which site a point is closest to. The medial axis of a polygon  $P$  is a Voronoi diagram for the interior of  $P$  where the sites are the complementary arcs in  $P$  of the convex vertices (i.e., interior angle  $< \pi$ ) and distance is measured within  $P$ . Equivalently, one can compute the medial axis by taking the Voronoi diagram for the polygon with all edges and vertices as sites and then removing the cell boundaries that terminate at a concave vertex (one with angle  $\leq \pi$ ). See Figure 15. Thus the medial axis can be computed by using algorithms for computing generalized Voronoi diagrams. Voronoi diagrams were defined by Voronoi in [130], but go back at least to Dirichlet [47] (indeed, in the theory of Kleinian groups the Voronoi cells of an orbit are called Dirichlet fundamental domains). For more about Voronoi diagrams see e.g., [4], [5], [8], [60], [61], [100], [105].

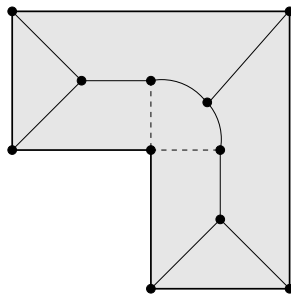


FIGURE 15. This shows the Voronoi cells when all the edges and vertices are sites. However, the dashed edges must be removed to give the medial axis.

It is a theorem of Chin, Snoeyink and Wang that the medial axis of a simple  $n$ -gon can be computed in  $O(n)$  time. I am not aware that their  $O(n)$  algorithm has been implemented, since it depends on the intricate algorithm of Chazelle that triangulates polygons in linear time. However, other asymptotically slower methods (e.g.,  $O(n \log n)$ ) have been implemented, and in practice the computation of the medial axis in  $\mathbb{R}^2$  is not considered a “bottleneck”. See [136], [137].

The basic strategy of the linear time algorithm of Chin, Snoeyink and Wang is fairly simple (although the details are not): (1) decompose the polygon into simpler polygonal pieces called monotone histograms using at most  $O(n)$  new edges, (2) compute the Voronoi diagram for each piece with work  $O(k)$  for a piece with  $k$  sides and finally (3) merge the Voronoi diagrams of the pieces using at most  $O(n)$  work.

The first step is accomplished using a celebrated result of Chazelle [30] that one can cut interior of  $P$  into trapezoids with vertical sides in linear time (this is equivalent to triangulating the polygon in linear time). Klein and Lingas [86] showed how to use Chazelle’s result to cut a polygon into “pseudo-normal histograms”; Chin, Snoeyink and Wang then show how to cut these into monotone histograms.

The next step is to show that the Voronoi diagram of a monotone histogram can be computed in linear time. The argument given in [33] follows the elegant argument of Aggarwal, Guibas, Saxe and Shor for the case of convex domains. In [1] the four authors use duality to reduce the problem to finding the three dimensional convex hull of  $n$  points whose vertical projections onto the plane are the vertices of a convex polygon.

The final step is to merge the Voronoi diagrams of all the pieces. The merge lemma used in [33] states:

**Lemma 5.** *Let  $Q$  be a polygon that is divided into two subpolygons  $Q_1$  and  $Q_2$  by a diagonal  $e$  (i.e., an line segment in  $P$  whose endpoints are vertices of  $P$ ). Let  $S_1$  be a subset sites (vertices and edges) in  $Q_1$  and  $S_2$  a subset of sites in  $Q_2$ . Given the Voronoi diagrams for  $S_1$  in  $Q_1$  and for  $S_2$  in  $Q_2$ , one can obtain the Voronoi diagram for  $S = S_1 \cup S_2$  in  $Q$  in time proportional to number of Voronoi edges for  $S_1$  and  $S_2$  that intersect  $e$  and the number of new edges that are added.*

This type of result was first used by Shamos and Hoey [111] and has been adapted by many authors since.

#### 4. THE DOME IS THE DISK

The two main results about the dome of  $\Omega$  say that (1) it is isometric to the hyperbolic disk and (2) it is “almost isometric” to the base domain  $\Omega$ . More precisely, equip the dome with the hyperbolic path metric  $\rho_S$  (shortest hyperbolic length of a path connecting two points and staying on the surface).

**Theorem 6** (Thurston, [124]). *Suppose  $\Omega$  is a simply connected plane domain (other than the whole plane or the complement of a circular arc) and let  $S$  be its dome. Then  $(S, \rho_S)$  is isometric to the hyperbolic unit disk. We will denote the isometry by  $\iota : S \rightarrow \mathbb{D}$ .*

**Theorem 7** (Sullivan [121], Epstein-Marden [52]). *Suppose  $\Omega$  is a simply connected plane domain (other than the whole plane or the complement of a circular arc). There is a  $K$ -quasiconformal map  $\sigma : \Omega \rightarrow S$  that extends continuously to the identity on the boundary ( $K$  is independent of  $\Omega$ ).*

In fact, there is a biLipschitz map between  $\Omega$  and its dome (each with their hyperbolic metric; see Theorem 49), but we will only use the quasiconformal version of the result. We place the additional restriction that  $\Omega$  is not the complement of a circular arc because in that case the convex hull of  $\partial\Omega$  is a hyperbolic half-plane and the dome should be interpreted as two copies of this half-plane joined along its edge with bending angle  $\pi$ . In order to simplify the discussion here, we simply omit this case (with the correct interpretations the results above still hold in this case; this is discussed in complete detail in Section 5 of [54]).

Explicit estimates of the constant in the Sullivan-Epstein-Marden theorem are given elsewhere in the literature. For example, it is proven in [14] that one can take  $K = 7.82$ . The estimates  $K \approx 80$  and  $K \leq 13.88$  are given in [52] and [54] respectively.

Although we will not use it here, it is worth noting that both these theorems have their origin in the theory hyperbolic of 3-manifolds. Such a manifold  $M$  is a quotient of the hyperbolic half-space,  $\mathbb{H}^3$ , by a discrete group  $G$  of isometries. The orbit of any point under this group accumulates only on the boundary of the half-space and the accumulation set (which is independent of the orbit except in trivial cases) is called the limit set  $\Lambda$ . The complement  $\Omega$  of  $\Lambda$  in the boundary of hyperbolic space is called the ordinary set. The group  $G$  acts discontinuously on  $\Omega$  and  $\partial_\infty M = \Omega/G$  is called the “boundary at infinity” of  $M$ . This is a Riemann surface (possibly with branch points). The manifold  $M$  contains closed geodesics and the closed convex hull of these is called the convex core of  $M$  and denoted  $C(M)$ . The lift of the convex core to  $\mathbb{H}^3$  is the hyperbolic convex hull of the limit set and its boundary is the dome of the ordinary set. Thus  $\partial C(M)$  is just the quotient of this dome by the group  $G$ . Theorem 6 implies that the boundary of  $C(M)$  is a surface of constant negative curvature, i.e., is isomorphic to the hyperbolic disk modulo a group of isometries. Theorem 7 says that  $\partial_\infty M$  and  $\partial C(M)$  are homeomorphic, indeed, are quasiconformal images of each

other with respect to their hyperbolic metrics. This fact was needed in the proof of Thurston’s hyperbolization theorem for 3-manifolds that fiber over the circle.

The proof of Theorem 6 for finitely bent domains simply consists of observing that if we deform the dome by bending it along a bending geodesic, we don’t change the path metric at all. Moreover, a finite number of such deformations converts a finitely bent dome into a hemisphere, and this is obviously isomorphic to the hyperbolic disk. More precisely, we are using the following simple lemma.

**Lemma 8.** *Suppose two surfaces  $S_1, S_2$  in  $\mathbb{H}^3$  are joined along a infinite hyperbolic geodesic and suppose  $\sigma$  is an elliptic Möbius transformation of  $\mathbb{H}^3$  that fixes this geodesic. Then a map to another surface that equals the identity on  $S_1$  and equals  $\sigma$  on  $S_2$  is an isometry between the path metric on  $S_1 \cup S_2$  and the path metric on the image.*

*Proof.* This becomes obvious if one normalizes so that the geodesic in question becomes a vertical line and  $\sigma$  becomes a (Euclidean) rotation around it, since it is then clear that the length of any path is left unchanged.  $\square$

Theorem 6 then follows by taking a finitely bent surface and “unbending” it one geodesic at a time, i.e., we can map it to a hemisphere by a series of maps, each of which is an isometry by the lemma. Since a hemisphere is isometric to the disk, we are done. In Figure 4 we illustrate the bending along a geodesic for a dome with two faces.

This proof gives us a geometric interpretation of the map  $\iota : \partial\Omega \rightarrow \partial\mathbb{D}$ . The disks making up a finitely bent domain have a tree structure and if  $\Omega$  is finitely bent then we fix a root disk  $D_0$  and write  $\Omega = D_0 \cup_j D_j \setminus D_j^*$ , where  $D_j^*$  denotes the parent disk of  $D_j$ . This gives  $\Omega \setminus D_0$  as a union of crescents. See Figure 17. We call these “tangential” crescents since one edge of the crescent follows  $\partial\Omega$  near each vertex (and to differentiate them from the “normal” crescents we will introduce later).

Each crescent in the tangential crescent decomposition has an “inner edge” (the one in the boundary of  $D_j^*$ ) and an “outer edge” (the other one) and there is a unique elliptic Möbius transformation that maps the outer edge to the inner one, fixing the two vertices of the crescent (this is just the restriction to the plane of the Möbius transformation of  $\mathbb{H}^3$  that removes the bending along the corresponding bending



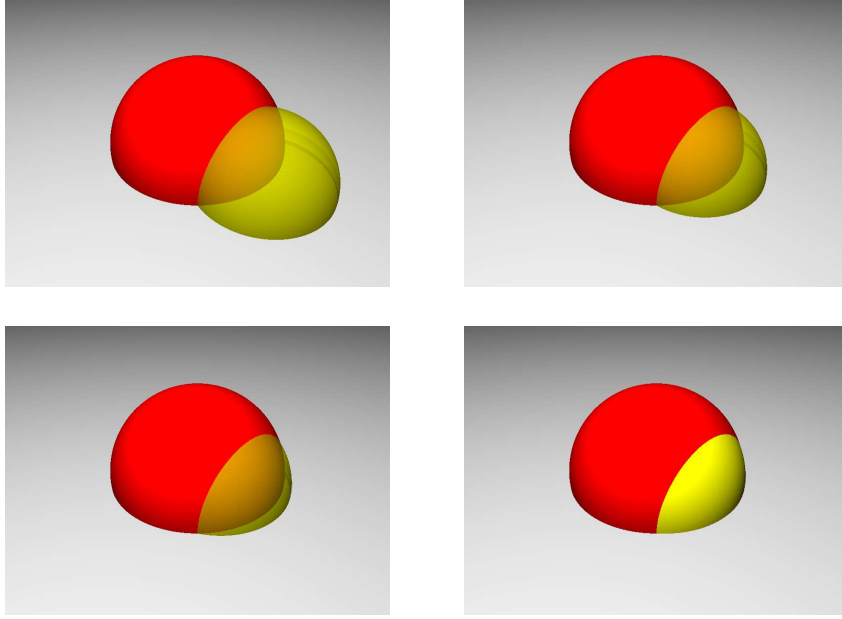


FIGURE 16. A dome consisting of two geodesic faces joined along an infinite geodesic. By bending the dome along the geodesic we get a one-parameter, isometric family of surfaces ending with a hemisphere, which is obviously isometric to the hyperbolic disk.

geodesic). The map  $\iota : \partial\Omega \rightarrow \partial\mathbb{D}$  is the composition of these maps along a path of crescents that connects an arc on  $\partial\Omega$  to an arc on  $\partial\mathbb{D}$ .

An alternate way to think of this is to foliate each crescent  $D_j \setminus D_j^*$  by circular arcs that are orthogonal to both boundary arcs. This gives a foliation of  $\Omega \setminus D_0$  by piecewise circular curves that connect  $x \in \partial\Omega$  to  $\iota(x) \in \partial\mathbb{D}$ . On the left of Figure 17 we have sketched the foliation in each of the crescents for a particular finitely bent domain (but without attempting to line up the leaves in different crescents) and on the right we have plotted the trajectories of a couple of boundary points that correspond to the vertices of the polygon we have approximated. This is the description given in the introduction. Some further examples are illustrated in Figure 18.

Theorem 7 implies that the mapping  $\iota : \partial\Omega \rightarrow \partial\mathbb{D}$  has a quasiconformal extension to a map  $\Omega \rightarrow \mathbb{D}$  that is  $K$ -quasiconformal with a bound  $K$ , independent of  $\Omega$ . Thus the geometric map we have described above is a rough approximation to the boundary values of the Riemann map. It is surprising (at least to the author) that

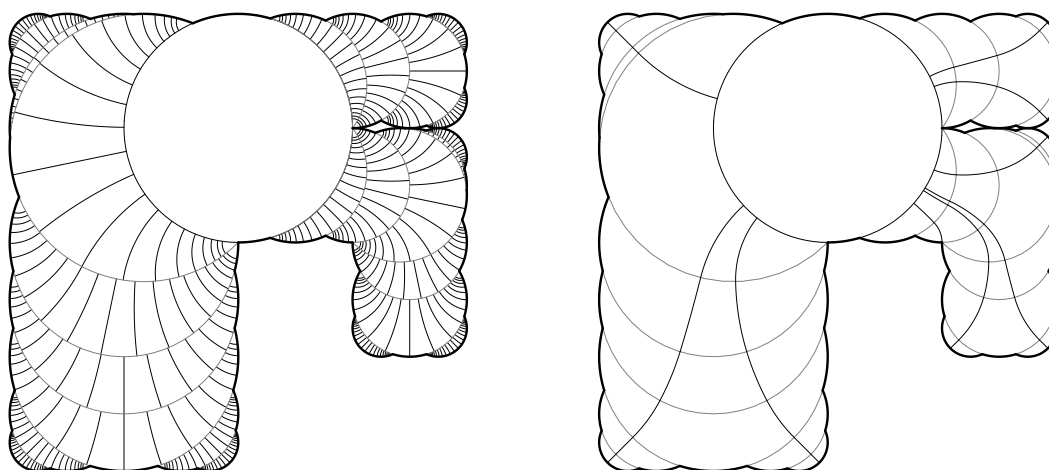


FIGURE 17. On the left is the foliation by orthogonal arcs in the tangential crescents. On the right we start at the vertices on the boundary of  $\Omega_2$  follow the corresponding trajectories of the vertices. Where these trajectories land on the circle are the  $\iota$  images of the vertices.

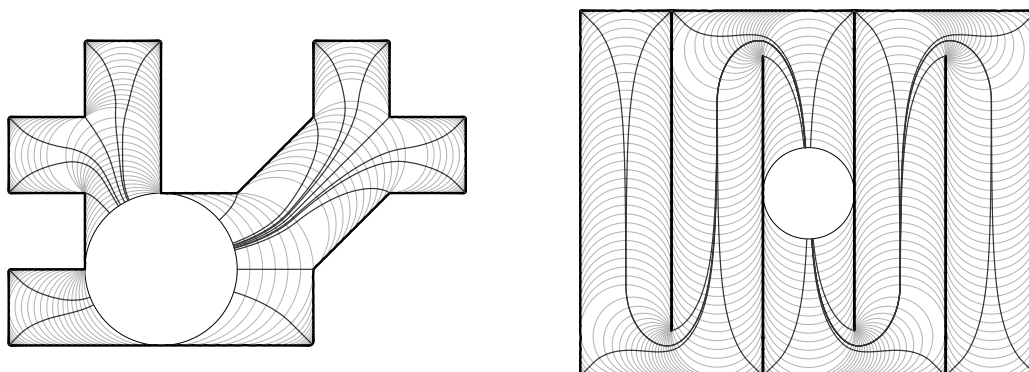


FIGURE 18. The medial axis flow for two more polygons which have been approximated by unions of medial axis disks. This flow defines the iota map from  $\partial\Omega$  to the chosen root disk of the medial axis.

there is such a simple, geometrically defined map that is close to the Riemann map with estimates independent of the domain.

## 5. THE NEAREST POINT RETRACTION AND NORMAL CRESCENTS

In the previous section we defined the map  $\iota$  and interpreted it geometrically by collapsing tangential crescents. In this section we will interpret  $\iota$  as collapsing crescents from a different decomposition of  $\Omega$  that more closely approximates the geometry of the dome.

Recall that  $S$  is the boundary of a convex set in  $\mathbb{H}^3$ , so that the nearest point retraction defines a Lipschitz map of the complement of this set onto its boundary. This map can be extended to  $\Omega \subset \partial\mathbb{H}^3 = \mathbb{R}^2$  as follows: given a point  $z \in \Omega$ , define nearest point retraction  $R : \Omega \rightarrow S$  by expanding horoball tangent at  $z \in \Omega$  until it first hits  $S$  at  $R(z)$  (a horoball in  $\mathbb{H}^3$  is a Euclidean ball tangent to the boundary). See Figure 19.

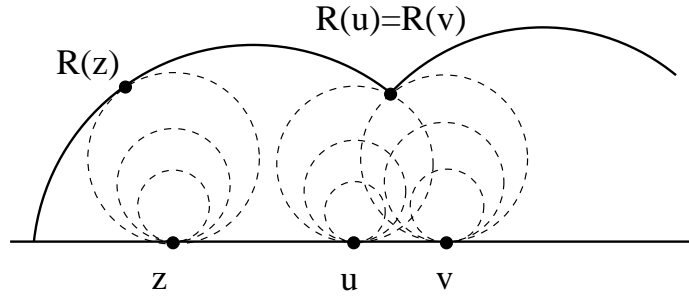


FIGURE 19. Defining the retraction map  $R : \Omega \rightarrow S$ : expand a sphere tangent at  $z$  until it touches  $S$  at  $R(z)$ . This map need not be 1-1.

Note that the map need not be 1-to-1, i.e., two points in  $\Omega$  can map to the same point on the dome. Thus it can't always be quasiconformal or even be a homeomorphism. However, it is always a quasi-isometry with bounds independent of  $\Omega$  and this implies that there is a quasiconformal map from  $\Omega$  to its dome with the same boundary values by Theorem 49. This implies Theorem 7, e.g., see [11]. Moreover,  $R$  is quasiconformal in some special cases; e.g., Epstein, Marden and Markovic prove in [55] that for Euclidean convex domains the retraction map is 2-quasiconformal.

This map is called the nearest point retraction because it is the continuous extension to the boundary of the map in  $\mathbb{H}^3$  that sends a point to the nearest point of  $S$  in the hyperbolic metric,  $\rho_{\mathbb{H}^3}$ . See Appendix A for the definition of the hyperbolic metric on  $\mathbb{D}$  and  $\mathbb{H}^3$ . The surface  $S$  has an important related metric,  $\rho_S$ . This is the hyperbolic path metric on  $S$  defined by taking the shortest hyperbolic length of all

paths that connect two points and stay on  $S$ . Clearly  $\rho_{\mathbb{H}^3}|_S \leq \rho_S$ . The base domain of  $\Omega$  has its own hyperbolic metric,  $\rho_\Omega$ , obtained by transporting the hyperbolic metric on  $\mathbb{D}$  by any conformal map.

The nearest retraction map  $R$  is  $C$ -Lipschitz from  $\rho_\Omega$  to  $\rho_S$  for some  $C < \infty$  (e.g., see [14]). It is easy to prove this for some  $C$ ; the sharp estimate of  $C = 2$  is given in [53] and earlier results are given in [24], [26], [52].

Now suppose  $\Omega$  is a finitely bent domain. Then the dome  $S$  of  $\Omega$  is a finite union of geodesic faces. On the interior of each face the retraction map has a well defined inverse and the images of the faces under  $R^{-1}$  are called the “gaps”. The inverse images of the bending geodesics are crescents that separate the gaps. These are called “normal crescents” since their two boundary arcs are perpendicular to the two arcs of  $\partial\Omega$  that meet at the common vertex. Therefore, we will call this decomposition of  $\Omega$  the “normal crescent decomposition”. Refer back to Figure 6; that picture shows a polygon, a finitely bent approximation, the normal crescent decomposition and the dome. See Figure 20 for more examples of gap/crescent decompositions.

If a gap  $G$  corresponds to a face  $F \subset S$  then  $G \subset D$ , the disk in  $\Omega$  that is the base of the hyperplane containing the face  $F$ . We will call  $D$  the “base disk” of  $G$ . Moreover,  $G$  is the hyperbolic convex hull in  $D$  of the set where  $F$  meets  $\partial\Omega$ . The angle of a normal crescent  $C$  is the same as the angle made by the faces of the dome that meet at the corresponding bending geodesic.  $C$  is foliated by circular arcs that are orthogonal to both boundary arcs and each of these arcs is collapsed to single point by  $R$ . Thus for a finitely bent domain  $\Omega$ ,  $R$  will never be a homeomorphism (unless  $\Omega$  is a disk).

The two vertices of each normal crescent are also the vertices of a crescent in the tangential crescent decomposition of  $\Omega$ . Moreover, corresponding crescents from the two decompositions have the same angle, and hence are simply images of each other by a  $\pi/2$  elliptic rotation around the two common vertices. See Figure 21. Collapsing the two types of crescents simply gives the two different continuous extensions to the interior of the same map on the boundary (namely  $\iota$ ).

Both decompositions cut  $\Omega$  into a “disk” and a union of crescents. In the tangential decomposition, it is a single connected disk, but in the normal decomposition the disk itself is broken into pieces called the gaps. The map  $\varphi = \iota \circ R : \Omega \rightarrow S \rightarrow \mathbb{D}$  is Möbius

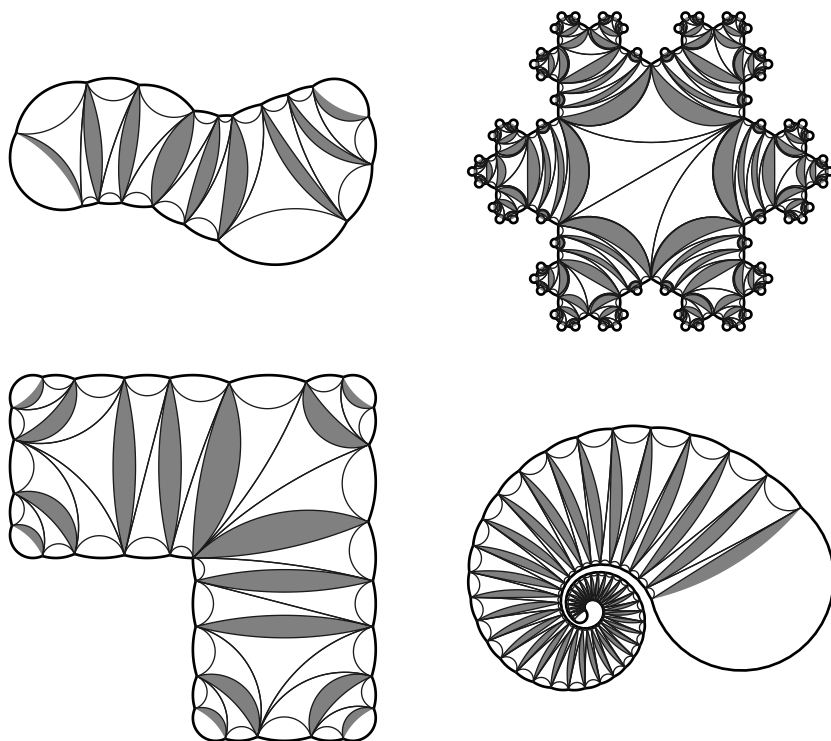


FIGURE 20. Normal crescent decompositions for some finitely bent domains. Also drawn are arcs triangulating the gaps. These are added to make the bending lamination complete (see Section 8).

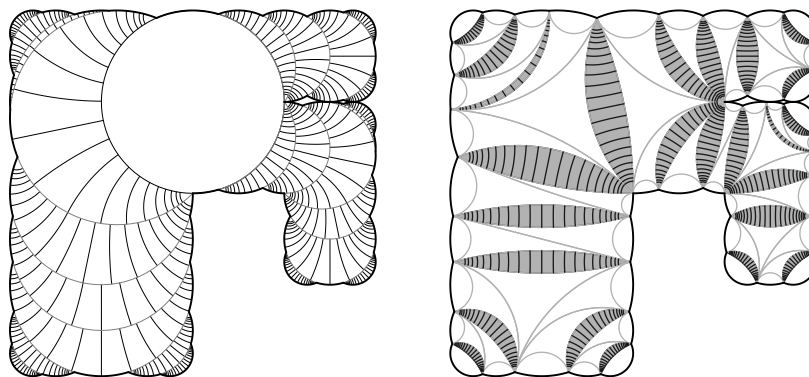


FIGURE 21. The tangential and normal crescent decomposition for a domain. There is a 1-to-1 correspondence between crescents in the two pictures; corresponding crescents have the same vertices and same angle, but are rotated by  $\pi/2$ .

on each gap and collapses every crescent to a hyperbolic geodesic in  $\mathbb{D}$ , thus the disk is written as a union of Möbius images of gaps. For example, see Figures 22. The picture on the left shows a normal crescent decomposition of a square and on the right are the  $\varphi$  images of the gaps in the disk. The images of the crescents is a finite union of geodesics that is called the “bending lamination” of  $\Omega$ . If we record the angle of each crescent and assign it to the corresponding geodesic in the bending lamination, then we get a “measured lamination”, and this data is enough to recover  $\Omega$ , up to a Möbius image. We will discuss laminations further in Section 8.

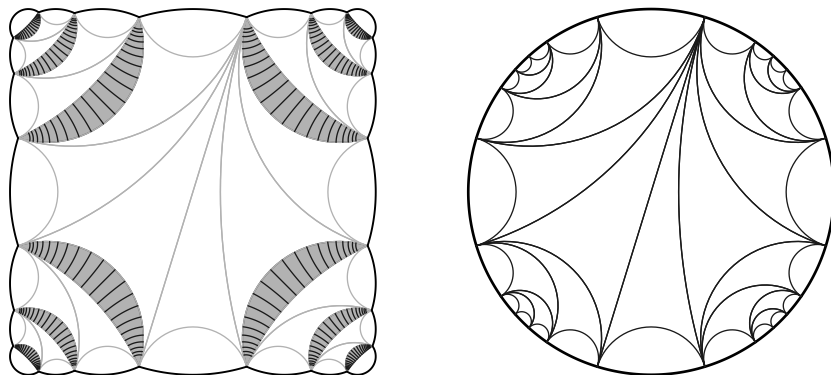


FIGURE 22. A normal crescent decomposition of a square and the corresponding bending lamination in the disk. We can recover the decomposition from the lamination by “thickening” each geodesics to a crescent of the correct angle.

We can recover the normal crescent decomposition from the bending lamination by “thickening” each bending geodesic to a crescent of the correct angle, and moving the gaps by the corresponding elliptic transformations. If we do this continuously, we obtain a family of domains connecting the disk to  $\Omega$ . For  $0 \leq t \leq 1$ , let  $\Omega_t$  be the domain obtained by replacing a crescent of angle  $\alpha$  in the normal decomposition by a crescent of angle  $t\alpha$ . See Figures 23 to 26 for some examples of these 1-parameter families. In general, the intermediate domains need not be planar, but we can think of them as Riemann surfaces that are constructed by gluing together crescents and gaps of given sizes along their edges. Figure 26 shows an example where the intermediate domains are not planar (one sees some small overlap for parameter value  $t = .99$ ; bigger overlaps could be produced by other examples).

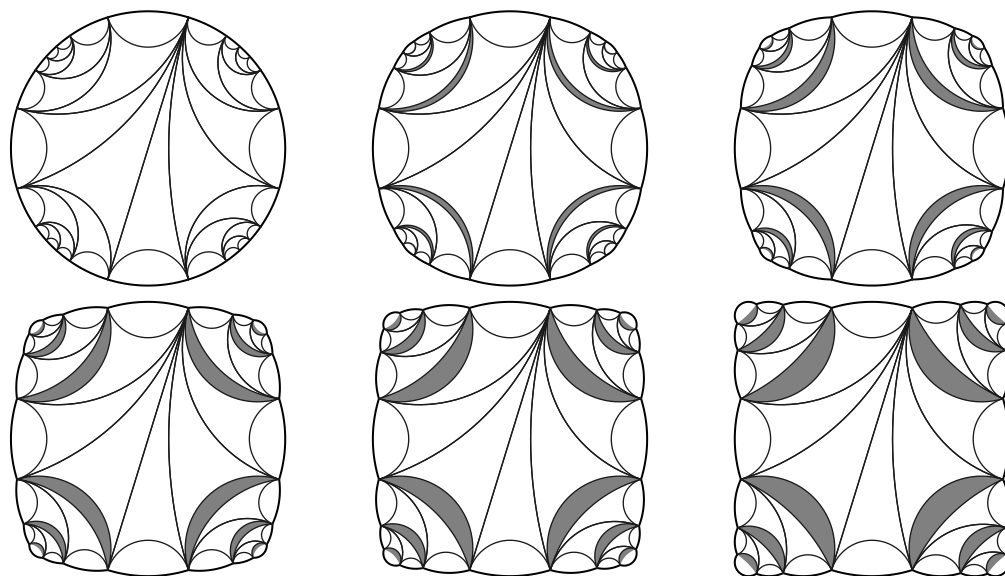


FIGURE 23. The one parameter family connecting the disk to a finitely bent approximation of the square. In each picture the angles have been multiplied by  $t = 0, .2, .4, .6, .8, 1$

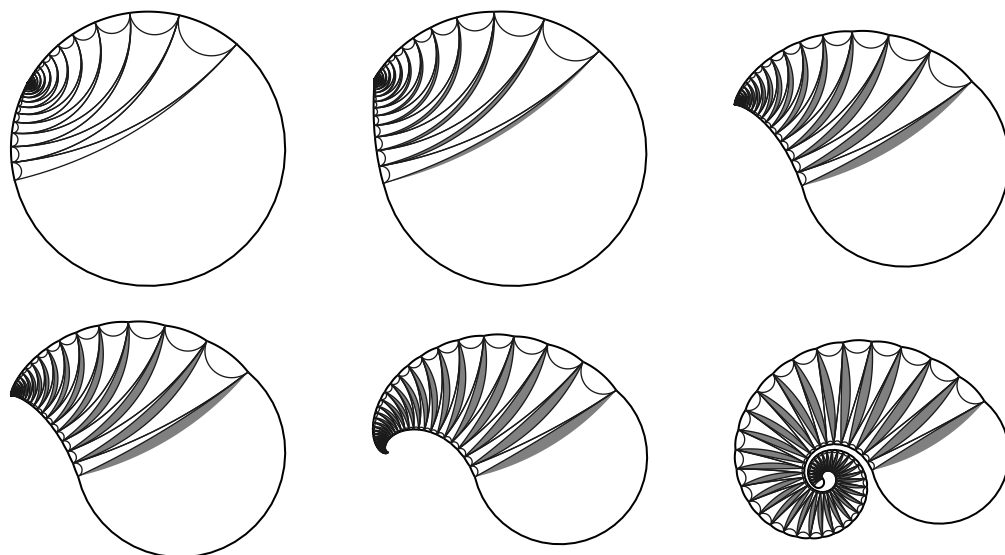


FIGURE 24. An approximate logarithmic spiral with  $t = 0, .2, .4, .6, .8, 1$ . Logarithmic spirals were used by Epstein and Markovic in [56] to disprove Thurston's  $K = 2$  conjecture. They showed that (in a precise sense) certain spirals have too much gray.

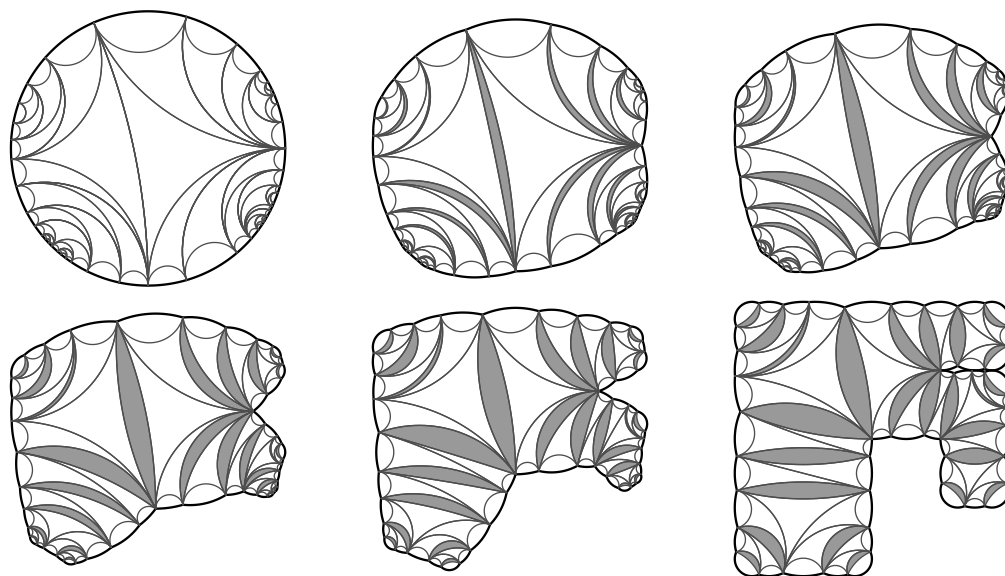


FIGURE 25. The domain from Figure 21 with  $t = 0, .2, .4, .6, .8, 1$ .

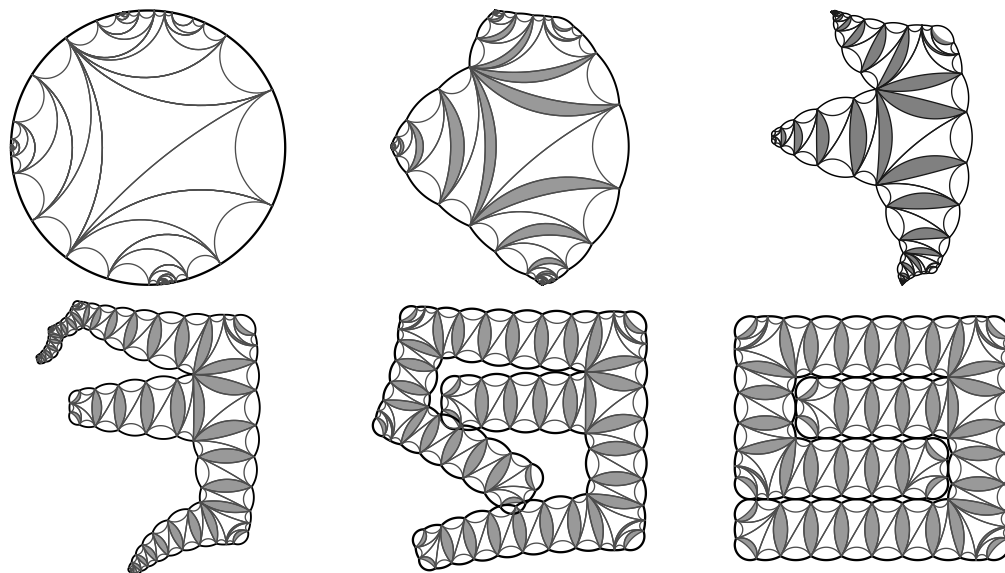


FIGURE 26. An example where intermediate domains need not be planar. The pictures correspond to multiplying the angles by  $t = 0, .4, .8, .95, .99, 1$ . Note that the parameter must be very close to 1 before we see the longer corridors clearly.



Given a pair of domains  $\Omega_s, \Omega_t$  with  $0 \leq s < t \leq 1$ , let  $\iota_{s,t} : \partial\Omega_t \rightarrow \partial\Omega_s$  be the obvious boundary map obtained multiplying the angle of each crescent by  $s/t$ . We will extend this boundary map to the interiors by writing each crescent  $C$  in  $\Omega_t$  of angle  $\alpha$  as a union of crescents  $C_1$ , of angle  $\alpha s/t$  and  $C_2$ , of angle  $\alpha(1 - s/t)$ . On  $C_1$  we collapse each leaf of the  $E$ -foliation to a point (hence  $C_1$  maps to a circular arc) and we let our map be Möbius on  $C_2$ . By continuity, this Möbius transformation would have to agree with the map on the gap that is adjacent to  $C_2$ . We will let  $\varphi_{s,t} : \Omega_t \rightarrow \Omega_s$  denote this map. Let  $\rho_s = \rho_{\Omega_s}$  denote the hyperbolic metric on  $\Omega_s$ . Suppose  $N$  is a large integer and choose points  $t_0 = 0, t_1 = \frac{1}{N}, \dots, t_N = 1$ . Let  $\Omega_k = \Omega_{t_k}$  for  $k = 0, \dots, N$ . Let  $\varphi_k : \Omega_{k+1} \rightarrow \Omega_k$  be defined by  $\varphi_k = \varphi_{\frac{k}{N}, \frac{k+1}{N}}$ .

## 6. $\varphi_{s,t}$ IS A QUASI-ISOMETRY

As noted before, the retraction map  $R : \Omega \rightarrow S$  is a quasi-isometry. Thus  $\varphi = \iota \circ R : \Omega \rightarrow \mathbb{D}$  is also a quasi-isometry between the hyperbolic metrics. The same is true for the maps  $\varphi_{s,t}$  for any  $0 \leq s < t \leq 1$ , with constant bounded by  $O(|s - t|)$ . This result is the goal of this section and the next.

Consider the bending lamination  $\Gamma$  associated to a finitely bent domain  $\Omega$ . Suppose a hyperbolic  $r$ -ball hits geodesics in  $\Gamma$  with angles  $\alpha_1, \dots, \alpha_m$ . We want to show that there is an upper bound  $\sum_j \alpha_j \leq B(r)$  that only depends on  $r$ . See [14], [52] for some variations of this idea. Estimates of  $B$  are also closely tied to results of Bridgeman [22], [23] on bending of surfaces in hyperbolic spaces. Here we shall give a simple conceptual proof without an explicit estimate. The number of bending geodesics that hit the  $r$ -ball has no uniform bound (if it did the lemma would be trivial since every crescent has angle  $\leq 2\pi$ ). However, the total bending of these geodesics is bounded in terms of  $r$ . This result (together with Lemma 31) is one of the main pillars on which the whole paper rests; the uniform estimate of bending eventually becomes the uniform estimates of time and accuracy given in Theorems 1 and 2.

**Lemma 9.** *There is a  $C < \infty$  so that  $B(r) \leq Ce^{3r}$ .*

*Proof.* Suppose  $\Omega$  is normalized so  $\infty \notin \Omega$ . The normalization implies that if  $\gamma$  is a bending geodesic in  $\mathbb{H}^3$  that hits the plane at 1 and  $-1$ , then the corresponding crescent is in the unit disk. Moreover, an easy estimate shows that a crescent with vertices  $\pm 1$  and angle  $\alpha$  has area  $\geq c\alpha$  for some fixed  $c > 0$ .

If  $\tilde{\gamma}$  is a bending geodesic with angle  $\beta$  that passes within hyperbolic distance  $r$  of  $(0, 0, 1)$  then the “highest” point of  $\tilde{\gamma}$  has Euclidean height at least  $e^{-r}$  above the plane  $\mathbb{R}^2$ . Thus its two endpoints on the plane are at least  $2 \cdot e^{-r}$  apart. Moreover at least one endpoint must be contained in the disk of diameter  $e^r$  around the origin (if not, then  $\tilde{\gamma}$  lies outside the hemisphere with this disk as its base, which means the hyperbolic distance to  $(1, 0, 0)$  is  $\geq r$ ).

Thus the part of the crescent corresponding to  $\tilde{\gamma}$  inside the ball  $B(0, e^r + 1)$  has area at least  $ce^{-r}\beta$ . Consider the set of all bending geodesics that come within hyperbolic distance  $r$  of the point  $(0, 0, 1) \in \mathbb{H}^3$  and let  $\{\alpha_n\}$  be an enumeration of the bending angles. Since the crescents are disjoint we deduce  $\sum_n \alpha_n \leq \frac{1}{c}\pi e^r (e^r + 1)^2 \leq Ce^{3r}$ , as desired. (Note that this argument is not sharp since the crescents can have small area only when they are close to the origin.)  $\square$

The following simple lemma quantifies the fact that an elliptic Möbius transformation with small rotation angle is close to the identity.

**Lemma 10.** *Suppose  $\sigma$  is an elliptic Möbius transformation with fixed points  $a, b$  and rotation angle  $\theta$ . If  $r = \max(|z - a|, |z - b|) \leq A|b - a| \leq |b - a|/(4\theta)$  and  $|\theta| \leq \frac{1}{4}$ , then we have*

$$|z - \sigma(z)| \leq 2A^2|\theta||z - a|,$$

where  $C$  depends only on  $A$ .

*Proof.* This is an explicit computation. The conclusion is invariant under scaling, so we may assume  $a = 1, b = -1$ , in which case  $\sigma$  has the form  $\sigma(z) = \tau^{-1}(\lambda\tau(z))$  where  $\lambda = e^{i\theta}$  and  $\tau(z) = (z - 1)/(z + 1)$ . Doing some arithmetic, and using  $|1 - \lambda| \leq |\theta|$ , we get

$$|\sigma(z) - z| = \left| \frac{(1 - \lambda) - (1 - \lambda)z^2}{(1 + \lambda) + (1 - \lambda)z} \right| \leq |\theta| \frac{|1 - z^2|}{1 - |\theta| - |\theta||z|} \leq 2A^2|\theta||z - 1|,$$

if  $|\theta| \leq \frac{1}{4}$  and  $|\theta z| \leq \frac{1}{4}$ .  $\square$

The following is the main result of this section. Recall that  $R : \Omega \rightarrow S$  denotes the nearest point retraction discussed in the previous section.

**Lemma 11.** *Suppose  $r > 0$  is given. There is an  $\epsilon > 0$ , depending only on  $r$ , so that if  $0 \leq s < t \leq 1$  and  $|s - t| \leq \epsilon$  then the following holds. Suppose  $G_1$  and  $G_2$  are*

gaps in the normal crescent decomposition of the finitely bent domain  $\Omega_s$  such that  $\rho_S(R(G_1), R(G_2)) \leq r$ . Suppose  $\tau_j$  are Möbius transformations so that  $\varphi_{s,t}^{-1}|_{G_j} = \tau_j$  for  $j = 1, 2$ . Then

$$\rho_t(\tau_1(z), \tau_2(z)) \leq C_r |t - s|,$$

for every  $z \in \Omega_s$  with  $\rho_s(z, G_1) \leq r$ .

*Proof.* The statement is invariant under renormalizing by Möbius transformations so we may assume that  $G_1$  has base disk  $\mathbb{D}$ , that  $z_1 = 0 \in G_1$  is within  $2r$  of  $G_2$ , and that  $\tau_1$  is the identity.

Then  $\tau_2$  is a composition of the elliptic transformations  $\{\sigma_j\}$  that correspond to the normal crescents  $\{C_j\}$  that separate  $G_1$  and  $G_2$ . By Lemma 9, the measure of the bending geodesics separating  $G_1$  and  $G_2$  is at most  $B(r)$ .

Since  $\rho_S(C_j, 0) \leq r$  for all  $j$ ,  $C_j$  has diameter  $\geq e^{-r}$  and one vertex is contained within  $D(0, e^r)$  by the proof of Lemma 9. By Lemma 10 this means that  $\sigma_j$  moves points in  $D(0, C)$  at most  $C|\theta_j|$  with  $C$  depending only on  $r$ , assuming  $\theta_j$  is small enough (depending only on  $r$ ). Thus

$$(1) \quad |\tau_2(z) - z| \leq C_r |s - t| \sum_j |\theta_j| = O(|s - t|),$$

for  $|z| \leq C$ , assuming  $|s - t|$  is small enough, depending only on  $r$ .

If  $\rho_t(0, z) \leq r$ , then  $|z| \leq A_r$  and  $\text{dist}(z, \partial\Omega_s) \geq B_r > 0$  with estimates that only depend on  $r$  (see Lemma 42, Appendix A). Thus for  $|s - t|$  small enough,  $\rho_t(z, 0) \leq r$  and  $|z - w| \leq \epsilon$  imply  $\rho_t(z, w) \leq C_r \epsilon$ . Hence for a given  $r$  we can choose  $|s - t|$  so small that (1) implies  $\rho_t(\tau_2(z), z) \leq O(|s - t|)$ , (with constant depending on  $r$ ).  $\square$

**Lemma 12.**  $\varphi_{s,t}$  is a quasi-isometry with constant  $O(|s - t|)$ .

This follows immediately from the following technical result that will be proven in Section 7. It also follows from a careful reading of [14], which gives an explicit construction of a quasiconformal map from  $\mathbb{D}$  to a finitely bent domain  $\Omega$  with boundary values  $\varphi^{-1}$ . The method can be adapted to give an explicit map  $\Omega_s \rightarrow \Omega_t$  that is quasiconformal with constant  $O(|s - t|)$ .

**Theorem 13.** Suppose  $\Omega_0, \Omega_1$  are simply connected and  $\varphi : \Omega_0 \rightarrow \Omega_1$  has the following property: there is a  $0 < C < \infty$  so that given any hyperbolic  $C$ -ball  $B$  in  $\Omega_0$ , there is a Möbius transformation  $\sigma$  so that  $\rho_{\Omega_0}(z, \sigma(\varphi(z))) \leq \epsilon$  for every

$z \in B$ . Then there is a hyperbolic  $(1 + O(\epsilon))$ -biLipschitz map  $\psi : \Omega_0 \rightarrow \Omega_1$  so that  $\sup_{z \in \Omega_0} \rho_{\Omega_1}(\varphi(z), \psi(z)) \leq O(\epsilon)$ . In particular,  $\varphi$  is a quasi-isometry between the hyperbolic metrics with constant  $O(\epsilon)$ .

**Corollary 14.** *There is a (hyperbolically)  $(1 + O(|s - t|))$ -biLipschitz map  $\psi_{s,t} : \Omega_s \rightarrow \Omega_t$  so that  $\psi_{s,t} = \varphi_{s,t}^{-1}$  on the boundary. If  $G$  is a gap or crescent and  $\varphi_{s,t}^{-1}$  is the Möbius transform  $\sigma$  on  $G$ , then  $\rho_t(\psi_{s,t}(z), \sigma(z)) \leq O(|s - t|)$  for  $z \in G$*

## 7. PIECEWISE MÖBIUS MAPS AND $\epsilon$ -DELAUNAY TRIANGULATIONS

Here we prove Theorem 13 from Section 6.

If we want to approximate a map  $f$  between polygons, a convenient thing to do is to decompose the interior into triangles, and approximate by a map that is linear on each triangle. If  $f$  is already linear in some subregion, we can arrange for the approximation to agree with it on the triangles that lie inside this subregion.

We would like to do the same thing for finitely bent domains. One problem is that the maps we wish to approximate are Möbius in some regions rather than linear, and a piecewise linear approximation will not preserve this. We could try to approximate circular arcs by line segments and Möbius transformations by linear maps, but instead we will slightly alter the idea of piecewise linear approximation.

Given a triangle  $T$ , let  $D$  be the disk containing the three vertices on its boundary and let  $\tilde{T}$  be the ideal hyperbolic triangle in  $D$  with these three vertices. We will say that a triangulation is  $\epsilon$ -Delaunay if whenever two Euclidean triangles  $T_1, T_2$  meet along an edge  $e$ , the sum of two the angles not incident on  $e$  is at most  $\pi - \epsilon$ . This means that between  $\tilde{T}_1$  and  $\tilde{T}_2$  there is a crescent of angle at least  $\epsilon$ . See Figure 27. A 0-Delaunay triangulation is the same as the usual notion of a Delaunay triangulation. Delaunay triangulations play an important role in computational geometry (see e.g., [8], [60], [61], [106]).

**Lemma 15.**  *$\epsilon$ -Delaunay triangulations are invariant under Möbius transformations.*

*Proof.* The  $\epsilon$ -Delaunay condition is equivalent to saying that if  $T_1$  and  $T_2$  are adjacent triangles then the boundaries of the corresponding disks  $D_1$  and  $D_2$  meet at exterior angle less than  $\pi - \epsilon$ . This is clearly invariant under Möbius transformations.  $\square$

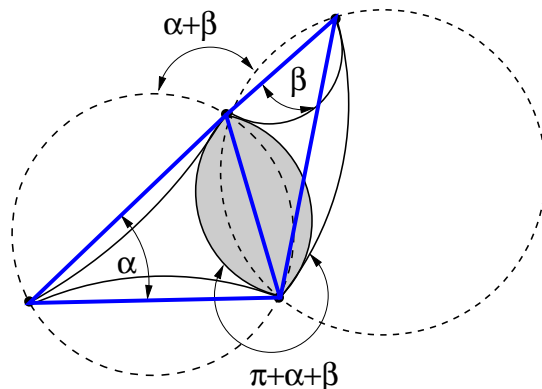


FIGURE 27. Two triangles share an edge and the angles opposite the edge sum to less than  $\pi$ . There is then a crescent of angle  $\pi - (\alpha + \beta)$  that separates the ideal hyperbolic triangles associated the two Euclidean triangles.

Suppose we are given a mapping between the boundaries of two crescents with interior angles  $\alpha_1, \alpha_2$  that agrees with a Möbius transformation on each boundary arc (but possibly different transformations on each arc). Normalizing so the vertices are 0 and  $\infty$ , the boundary maps must be of the form  $z \rightarrow \lambda_i z$  for  $i = 1, 2$ . Mapping the crescents to strips  $S_i = \{z = x + iy : 0 \leq y \leq \alpha_i\}$  by a logarithm, these maps become  $z \rightarrow z + t_i$ . The boundary map can be extended to the interior by a unique affine map  $T : (x, y) \rightarrow (x + t_1 + (t_2 - t_1)y/\alpha_1, y\frac{\alpha_2}{\alpha_1})$ . When this map is conjugated back to a map between the crescents, it defines a quasi-conformal map with minimal possible dilatation extending the given boundary values (e.g. Theorem 3.1 of [56] for a simple proof; strict equality actually holds [9], [120]). We shall call such a map an affine-crescent map.

Suppose we are given an  $\epsilon$ -Delaunay triangulation in a region  $\Omega$  and a map  $f : \Omega \rightarrow \Omega'$  that sends the vertices to the vertices of another  $\epsilon$ -Delaunay triangulation. On each  $\tilde{T}$ , define  $g$  to be the Möbius transformation defined by the images of the three vertices. On the crescents separating two ideal triangles, define  $g$  to be the affine crescent map extending the definition on the boundary of the crescent. Thus  $g$  is an approximation to  $f$  that is Möbius on the ideal triangles and quasiconformal on the crescents. If  $f$  is Möbius on the quadrilateral formed by two adjacent triangles, then it is  $g = f$  on the two corresponding ideal triangles and the crescent separating them.

Otherwise the quasiconformal constant of  $g$  is bounded in terms of the quasiconformal constant of  $f$  and the hyperbolic size of the triangles.

We will call an (infinite)  $\epsilon$ -Delaunay triangulation an  $(\epsilon, s)$ -triangulation for  $\Omega$  if every edge has hyperbolic diameter  $\sim s$  in  $\Omega$  and the circumcircle of every triangle has hyperbolic diameter  $\sim s$ . Next we want to observe that such a triangulation always exists.

The plane can be tiled by a collection equilateral triangles  $\mathcal{T}_n$  of side length  $2^{-n}$  in such a way that the each triangle of size  $2^{-n}$  is a union of four triangles in  $\mathcal{T}_{n+1}$ . Given a point  $x \in \Omega$  and  $0 < \lambda < \frac{1}{4}$  there is a triangle  $T \in \mathcal{T}_n$  that contains  $x$  and so that

$$(\lambda/2)\text{dist}(T, \partial\Omega) \leq \ell(T) \leq \lambda\text{dist}(T, \partial\Omega)$$

and it is unique except when  $x$  is on the common boundary of a finite number ( $\leq 6$ ) of such triangles. Any two triangles that satisfy this condition have adjacent sizes (since they are both comparable to the same number within a factor of two).

So we can cover  $\Omega$  by a union of triangles whose interiors are disjoint and each is approximately size  $\lambda$  in the hyperbolic metric. We claim that by adding some extra edges we can preserve this property and also get a  $\epsilon$ -Delaunay triangulation. To see how, form a triangular mesh by taking the lattice triangles whose size is comparable to the distance to the boundary.

We can also arrange that if two triangles meet a common triangle, then they must be of adjacent sizes. To see this, suppose  $T_1$  and  $T_2$  are adjacent and  $T_2$  and  $T_3$  are adjacent and that  $T_1$  is the largest of the three triangles. Let  $\ell(T)$  denote the side length of an equilateral triangle. Then

$$\begin{aligned} \ell(T_3) &\geq (\lambda/2\sqrt{2})\text{dist}(T_3, \partial\Omega) \\ &\geq (\lambda/2\sqrt{2})[\text{dist}(T_1, \partial\Omega) - \ell(T_2) - \ell(T_3)] \\ &\geq (\lambda/2\sqrt{2})\left(\frac{1}{\lambda} - 1 - 1\right)\ell(T_1) \\ &\geq \left(\frac{1}{2\sqrt{2}} - \frac{\lambda}{\sqrt{2}}\right)\ell(T_1) \\ &> \frac{1}{4}\ell(T_1), \end{aligned}$$

if  $\lambda$  is small enough. Since  $\ell(T_1)/\ell(T_3)$  is a power of 2 we must have  $\ell(T_3) \geq \ell(T_1)/2$ , as desired.

If two adjacent triangles are different sizes then some interior edges must be added to the larger one to make it a triangulation (but the smaller one does not hit an even smaller one by our previous calculation, so it does not need to be divided). There are three cases.

- (1) If the larger one is bordered on all three sides by smaller ones, then we divide it into four equilateral triangles in the usual way.
- (2) If is bounded on exactly one side by smaller triangles, we add the bisector of the opposite angle.
- (3) If it is bounded on exactly two sides by smaller triangles, we add the segment parallel to the third side  $e$  and half its length and the three segments connecting the midpoint of the new segment to corners of the triangle.

See Figure 28. This is clearly  $\epsilon$ -Delaunay. Indeed the worse case is in the third case above. The bottom triangle has two angles of size  $\alpha = \arctan(\sqrt{3}/2) \approx .713714 \approx .22718\pi$  and one of angle  $\beta = (\pi - 2\alpha) \approx .544\pi$ . Since  $\alpha$  is opposite an angle of size  $\frac{2}{3}\pi$  and  $\beta$  is opposite angle of  $\frac{1}{3}\pi$ , we see that every possible quadrilateral is at least  $.106\pi$ -Delaunay.

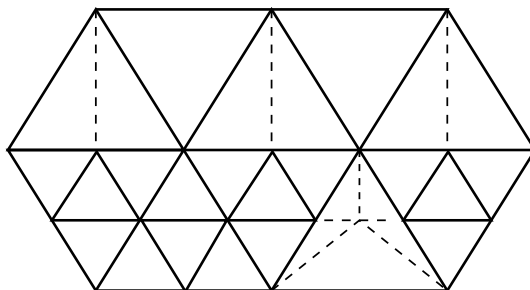


FIGURE 28. When triangles of different size meet we subdivide the larger one to make a triangulation. This produces  $\epsilon$ -Delaunay triangulations for a uniform  $\epsilon > 0$

The proof of Theorem 13 is now quite simple. Take a  $(\epsilon_0, s)$ -triangulation of  $\Omega_1$ , restrict the map  $\varphi$  to the vertices and take  $\psi$  to the piecewise Möbius extension of these values to  $\Omega_1$ . If  $s$  is smaller than  $C/2$  then on the union of any two adjacent triangles, the map  $\varphi$  is  $\epsilon$ -close to a Möbius transformation, and this implies  $\psi$  is hyperbolic biLipschitz with constant  $1 + O(\epsilon)$  where the constant depends only on  $\epsilon_0$  and  $s$ . This proves Theorem 13.

## 8. COMPUTING THE BENDING LAMINATION IN LINEAR TIME

We have now finished introducing the  $\iota$  map and describing the relevant estimates. We now start our discussion of the algorithm for computing conformal maps, starting with the construction of the bending lamination of a finitely bent domain in linear time. This will lead to our decomposition of the plane, the representation of conformal maps and the method for improving such representations.

Recall that  $R$  denotes the nearest point retraction from a planar domain to its dome. Given a finitely bent domain  $\Omega$ , we noted above that  $\varphi = \iota \circ R$  is a continuous map of  $\Omega$  to  $\mathbb{D}$ , equals  $\iota$  on the boundary, is a Möbius transformation on each gap, and collapses the crescents to a union of geodesics  $\Gamma$  in  $\mathbb{D}$  called the bending lamination. To each geodesic  $\gamma \in \Gamma$  we associate the angle of the corresponding crescent. This is called the bending measure of the geodesic and is an example of a transverse measure on a lamination.

A finite lamination  $\Gamma$  in the disk lies in the hyperbolic convex hull of its endpoints. If it triangulates the convex hull we say it is complete. We shall assume that our bending laminations are complete, which is always possible by adding at most  $O(n)$  extra geodesics with bending angle 0 (since we only need  $2n - 3$  edges to triangulate  $n$  points).

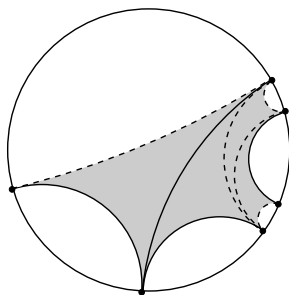


FIGURE 29. The convex hull of six points, a lamination with these endpoints (solid lines) and a completion of it (dashed lines).

Next we will check that  $\iota$  and the bending lamination of a finitely bent domain  $\Omega$  can be constructed in linear time, given the medial axis of  $\Omega$ . This is fairly straightforward, but we record it formally with some definitions and a lemma. Suppose we have a finite collection of disks,  $\mathcal{D}$ , in the plane and an adjacency relation between them that makes the collection into the vertices of a tree. Suppose the disk  $D_0$  has



been designated the root of the tree. Then any other disk  $D$  has a unique “parent”  $D^*$  that is adjacent to  $D$  but closer to the root. Assume that for every (non-root) disk we are given a map  $\tau_D : D \rightarrow D^*$ . Then we can define a map  $\sigma_D : D \rightarrow D_0$  as follows. If  $D = D_0$ , the map is the identity. Otherwise, there is a unique shortest path of disks  $D_0, \dots, D_k = D$  between  $D_0$  and  $D$ . Note that each disk is preceded by its parent. Thus  $\sigma = \tau_{D_1} \circ \dots \circ \tau_{D_k}$  is a mapping from  $D$  to  $D_0$  as desired. We will refer to this as a “tree-of-disks” map.

**Lemma 16.** *With notation as above, assume that every map  $\tau_D$  is Möbius. Then given  $n$  points  $\mathbf{v} = \{v_1, \dots, v_n\}$ , with  $v_k \in \partial D_k$  for  $k = 1, \dots, n$ , we can compute the  $n$  image points  $\sigma(\mathbf{v}) \subset \partial D_0$  in at most  $O(n)$  steps.*

*Proof.* If  $D \in \mathcal{D}$  has positive radius, choose three distinct reference points  $z_1^D, z_2^D, z_3^D$  on  $\partial D$ ; otherwise let this collection be empty. Every other point  $z$  on  $\partial D$  is uniquely determined by the cross ratio  $\text{cr}(z_1^D, z_2^D, z_3^D, z)$ . Label each point  $v$  in  $\mathbf{v}$  with the minimal  $k$  so that  $v$  is on the boundary of a  $k$ th generation disk  $D$ . For  $k = 0$  we do nothing to the vertex. For  $k > 0$ , compute  $\tau_D(v) \in \partial D^*$  and record the cross ratio  $\text{cr}(z_1^{D^*}, z_2^{D^*}, z_3^{D^*}, \tau_D(v))$ . Also compute and record the images of the three reference points for  $D$ , i.e.,  $\text{cr}(z_1^{D^*}, z_2^{D^*}, z_3^{D^*}, \tau_D(z_k^D))$  for  $k = 1, 2, 3$ .

If a vertex is on  $\partial D_0$  then it maps to itself. If  $D$  is a first generation disk, then we just compute  $\tau_D(v) \in \partial D_0$  and compute the  $\tau_D$  images of the three reference points for  $D$ . For each child of  $D'$  of  $D$ , we can now compute  $\sigma_{D'}$  for any associated vertices using the previously recorded cross ratios with respect to the reference points for  $D$  and we can also compute the images on  $\partial D_0$  for the reference points for  $D'$ . In general, if  $D$  is a disk and we have already computed where the reference points for its parent are mapped on  $\partial D_0$ , we can use the recorded cross ratio information to compute where the associated vertices and reference points for  $D$  map to. This allows us to map every point of  $\mathbf{v}$  to  $\partial D_0$  in  $O(n)$  steps.  $\square$

To construct the bending lamination of a finitely bent domain we apply this lemma to the collection of base disks corresponding to the gaps of the normal crescent decomposition and with two gaps being adjacent iff they are separated by a single crescent. In this case adjacent disks either (1) intersect at exactly two points and we take the elliptic transformation that fixes these points and moves the child to the

parent, or (2) the disks coincide (if the crescent had bending angle 0) and we take the identity map. We can also compute the gaps and the Möbius transformations mapping these gaps to the ones in  $\Omega$  in time  $O(n)$ .

In general, the disks in a “tree-of-disks” need not intersect. In [17], this lemma is used to construct the exact  $\iota$  map for a polygon. The vertices are the medial axis disks corresponding to the vertices of the medial axis with adjacency inherited from the medial axis. Adjacent disks need not intersect (e.g., consider two ends of a long edge-edge bisector), but we can still define an explicit Möbius transformation between them (but not an elliptic transformation in this case).

## 9. COVERING THE BENDING LAMINATION

Our goal in this section is to cover the bending lamination of a finitely bent domain by standard regions. Our standard regions will be “Whitney boxes”, which are approximately unit hyperbolic neighborhoods of points, and “Carleson towers”, which look like unit neighborhoods of long hyperbolic geodesic segments.

The construction can be carried out either in the unit disk or the upper half-plane. It is slightly easier to draw accurate figures in the upper half-plane, so we will describe it there, and only trivial changes are needed to move it to the unit disk.

Given an interval  $I \subset \mathbb{R}$ , the corresponding Carleson square is the region in the upper half-plane of the form  $\{z = x + iy : x \in I, 0 < y < |I|\}$ . The “top-half” of  $Q$  is  $T(Q) = \{z \in Q : y > |I|/2\}$ . This will be called a Whitney box, and its Euclidean diameter is comparable to its Euclidean distance from  $\mathbb{R}$  (abusing notation we may also call them Whitney “squares”, even though they are Euclidean rectangles; the main point is that they are approximately unit size in the hyperbolic metric). When  $I$  ranges over all dyadic intervals (i.e., all intervals of the form  $[j2^{-n}, (j+1)2^{-n})$ ), the corresponding Whitney boxes partition the upper half-plane into pieces with approximately unit hyperbolic size. See Figure 30. Carleson squares are named after Lennart Carleson who used them in his solution of the corona problem and they are now ubiquitous in function theory [27], [64].

Dyadic Carleson squares form a tree under intersection of the interiors. Each square has a unique parent and two children. The parent of a dyadic Carleson square  $Q$  will be denoted  $Q^*$ . This obviously also induces a tree structure on Whitney boxes.

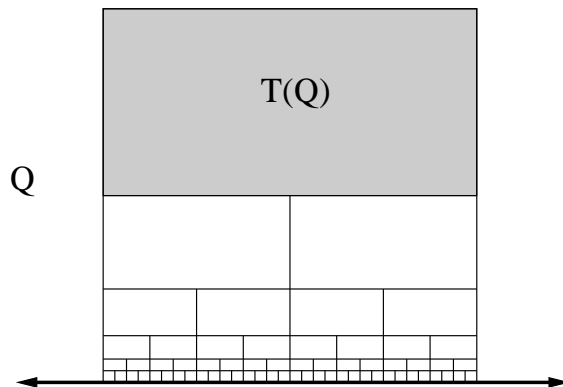


FIGURE 30. A decomposition of a Carleson square into dyadic Whitney boxes. [64]

We will say two dyadic Whitney boxes are neighbors if they are the same size and adjacent; each box therefore has a “left” and a “right” neighbor. One of these is a “sibling” in the sense that it shares a parent, while the other does not.

Suppose  $\Gamma$  is a complete, finite geodesic lamination in  $\mathbb{H}$ . We assume that  $\Gamma$  has been normalized so that its set of endpoints  $S$  satisfies  $\{0, 1\} \subset S \subset [0, 1]$ .

For  $x \in \mathbb{R}$ , let  $W(x) \subset \mathbb{H}$  be the Euclidean cone of angle  $\pi/2$  and vertex  $x$  whose axis is vertical. This is called the Stolz cone with vertex  $x$ . Then  $W = \cup_{x \in S} W(x)$  is an infinite polygon with  $2n$  sides. See Figure 31. This type of region is called a sawtooth domain and is also approximately a unit neighborhood of  $\Gamma$  (at least if we truncate it at height 2). Clearly we can compute  $W$  from  $S$  in linear time if we are given  $S$  as an ordered set.

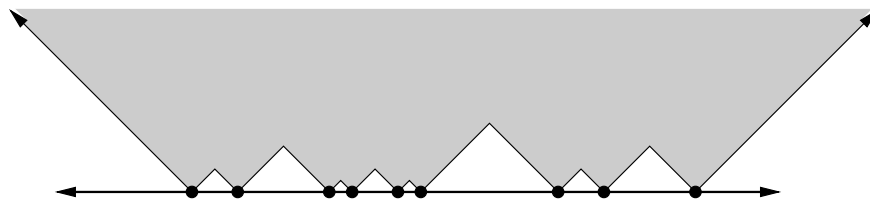


FIGURE 31. The sawtooth domain associated to the set  $S$ . This region is approximately a unit neighborhood of the bending lamination and has only  $O(n)$  boundary arcs.

We can compute the medial axis of  $W$  in time  $O(n)$  (we don’t even need the full strength of the theorem of Choi-Snoeyink-Wang:  $W$  is a monotone histogram so a modification of the simpler algorithm from [1] for convex polygons will work in linear

time, see [33]). In the medial axis of  $W$ , an edge-edge bisector must be vertical. Suppose  $A_0$  is a large number (to be fixed later, but  $A_0 = 20$  will work) and consider an edge-edge bisector  $e$  of hyperbolic length  $\geq A_0$ .

First, suppose  $e$  has finite hyperbolic length. This simply means that  $e$  is bounded away from  $\infty$  and the real line (i.e., it is a compact subset of  $\mathbb{H}$ ). Let  $Q_1, Q_2$  denote the Whitney boxes that contain the top and bottom endpoints of  $e$  respectively. These must be distinct because we are assuming  $e$  has large length, so its endpoints are in boxes far apart. Let  $e^*$  and  $Q_1^*$  denote the vertical projections of  $e$  and  $Q_1$  onto the real axis. If  $e^*$  is contained in the middle third of  $Q_1^*$  then let  $Q_3 = Q_1$ . If  $e^*$  is in the left third of  $Q_1^*$  then let  $Q_3$  denote the union of  $Q_1$  and its neighbor to the left. If  $e^*$  is in the right third, we take the union with the neighbor to the right. In every case,  $Q_2^*$  now hits the middle third of  $Q_3^*$ .

The corresponding Carleson tower is the trapezoid that has the bottom edge of  $Q_3$  and the top edge of  $Q_2$  as its bases. See Figure 32. Each tower is associated to a unique edge of the medial axis so obviously there are at most  $O(n)$  towers associated to a set  $S$  with  $n$  points. The corresponding Carleson arch is  $Q_4 \setminus Q_5$  where  $Q_4$  is the union of Carleson squares with top edge contained in the bottom edge of  $Q_3$  and  $Q_5$  is the Carleson square whose top edge is the top edge of  $Q_2$ .

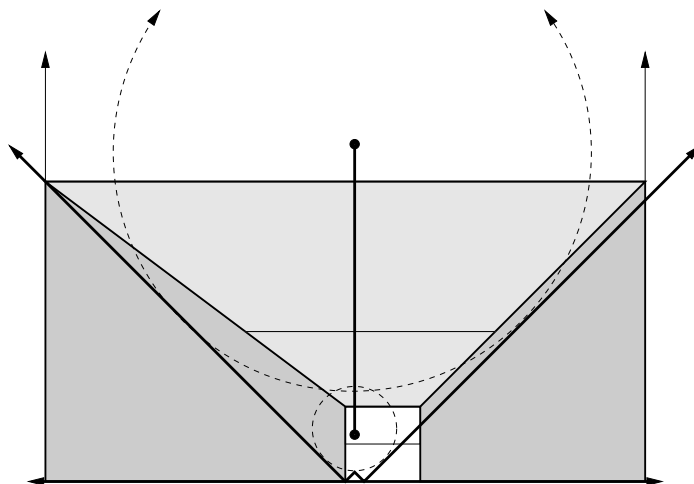


FIGURE 32. The union of shaded areas is a Carleson arch. The lighter shaded trapezoid is the corresponding Carleson tower.

The decomposition piece associated to  $e$  is  $Q = Q_3 \setminus Q_2$  and is called an arch. It meets the real line in two intervals since the base of  $Q_2$  is much shorter than the base of  $Q_3$  and hits the center third of  $Q_3$ 's base. If  $e$  has hyperbolic length  $L$  then the resulting arch is said to have hyperbolic “width”  $L$  and the extremal distance in  $\mathbb{H}$  between the two components of  $Q \cap \mathbb{R}$  is  $\frac{\pi}{L} + O(1)$ . We will call this an  $\epsilon$ -arch if  $\epsilon \geq \pi/L$ . Note that if  $\epsilon$  is small, then the two boundary components of a  $\epsilon$ -arch in  $\mathbb{H}$  are very far apart in the hyperbolic metric ( $\sim 1/\epsilon$ ).

If  $e$  has infinite length then the corresponding Carleson tower is a triangle with one vertex on  $\mathbb{R}$  where  $e$  hits the line, and opposite side that is the bottom of  $Q_3$  (defined as above). The Carleson arch is “degenerate” in this case: it is the same as the union of Carleson squares  $Q_4$  above, except that it comes with a special marked point in the middle third of its base.

Also note that any two hyperbolic geodesics connecting the top and bottom edges of the corresponding Carleson tower must be within  $O(e^{-d})$  of each other when they are more than hyperbolic distance  $d$  from either arch boundary. Thus the convex hull is thin in the arches, in the sense that removing a small ball there will disconnect it. This is not true outside the arches.

If we are given  $A > A_0$  then we let  $e'$  denote the “central part” of  $e$ , i.e., the points of  $e$  that are at least hyperbolic distance  $A$  from the endpoints of  $e$ . Associated to  $e'$  is a Carleson arch called the “central arch” or “ $A$ -arch” associated to  $e$ . Let  $\{e_j\}$  be an enumeration of the edge-edge bisectors of length  $\geq A_0$  in the medial axis of  $W$ , let  $A_j$  be the Carleson arch associated to  $e_j$  and  $A'_j$  the arch associated to its central part  $e'_j$  (possibly empty if  $e$  is shorter than  $2A$ ). Let  $\mathcal{K}$  be an enumeration of the connected components of  $\mathbb{H} \setminus \cup_j A'_j$  and let  $\mathcal{N}$  be the  $A_0$ -arches. ( $\mathcal{N}$  is for “thin” and  $\mathcal{K}$  is for “thick”.) Then the sets in  $\mathcal{N}$  and  $\mathcal{K}$  cover the whole upper half-plane and each set only overlaps sets of the other type. These overlaps are themselves Carleson arches corresponding to segments of hyperbolic length  $A - A_0$ . This covering of  $\mathbb{H}$  will be referred to as a thick/thin decomposition of  $\mathbb{H}$  with  $\eta$ -thin overlaps, where  $\eta^{-1} \approx A - A_0$ . We will use it later to define a thick/thin decomposition of a polygon in Section 12.

**Lemma 17.** *The number of Whitney boxes that hit  $C(S)$  but do not hit any central Carleson arch is at most  $O(An)$ .*

*Proof.* First suppose  $A = A_0$ . Since  $\Gamma$  is complete and contains  $n$  geodesics, its hyperbolic convex hull can be split into  $n - 2$  ideal hyperbolic triangles and hence the hyperbolic convex hull has hyperbolic area bounded by  $\pi(n - 2)$ . See Appendix A for a discussion of hyperbolic area. Thus it is enough to show that there is a  $\delta > 0$  and a  $C < \infty$  so that each Whitney box  $Q$  can be associated to a hyperbolic ball of area  $\delta$  contained in the convex hull of  $\Gamma$  and within hyperbolic distance  $C$  of  $Q$ . For, if we place  $M$  balls of area  $\delta$  into a set of area  $\leq \pi n$ , then at least  $M\delta/\pi n$  of them intersect in a common point. Since any point can only have a bounded number of distinct Whitney boxes within hyperbolic distance  $C$  of it, we see that  $M$  must be bounded by a multiple of  $n$  (the constant depending on  $\delta$  and  $C$ ). If  $Q$  is a Whitney box that hits  $C(S)$ , but does not hit any  $\epsilon$ -Carleson arch, then either it is about unit size (there are only  $O(1)$  such boxes hitting  $C(S)$ ) or  $2Q \cap C(S)$  contains a ball with radius bounded below uniformly, which completes the proof.

If  $A > A_0$  then the gap between and  $A_0$ -arch and its central  $A$ -arch can be filled by  $O(A)$  Whitney boxes. Since there are  $O(n)$  arches, this is at most  $O(An)$  extra boxes.  $\square$

Thus we know that given  $n$  ordered points in  $\mathbb{R}$  the convex hull of these points can be covered by  $O(n)$  Carleson towers and  $O(n)$  Whitney boxes. Next we wish to show these towers and boxes can actually be found in time  $O(n)$ .

**Lemma 18.** *Suppose  $\Gamma$  is a finite, complete geodesic lamination containing  $n$  geodesics. Then in time  $O(n)$  we can find a covering of  $\Gamma$  by at most  $O(n)$  dyadic Whitney boxes and Carleson towers.*

*Proof.* Compute the medial axis of the sawtooth domain  $W$  corresponding to the set of endpoints  $S$ . Locate all the edge-edge bisectors of hyperbolic length  $\geq A_0$  and record the associated Carleson towers.

Each tower has a top and bottom horizontal edge. Extend these edges until they hit the boundary of  $W$  (recall that we know which edges of  $W$  get hit). Near a tower,  $W$  looks very close to a Stolz cone, so the length of these edges is close to 1 if  $A_0$  is large enough. In particular, for large  $A_0$  it has length  $< 2$  and so at most three Whitney boxes suffice to cover each of these edges. (This determines our choice of  $A_0$ ).

These edges cut  $W$  into connected components. After we remove the components corresponding to towers, we have at most  $O(n)$  components remaining. We claim that if one of these components hits  $m$  dyadic Whitney boxes then we can find all these boxes in time  $O(m)$ .

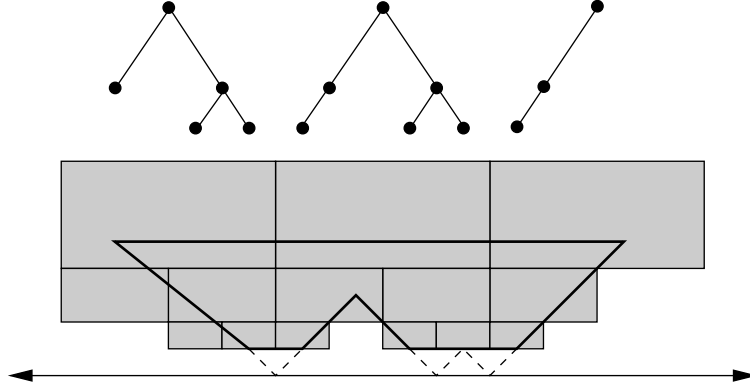


FIGURE 33. A truncated component of  $W$  and the dyadic Whitney boxes that hit it. These boxes form vertices of at most three trees rooted at the topmost boxes.

To do so consider one such component  $W_0$ . It has a single horizontal “top” edge of length  $L$  and a bottom edge that is polygonal curve. Project each segment of this curve vertically to the real line and choose a dyadic interval contained in each projection and of comparable size. Then enumerate all the dyadic intervals which contain at least one of our choice and have length  $\leq L$ . If there are  $m$  such they can be listed in time  $O(m)$  (see Lemma 50 of Appendix A). The corresponding Whitney boxes, plus a constant number of their neighbors, cover  $W_0$ , so we are done.  $\square$

As a consequence of the proof, we see that we can also record the adjacency relations between the chosen boxes in time  $O(n)$ .

## 10. EXTENDING THE CONVEX HULL COVER TO ALL OF $\mathbb{H}$

Given a finite set of points  $S \subset [-1, 1]$  we will construct the corresponding “Carleson-Whitney” decomposition of the upper half-plane by modifying the cover of the convex hyperbolic hull of  $S$  from Section 9. This decomposition of the upper half-plane will consist of the outside of some fixed Carleson square  $Q_0$  and a finite number of pieces whose union is all of  $Q_0$ . These pieces come in four types (see Figure 34:

- (1) Carleson squares,
- (2) Whitney squares, which are obtained by dividing a Whitney box into a bounded number of equal sized Euclidean squares,
- (3) Carleson arches, which consist of a Carleson square with a smaller Carleson square removed from it; we assume the base of the smaller square hits the middle third of the base of the larger square and is much smaller.
- (4) Degenerate arches, where the smaller square is replaced by a single point of  $S$ , contained in the center third of the base. Moreover, every point of  $S$  will be associated to a degenerate arch in this way. Note that these pieces are really Carleson squares, but it is convenient to consider them separately from squares  $Q$  whose closures do not contain a point of  $S$ .

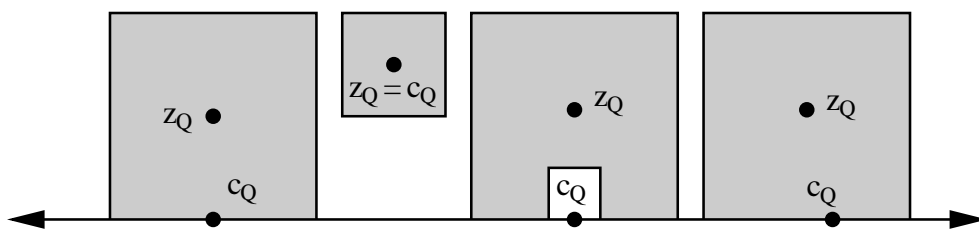


FIGURE 34. The shapes of pieces used in a Carleson-Whitney decomposition: Carleson squares, Whitney squares, Carleson arches and degenerate Carleson arches.

In practice, we could avoid arches by simply using more Whitney type squares but we would lose the linear dependence on  $n$ . For many domains, however, this might not be much of a loss, and would simplify much of what follows. Moreover, when using finite, rather than infinite, precision it may be more practical to simply cover any arches by a union of Whitney and Carleson boxes.

To construct the covering we fix some  $\epsilon > 0$ , take the hyperbolic convex hull of  $S$  and cover it by  $O(n)$   $\epsilon$ -Carleson arches and Whitney boxes as in Section 9. The remaining parts of  $Q_0$  can be written as a union of Carleson squares  $Q$  whose top edges meet the bottom edges of Whitney boxes in the cover above. The part of the boundary of  $Q$  that hits the existing cover is a connected piece  $E$  of the boundary that contains the top edge. We then subdivide the Carleson box near  $E$  into Whitney type and Carleson squares so that any two adjacent squares have comparable size and that subsquares touching  $E$  have size comparable to the distance from  $\mathbb{R}$ . See Figure



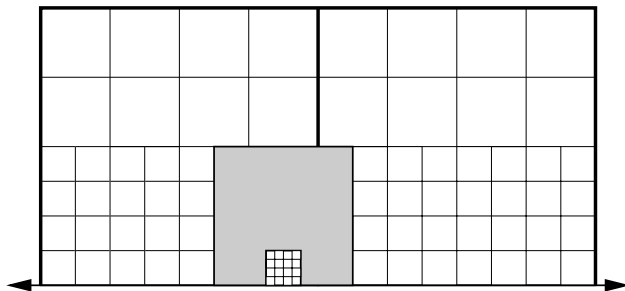


FIGURE 35. Definition of a Carleson arch. The bounding squares of an arch need not be dyadic, in which case we tile the region around them by Whitney boxes and Carleson squares to fill in a union of dyadic squares.

36 to see how to do this. This insures that in our decomposition of  $\mathbb{H}$  when two pieces meet, the intersecting boundary components have comparable size (this is also true for the pieces themselves, except for arches, which may be much larger than adjacent pieces underneath them; however, the lower boundary of the arch is comparable in size to the adjacent pieces). Moreover, the number of squares created is bounded by a multiple of the number of Whitney squares in the cover, so is  $O(n)$ .

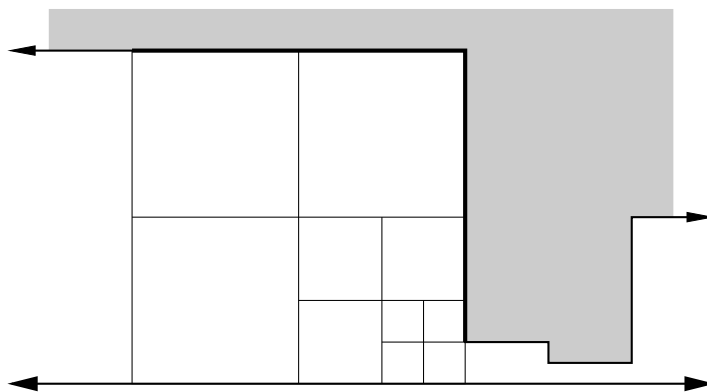


FIGURE 36. A Carleson square that lies below our cover of the convex hull can be subdivided into subsquares so that any two adjacent squares have comparable size. The number of squares needed is bounded by a multiple of the number of squares in the covering region and hence is  $O(n)$ .

The final step of the construction is to subdivide pieces as follows. Each Whitney square is subdivided into a bounded number of Whitney type squares  $Q$  with the

property that  $MQ$  does not hit a point of  $S$  ( $M$  is a fixed large number to be specified later and  $MQ$  denotes the box concentric with  $Q$  and  $M$  times larger). For example, see Figure 37. Similarly, we divide Carleson squares into a bounded number of Whitney type squares and Carleson squares so that each can be expanded by a factor of  $M$  without hitting  $S$  (this can be done since each point of  $S$  is contained in a degenerate Carleson arch, and hence any Carleson square in our decomposition is separated from  $S$  by a uniform multiple of its diameter). We will call these  $M$ -Whitney squares or  $M$ -Carleson squares for  $S$ . Similarly we replace arches by thinner arches  $Q$  so that  $MQ$  misses  $S$  and tile the resulting gaps by Whitney type squares and Carleson boxes (for an arch  $MQ$  means expanding the bigger square by a factor of  $M$  and shrinking the smaller one by a factor of  $M$ ).

$M$  will be fixed later to insure various properties. For example, it is easy to verify the following fact we will need using hyperbolic geometry and the fact that Möbius transformations are hyperbolic isometries.

**Lemma 19.** *If  $M$  is large enough the following holds. Suppose  $Q_1$  is an  $M$ -Whitney square for  $S$  and  $Q_2$  is a  $M$ -Whitney square for  $\tau(S)$  where  $\tau$  is a Möbius transformation of  $\mathbb{H}$  to itself and that  $\tau(Q_1) \cap Q_2 \neq \emptyset$ . Then  $2Q_2 \subset \tau(10Q_1)$ .*

A similar result holds for Carleson squares. For Whitney and Carleson squares,

$$\text{diam}(Q) \sim \frac{1}{M} \text{dist}(Q, S),$$

but this is not true for arches. However, if  $E$  is a boundary component of an arch then it is true that

$$\text{diam}(E) \sim \text{dist}(E, S).$$

The pieces of our decomposition form the vertices of a tree, where the parent of a piece is the piece that is adjacent and directly above it. The leaves of the tree are either Carleson squares or degenerate Carleson arches. We will also consider the graph that results from adding edges corresponding to adjacency of pieces (left/right as well as up/down).

Given an element of such a decomposition we consider the part of its boundary in the open upper half-plane. For Whitney type squares this is a square, for Carleson squares it is an arc (the top and sides of the rectangle) and for arches there are two components, each of which is the top and sides of a square. Given a boundary

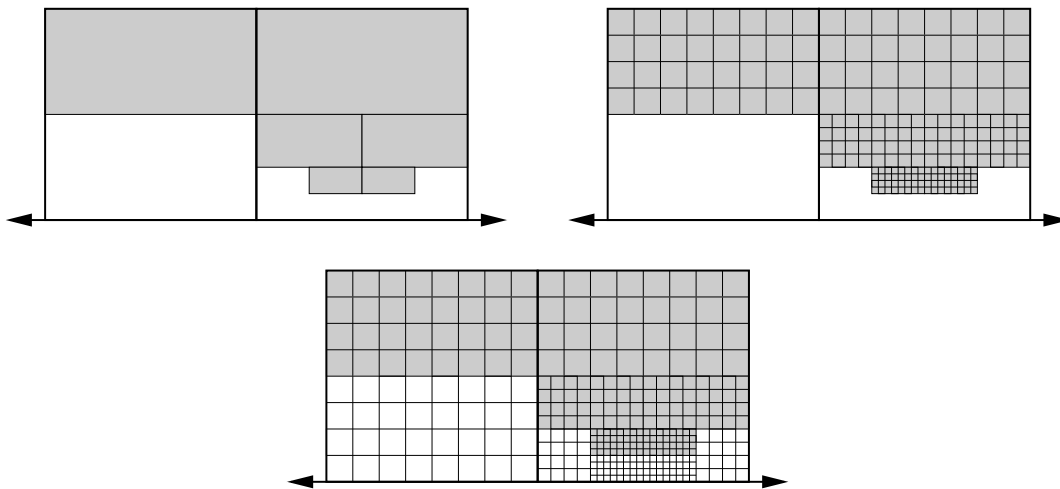


FIGURE 37. On the upper left is a collection of Whitney squares, on the upper right a division of these into Whitney type squares and on the bottom we subdivide the region below the Whitney squares into Whitney type squares and Carleson squares so that adjacent squares are of comparable sizes.

component  $E$  of one of these types, we let  $\text{diam}(E)$  denote its Euclidean diameter and let  $N_s(E)$  be the  $s \cdot \text{diam}(E)$  Euclidean neighborhood of  $E$ . Throughout the paper we only need one fixed value of  $s < \frac{1}{4}$ , say  $s = 1/10$ . Let  $N_s$  be the union of these sets over all boundary components of all pieces of our decomposition. Similarly we define  $N_s(\partial Q)$  to be the union of  $N_s(E)$  over all boundary components of  $Q$  (one such for boxes, two for arches) and let  $N_s(Q)$  be the union of this with  $Q$ .

If  $Q$  is a piece of our decomposition, we let  $z_Q$  denote its center (for squares) or the center of the larger square (for arches). Similarly, we let  $c_Q$  denote its center if  $Q$  is a Whitney type square; the center of its base if  $Q$  is a Carleson square; and the center of the base of the smaller square if  $Q$  is a Carleson arch and the associated point of  $S$  for degenerate arches. See Figures 34 and 38.

Given a disk  $D = D(x, s)$  and a number  $r > 0$  we let  $rD = D(x, rs)$ . Similarly, given an annulus  $A = \{s < |z - x| < t\}$  we let  $rA = \{s/r < |z - c_Q| < rt\}$ . With this notation we see that each piece  $Q$  of our decomposition contains a disk or half-annulus  $D_Q$  such that

$$D_Q \subset Q \setminus N_s(\partial Q) \subset N_s(Q) \subset \lambda_s D_Q,$$

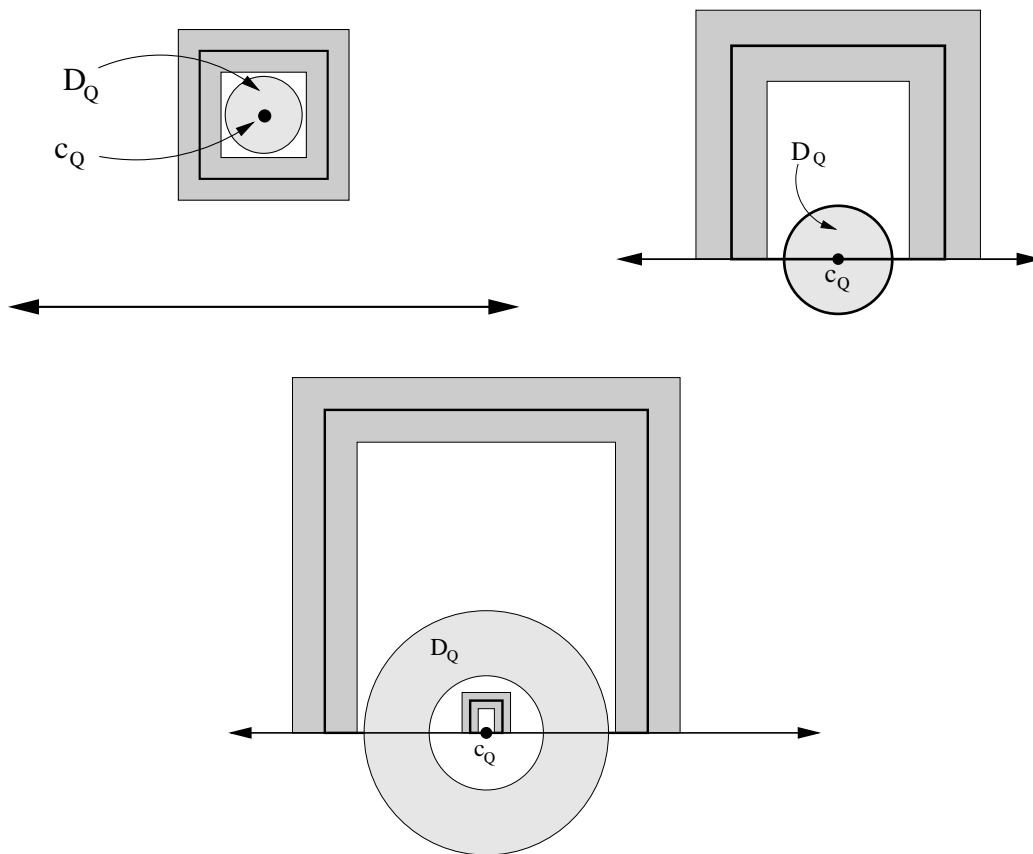


FIGURE 38. This shows the boundary neighborhoods (darker), centers and empty regions (lighter) for Whitney squares, Carleson squares and Carleson arches. For a degenerate arch these are the same as for the Carleson square. The picture of the arch is deceptive since the scales for the two boundary components should be much farther apart, and the empty region much “thicker”.

where a little arithmetic shows

$$(2) \quad \lambda_s = \frac{\sqrt{(1+s)^2 + (\frac{1}{2} + s)^2}}{\frac{1}{2} - s},$$

and where  $D_Q$  denotes a disk for square pieces and an annulus for arch pieces; we use the same letter in both cases to simplify notation. We call these the “empty regions” associated to each piece of the decomposition; “empty” because when we define quasiconformal mappings from  $\mathbb{H}$  to  $\Omega$ , the Beltrami dilatation  $\mu$  will be supported in  $N_s$ , which is disjoint from  $D_Q$ . Thus our maps will be conformal in the empty regions

and so will have power series or Laurent series expansions there. These series will be how we record our quasiconformal maps.

Given the decomposition  $\mathcal{W}$  we let  $\mathcal{B}$  (for “boundary”) be collection of  $O(n)$  closed squares with disjoint interiors that lie in  $N_s$  and whose union cover  $N_s$ . See Figure 39. Only a uniformly bounded number of squares are used for each boundary component and each such square is associated to a disk in the arch (and disjoint from the covered neighborhood of the boundary) whose triple covers the square. This disk is the “empty region” associated to the square.

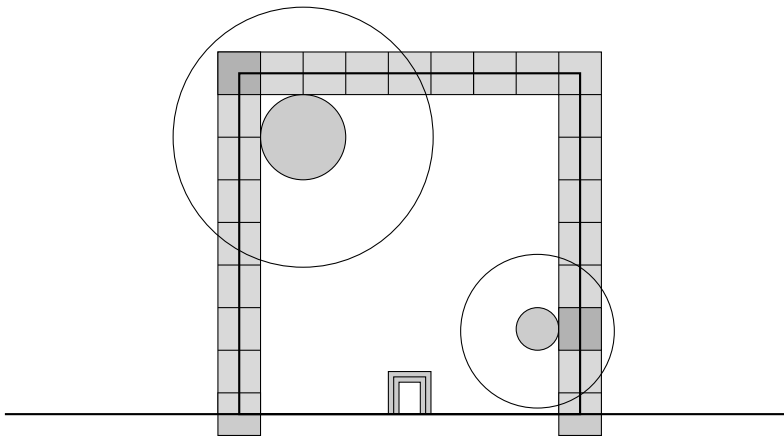


FIGURE 39. A neighborhood of an arch boundary can be covered by squares, and each square is associated to a disk inside the arch whose triple covers the square. These disks are the “empty regions” associated to the squares and will be used to define “partial representations” in Section 11.

## 11. $\epsilon$ -REPRESENTATIONS OF POLYGONAL DOMAINS

One problem in approximating a conformal map  $f : \mathbb{D} \rightarrow \Omega$  (or in the reverse direction) is to decide how to represent the function. One obvious approach would be to use a truncation of the power series of  $f$ ,  $f_n(z) = \sum_{k=0}^n a_k z^k$ , but this converges slowly (since  $f'$  is discontinuous at the prevertices) and the number of terms needed for a given accuracy depends on the geometry of the domain. We will use a representation using  $O(n)$  different series that avoids these problems.

Given a Carleson-Whitney decomposition  $\mathcal{W}$ , it is easy to see that there is a corresponding piecewise polynomial partition of unity  $\{\varphi_k\}$  whose gradients are supported

in  $N_s$ . More precisely, there is a collection of piecewise polynomial functions (uniformly bounded degree) such that

- (1)  $0 \leq \varphi_k \leq 1$ ,
- (2)  $\text{supp}(\varphi_k) \subset N_s(Q_k)$ ,
- (3)  $\sum_k \varphi_k(z) = 1$  for all  $z$ ,
- (4)  $\text{supp}(\nabla\varphi_k) \subset N_s(\partial Q_k)$ ,
- (5)  $|\nabla\varphi_k(z)| \leq C/(s \cdot \text{diam}(E))$  for  $z \in N_s(E)$ , when  $E$  is a component of  $\partial Q_k$ .
- (6)  $|\nabla^2\varphi_k(z)| \leq C/(s \cdot \text{diam}(E))^2$  for  $z \in N_s(E)$ , when  $E$  is a component of  $\partial Q_k$ .

To prove this, consider Figure 40. On the top it shows part of the decomposition and a covering of the boundary arcs by small shaded squares and trapezoids (which allow the squares to shrink as we approach the boundary). Outside these shaded regions our functions are constant; either 0 or 1. Within the shaded squares they interpolate between 0 and 1. There are only five types of regions, and we need only show how to build partition functions for each type.

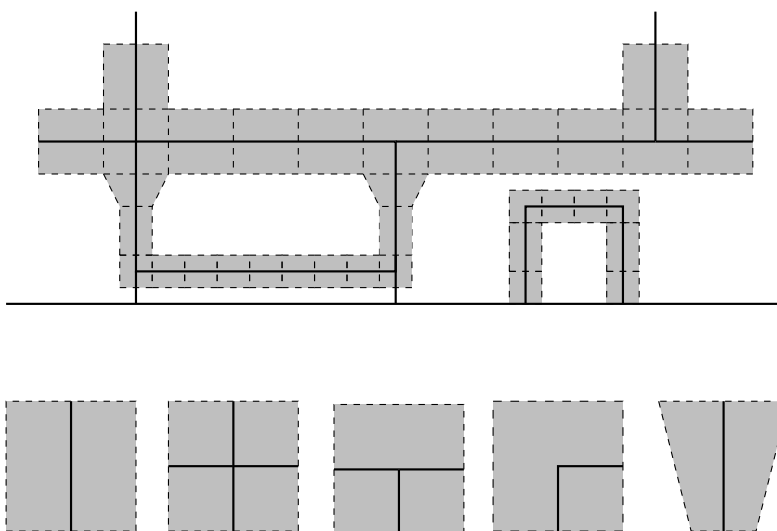


FIGURE 40. The partition of unity is non-constant only of these types of regions.

Let  $f(x) = (1 - x^2)$  and

$$g(x) = \int_{-1}^x f(t)dt / \int_{-1}^1 f(t)dt = \frac{1}{2} + \frac{3}{4}(x - \frac{1}{3}x^3).$$

Then  $g(-1) = 0, g(1) = 1$  and  $g' = 0$  at these two points (by starting with  $f(x) = (1 - x^2)^k$  we could get higher derivatives to also vanish, if needed). Let  $h(x) = g(x)$  if  $-1 \leq x \leq 1$ ,  $h(x) = 0$  for  $x < -1$  and  $h(x) = 1$  for  $x > 1$ . For the leftmost square on the bottom of Figure 40 we can take the functions  $\varphi(x, y) = h(2x)$  and  $1 - \varphi$  (if  $Q = [-1, 1]^2$ ; otherwise we apply a Euclidean similarity to make  $\varphi$  fit into  $Q$ ). These are illustrated in the top row of Figure 41. The next three squares in Figure 40 are handled by the functions

$$\begin{aligned} &h(2x)h(2y), (1 - h(2x))h(2y), (1 - h(2x))(1 - h(2y)), h(2x)(1 - h(2y)). \\ &h(2y), h(2x)(1 - h(2y)), (1 - h(2x))(1 - h(2y)) \\ &h(2x)(1 - h(2y)), 1 - h(2x)(1 - h(2y)), \end{aligned}$$

respectively. The trapezoid uses

$$h(2x \cdot (2 - h(2y))), 1 - h(2x \cdot (2 - h(2y))).$$

It is easy to check that these function have the desired properties.

Now suppose that for each piece  $Q_k \in \mathcal{W}$  of our decomposition we have a conformal map  $f_k$  defined on  $N_s(Q)$  (we think of this as a local approximation to the globally defined conformal map  $f$ ). This collection of functions is denoted  $\mathcal{F}$  and has the same index set,  $I$ , as  $\mathcal{W}$ . We say that  $\mathcal{F}$  represents  $\Omega$  if each point of  $S$  is mapped to the corresponding vertex of  $\partial\Omega$ , and each component (if there is more than one) of  $\partial Q_k \cap \mathbb{R}$  is mapped into the corresponding edge of  $\Omega$ . Such a  $\mathcal{F}$  is an  $\epsilon$ -representation if each  $f_k$  is 1-biLipschitz with respect to the hyperbolic metrics and whenever  $E_1$  and  $E_2$  are boundary components of pieces such that  $N_s(E_1)$  and  $N_s(E_2)$  overlap, then

$$(3) \quad |f_1(z) - f_2(z)| \leq \epsilon \cdot \text{diam}(f_1(E_1)), \quad z \in N_s(E_1) \cap N_s(E_2).$$

We define the norm of our collection,  $\|\mathcal{F}\|$  to be the smallest  $\epsilon$  for which (3) holds for every pair of adjacent elements of  $\mathcal{W}$ .

If  $E$  is a boundary component of piece  $Q_k$ , define

$$\partial F(E) = \frac{\text{diam}(f_k(E))}{\text{diam}(E)}.$$

If  $Q_k$  is a Whitney square then  $f_k$  is conformal on a neighborhood of  $Q_k$ . For other pieces, we can apply Schwarz reflection to see  $f_k$  can be extended to be conformal on a neighborhood  $N_s(E)$  for a uniform  $s$ . So by Koebe's distortion theorem,  $|f'|$

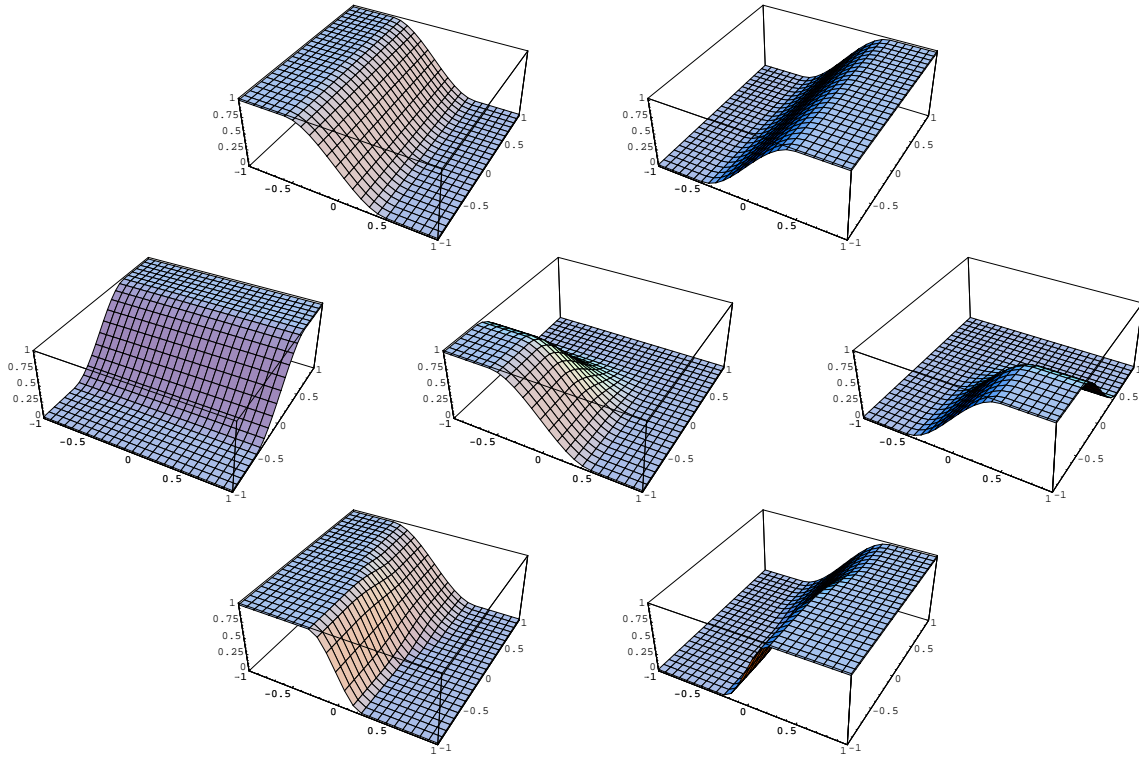


FIGURE 41. Some of the functions used in our piecewise polynomial partition of unity. The three rows correspond to the leftmost, center and rightmost regions at the bottom of Figure 40.

is comparable at any two points of  $E$  with uniform bounds. Thus given boundary components  $E_1, E_2$  of two adjacent pieces, the following are all comparable to each other and any of them could be used in (3):

$$\partial F(E_1)\text{diam}(E_1), \quad |\partial f_1(z)|\text{diam}(E_1), \quad |\partial f_2(z)|\text{diam}(E_2), \quad z \in E_1 \cup E_2.$$

It will be convenient to express (3) in a way that suppresses the  $\text{diam}(f_1(E_1))$  term. Roughly, (3) says that adjacent functions are close to agreeing in the hyperbolic metric of the image domain. This is precisely true for Whitney boxes where  $d\rho_\Omega \sim ds/\text{dist}(z, \partial\Omega) \sim ds/\text{diam}(f_1(E_1))$ , but not for boundary pieces. We can make it true for all pieces by replacing the hyperbolic metric  $\rho_\Omega$  by a related metric  $\tilde{\rho}_\Omega$ . Suppose we have a finite set  $S \subset \mathbb{T}$  that divides the circle into disjoint arcs  $\{I_j\}$ . For each arc, take the disk  $D_j$  (or possibly a half-plane or disk complement) that intersects  $\mathbb{D}$  along this arc and is orthogonal to  $\mathbb{T}$ . Take the union of these disks



and  $\mathbb{D}$ . The result is a simply connected domain  $\Omega_S$  that contains  $\mathbb{D}$  and so that  $S \subset \partial\Omega_S$ . Let  $\tilde{\rho}_S$  be the hyperbolic metric on  $\Omega_S$ . If  $f : \mathbb{D} \rightarrow \Omega$  is a conformal map to a polygonal domain and  $S$  is the set of conformal prevertices, define  $\tilde{\rho}_\Omega$  on  $\Omega$  by pushing  $\tilde{\rho}_S$  forward by  $f$ . Clearly for a boundary component of a decomposition piece in  $\mathbb{D}$ ,  $\text{diam}(E) \sim \text{dist}(E, \partial\Omega_S)$ , which means  $d\tilde{\rho}_S \sim ds/\text{diam}(E)$  on  $E$ . Therefore by Koebe's distortion theorem, (3) is equivalent to

$$(4) \quad \tilde{\rho}_\Omega(f_1(z), f_2(z)) = O(\epsilon) \text{ for all } z \in N_s(E).$$

This is a little cleaner looking than (3) and also is more clearly conformally invariant: if  $g : \Omega_1 \rightarrow \Omega_2$  is a conformal map of a polygonal domain to a circular arc domain that maps edges into edges then

$$\tilde{\rho}_{\Omega_1}(z, w) = \tilde{\rho}_{\Omega_2}(g(z), g(w)).$$

In particular, this works for the conformal map to the disk. This will allow us to estimate (4) assuming we have maps into the unit disk; this will be convenient in certain proofs, while the more concrete version (3) is more appropriate for certain explicit calculations. We could also have used the hyperbolic metric on the plane punctured at the points of  $E$ ; away from these points this is approximately the same size as  $\tilde{\rho}$ , but near each point the asymptotics are different (but we never use the metric there, so either choice would be fine).

Occasionally we will want to measure the distance between a collection  $\mathcal{F}$  and a single function  $f$  defined on  $\mathbb{H}$ . We write

$$\tilde{\rho}_\Omega(f, \mathcal{F}) = \sup_j \sup_{z \in Q_j} \tilde{\rho}_\Omega(f(z), f_j(z)).$$

Given a collection of functions satisfying (3), define

$$(5) \quad F = \sum_{k \in I} f_k \varphi_k,$$

Note that whenever we take a non-trivial combination of  $f_k$ 's along the boundary, the values must lie on the same edge of  $\partial\Omega$ . Thus any convex combination also lies on this edge, and hence  $F$  maps  $\mathbb{R}$  to  $\partial\Omega$ . If we try to define representations of domains with curved boundaries, we lose this property (but we shall see how to deal with this in Section 13).

**Lemma 20.**  *$F$  is quasiconformal with constant  $1 + O(\|\mathcal{F}\|)$ , if  $\|\mathcal{F}\|$  is small enough.*

*Proof.* First note that  $F$  is a continuous mapping of  $\mathbb{H}$  into  $\Omega$  and that it maps  $\mathbb{R}$  onto  $\partial\Omega$ . If two functions  $f_1, f_2$  are close in the sense of (3), then the Cauchy estimates imply their derivatives are also close in the sense

$$(6) \quad |\partial f_1(z) - \partial f_2(z)| \leq C\epsilon |\partial F(E_j)|$$

for  $j = 1$  or  $2$ . Note that (all sums are over  $k \in I$ , the index set of  $\mathcal{W}$ ),

$$\partial F = \sum_k (\partial f_k \cdot \varphi_k + f_k \cdot \partial \varphi_k),$$

$$\bar{\partial} F = \sum_k f_k \cdot \bar{\partial} \varphi_k,$$

because  $\bar{\partial} f_k = 0$ . Since only a bounded number of terms of our partition of unity are non-zero at any point we have

$$(7) \quad \sum_k |\nabla \varphi_k(z)| \leq \frac{C}{\text{diam}(E)}, \quad z \in N_s(E).$$

Also, since the  $\sum_k \varphi_k \equiv 1$  we know  $\sum_k \partial \varphi_k = \sum_k \bar{\partial} \varphi_k = 0$ . Note that if  $\sum_k a_k = 0$  and  $|b_k - b| \leq \epsilon$ , then

$$(8) \quad \left| \sum_k a_k b_k \right| = \left| \sum_k a_k (b_k - b) \right| \leq \epsilon \sum_k |a_k|.$$

Hence by (3), (7) and (8),

$$|\bar{\partial} F| \leq \frac{C\epsilon \cdot \text{diam}(f(E))}{\text{diam}(E)} \leq C\epsilon |\partial f(E)|.$$

Because  $\sum \varphi_k \equiv 1$ ,

$$\partial F = \partial f + \sum_k ((f_k)_z - \partial f) \varphi_k + f_k \cdot (\varphi_k)_z = \partial f + I + II.$$

Thus  $|\partial F - \partial f| \leq I + II$  and we can estimate these terms as

$$I \leq \sum_k \frac{|f_k(z) - f(z)| |\partial F(E)|}{\text{diam}(E)} \leq C\epsilon |\partial f(E)|,$$

$$II \leq \frac{C\epsilon |\text{diam} f(E)|}{\text{diam}(E)} \leq C\epsilon |\partial F(E)|.$$

Thus,

$$\begin{aligned}
|\mu_F(z)| = \left| \frac{\bar{\partial}F}{\partial F}(z) \right| &\leq \left| \frac{\sum f_j(z) \bar{\partial} \varphi_j(z)}{\sum \partial f_j(z) \cdot \varphi_j(z) + f_j(z) \cdot \partial \varphi_j(z)} \right| \\
&\leq \frac{C\epsilon |\partial F(E)|}{|\partial F(E)| - C\epsilon |\partial F(E)|} \\
&\leq C\epsilon.
\end{aligned}$$

In particular, if  $\|\mathcal{F}\| \leq \epsilon$ , then  $F$  is a  $(1 + C\epsilon)$ -quasiconformal map of  $\mathbb{H}$  to  $\Omega$ .  $\square$

Next we define a collection  $\mathcal{E}$  of elementary mapping functions. All of these can be considered as conformal maps of the upper half-plane to regions bounded by at most three straight edges (segments, rays or lines) with at most one bounded segment used. As special cases we take the functions  $f(z) = az + b$  (one boundary line),  $f(z) = az^\alpha + b$  (two boundary rays) and  $f(z) = a \log z + b$  (two parallel boundary lines). When there are three sides there must be two rays and a finite segment and such a map is given by the Schwarz-Christoffel formula; it is elementary in the sense that there is no parameter problem to solve; when there are three sides we can take  $\infty$  to map to itself and  $\pm 1$  to map to the finite vertices. See Appendix A

Suppose  $f : \mathbb{H} \rightarrow \Omega$  is conformal and  $S$  consists of the preimages of the vertices of  $P = \partial\Omega$ . The main observation we need to make is that on each piece of our Carleson-Whitney decomposition  $Q_k$  we can write  $f = f_k \circ g_k$  where  $f_k \in \mathcal{E}$  and  $g_k$  is conformal on  $MQ_k$  for Whitney squares and on  $M(Q_k \cup Q_k^*)$  ( $Q^*$  is the reflection of  $Q$  across  $\mathbb{R}$ ) for other pieces, and hence  $g_k$  has a uniformly convergent power or Laurent series on  $D_k$ . In the case of Whitney type squares or Carleson squares with no vertex, this is clear and we can take  $f_k$  to be the identity. For degenerate arches this is also clear with  $f_k$  being a power function, for if the vertex  $v$  has interior angle  $\alpha$  then  $f(z)^{\pi/\alpha}$  can be extended conformally by Schwarz reflection.

The other elements of  $\mathcal{E}$  are only needed for arches. In this case the two components of  $\partial MQ \cap \mathbb{R}$  map to line segments, and we can choose  $h \in \mathcal{E}$  so that  $h^{-1} \circ f$  will map both these to disjoint line segments into  $\mathbb{R}$ . Hence  $h^{-1} \circ f$  will have a conformal extension to  $MQ \cup MQ^*$ .

One of the main difficulties with extending our methods to non-polygons is to define the analogous class of maps  $\mathcal{E}$ . We shall see in Section 13 how to do this for some circular arc polygons, but even in this case problems arise if we need to map two

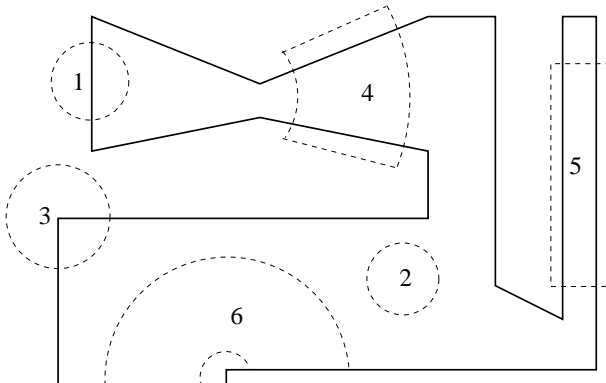


FIGURE 42. This shows parts of a polygon that correspond to using different elements of  $\mathcal{E}$ . In regions 1 and 2 we would use the identity, in regions 3 and 4 a power function, a logarithm in region 5 and a 3-sided Schwarz-Christoffel map in region 6.

circular arcs into a line simultaneously, so arches can't be used in general. For more general curved boundaries, it may be difficult even to define maps at the vertices.

Let  $g_{k,p} = \sum_{j=-p}^p a_n(z - z_k)^j$  be the truncation of the power or Laurent series for  $g_k$  around the point  $z_k = z_{Q_k}$ . Then since  $g_k$  is conformal on  $10Q_k$ , we have

$$|g_k(z) - g_{k,p}(z)| \leq C \text{diam}(g_k(E)) \lambda^p,$$

for a boundary component  $E$  of  $Q_k$  and for  $z \in N_s(E)$  and some fixed  $\lambda < 1$ . Thus

$$|f(z) - f_k(g_{k,p}(z))| \leq C \text{diam}(f(E)) \lambda^p,$$

for  $z \in N_s(E)$  and some fixed  $\lambda < 1$ . We can formalize this a bit with some notation.

An  $\epsilon$ -representation of  $\Omega$  is a triple  $(S, \mathcal{W}, \mathcal{F})$  consisting of:

- (1) An ordered set  $S \subset \mathbb{R}$  of  $n$  points,
- (2) A Carleson-Whitney decomposition  $\mathcal{W}$  of  $\mathbb{H}$  with  $O(n)$  pieces that extends a covering of the hyperbolic convex hull of  $S$ , together with the adjacency structure of the pieces and with a piecewise polynomial partition of unity  $\{\varphi_k\}$  as described above,
- (3) A collection of functions  $\mathcal{F}$  of norm  $\epsilon$ , and each function has the form  $f_k(z) = h_k(g_k(z))$  where  $g_k$  consists of  $p = O(|\log \epsilon|)$  terms of a power series (for the square pieces) or Laurent series (for the arches) and  $h_k \in \mathcal{E}$ ,

It may be a good idea to use Laurent series to implement the algorithm, but we would like to avoid the use of Laurent series in the proof in order to make use of known

results about fast manipulations of power series, without having to extend them to allow negative powers. It turns out that our iteration to improve representations only needs the series expansions near the boundary of our decomposition regions and we can always convert a Laurent series to power series on a collection of disks that cover each boundary component. Therefore, we define a partial  $\epsilon$ -representation as a triple  $(S, \mathcal{B}, \mathcal{G})$  where  $\mathcal{B}$  is the covering of the boundary of the decomposition introduced at the end of Section 10 and  $\mathcal{G}$  consists of power series on the corresponding empty regions that satisfy (3). For Whitney or Carleson squares, this is the same as before, but for arches we have “thrown away” the representation in the middle of the arch, keeping power series representations that are valid only near the boundary of the arch.

Clearly a representation can be turned into a partial representation by restricting an element of  $\mathcal{F}$  to a disk and computing its power series there. Conversely, a partial representation can be converted back to a representation by using the power series near the boundary to compute integrals of the form  $\int f(z)z^k dz$  around the boundary of an arch and thus recover the coefficients of the Laurent series. Moreover, we shall see in Appendix B that these conversions can be done quickly.

Next, we deal with a technical point concerning  $\epsilon$ -approximations. Later we will want to take power series expansions that are good approximations to the desired conformal map on the empty disks of our decomposition and deduce that they are still good approximations on a larger disk that includes the entire piece.

More generally, suppose  $f$  is a conformal map defined on  $D(0, 2)$ . Suppose we know the power series of an analytic function  $h$ , defined on the smaller disk  $D(0, 1)$  so that  $|h - f| \leq \epsilon$  on the smaller disk. Can we use  $h$  to get an approximation to  $f$  on a larger disk, say  $D(0, r)$  for some  $1 < r < 2$ ? Note that  $h$  itself may not work. For example, if  $f(z) = z$  and  $h(z) = z + (\frac{8}{9}z)^{1000}$  then  $h$  is a good approximation for  $|z| < 1$  but not for  $|z| > 9/8$ . However, if we truncate the power series for  $h$  appropriately, then we obtain a uniformly good approximation for  $f$  on a uniformly larger disk. More precisely:

**Lemma 21.** *There is a  $C < \infty$  so that given  $0 < \beta < 1$  and  $1 < r = R^\beta < R < \infty$ , the following holds. Suppose  $D = \{z : |z| < t\}$  and suppose  $f(z) = \sum_{n=-\infty}^{\infty} a_n z^n$  is a conformal on  $2R \cdot D = \{z : |z| \leq 2Rt\}$ . Suppose also that  $h(z) = \sum_{n=0}^{\infty} b_n z^n$  is*

holomorphic on  $D$  and that  $|f - h| \leq \epsilon$  on  $D$ . Let  $g(z) = \sum_{n=0}^q b_n z^n$  be the truncated power series for  $h$  where  $q = \lfloor c \log \frac{1}{\epsilon} \rfloor$ ,  $c = 1/\log R$ . Then

$$|f(z) - g(z)| \leq \frac{C\epsilon^{1-\beta}}{1 - R^{\beta-1}} |f'(0)|,$$

for all  $z \in rD$ .

*Proof.* Without loss of generality we assume  $t = 1$ . Also, normalize  $f$  so that  $a_0 = 0$  and  $|a_1| = 1$ . Because  $f$  is conformal on  $2RD$ , this implies  $f(RD)$  has uniformly bounded diameter (Koebe distortion theorem, Appendix A). Thus  $|a_n| \leq CR^{-n}$ ,  $n \geq 0$  since the usual formula

$$a_n = \frac{1}{2\pi i} \int_{|z|=R} \frac{f(w)dw}{w^{n+1}},$$

bounds the coefficients in terms of the maximum of  $|f|$ . Also, if  $\|f - g\|_\infty < \epsilon$  for  $z \in D$ , then  $|a_n - b_n| \leq C\epsilon$  for  $n \geq 0$ . The rest of the proof is a simple exercise summing series, i.e., for  $1 < |z| \leq r$ ,

$$\begin{aligned} |f(z) - \sum_{k=0}^q b_k z^k| &\leq \left| \sum_{|k|>q+1} a_k z^k \right| + \sum_{|k|\leq q} |a_k - b_k| |z|^k \\ &\leq C \sum_{k=q+1}^{\infty} \left(\frac{r}{R}\right)^k + C\epsilon \sum_{k=0}^q r^k \\ &\leq \frac{C}{1 - (r/R)} \left(\frac{r}{R}\right)^q + C\epsilon r^q \\ &\leq \frac{C}{1 - R^{\beta-1}} \left(\frac{r}{R}\right)^{c|\log \epsilon|} + C\epsilon r^{c|\log \epsilon|} \\ &\leq C\epsilon^{c \log \frac{R}{r}} + C\epsilon^{1-c \log r}. \end{aligned}$$

Taking  $c = 1/\log R$  and  $\beta = \log r/\log R$ , the last line becomes  $O(\epsilon^{1-\beta})$ , as desired.  $\square$

## 12. THE THICK/THIN DECOMPOSITION OF A POLYGON

Suppose  $\Omega$  is simply connected domain with  $n$  specified boundary points  $V$ , let  $f$  be a conformal map of  $\mathbb{H}$  onto  $\Omega$  and let  $S = f^{-1}(V)$ . Construct the covering of the hyperbolic convex hull of  $S$  as in Section 9. If no  $\epsilon$ -Carleson arches are needed to cover  $C(S)$  then we say  $(\Omega, V)$  is  $\epsilon$ -thick (or just “thick”, if  $\epsilon$  is understood from

context). If  $\Omega$  has a polygonal boundary we let  $V$  be the vertices and this defines a “thick polygon”.

A more geometric way to think of thick polygons uses extremal distance. Suppose  $e_1, e_2$  are non-adjacent edges of  $\Omega$ . We say the pair of edges is  $\epsilon$ -thin in  $\Omega$  if the extremal distance between them is  $\leq \epsilon$ , i.e., if the modulus of the path family connecting these edges inside  $\Omega$  is  $\geq \frac{\pi}{\epsilon}$ . By our remarks in Section Lemma 9, such a pair corresponds to an  $\delta$ -Carleson arch with  $\delta \sim \epsilon$ . Indeed, thin pairs of non-adjacent sides are in 1-1 correspondence with Carleson arches (except for the possibility that one side has unbounded preimage under  $f$ , and gives two arches in the decomposition of  $\mathbb{H}$ ). Thus if a polygonal domain is  $\delta$ -thick in the sense of the previous paragraph, then every non-adjacent pair of edges is  $\epsilon$ -thick for some  $\epsilon \simeq \delta$ , and conversely. Some examples of thick and not thick polygons are given in Figures 43 and 44.

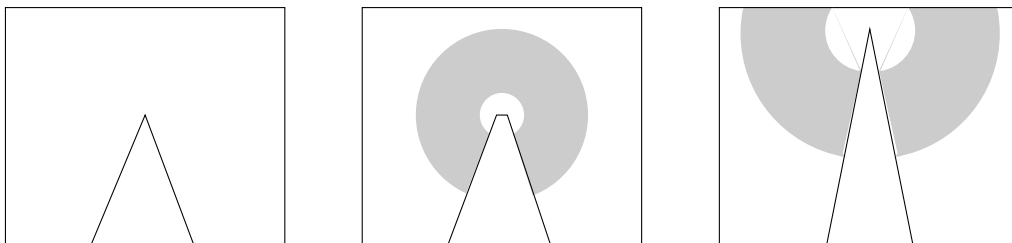


FIGURE 43. A thick polygon and two non-thick variations. The shaded areas join non-adjacent edges with small extremal distance and correspond to Carleson arches.

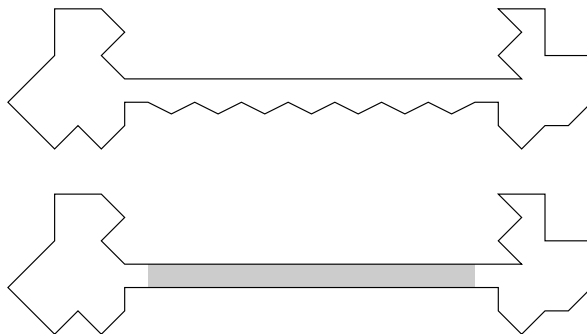


FIGURE 44. The polygon on top is thick, but not the one on the bottom.

We can always add more vertices to the boundary to make a polygon thick, although there is no bound on how many we might have to add. Also note that adding

vertices can convert a thick polygon to a non-thick one, i.e., add two vertices  $\epsilon$  apart to the middle of an edge of length 1.

Another way to approach thick and thin parts is to consider the Riemann surface obtained by reflecting the dome of  $\Omega$  across  $\mathbb{R}^2$  and removing the vertices of  $\partial\Omega$ . This is a punctured Riemann surface (isometric to the unit sphere with the  $\iota$ -preimages removed) and the thin parts of  $\Omega$  correspond to the thin parts of this surface, and the polygon is thick if this surface has no hyperbolic thin parts. We will not pursue this connection between polygons and surfaces further here, but it may prove interesting (e.g., what does Mumford's compactness theorem for surfaces say about polygons?).

**Lemma 22.** *If  $(\Omega, V)$  is  $\epsilon$ -thick then any  $K$ -quasiconformal image is  $\epsilon/K$ -thick.*

*Proof.* Obvious since conformal modulus can be changed by at most a factor of  $K$ .  $\square$

Because of this lemma, we can deduce that a polygon is  $\epsilon$ -thick by computing the  $\iota$  preimages of the vertices and making sure there are no  $\epsilon/K$ -arches in its covering, where  $K$  is the universal quasiconformal bound on the extension of the  $\iota$  map to the interior. Thus in time  $O(n)$  we can determine (up to a bounded factor of  $K$ ) the degree of thickness of a polygon.

It will also be convenient to define a class of polygons called “thin”. A thin polygon has two special edges that we call the “long edges”, and which may be either adjacent or non-adjacent. In the first case, (which we call parabolic) assume both long edges start at 0 and end at points  $\{a, b\} \in A_R = \{z : R \leq |z| \leq 2R\}$ . We assume the other edges of the polygon all lie in  $A_R$ , have lengths comparable to  $|a - b|$  and interior angles bounded away from 0 and  $2\pi$ .

In the second case (which we call hyperbolic), the long edges start at points  $a, b$  in  $A_1 = \{z : 1 \leq |z| \leq 2\}$  and end at points  $c, d$  in  $A_R = \{z : R \leq |z| \leq 2R\}$ ,  $R \geq 4$ . The remaining sides of a thin polygon all lie in either  $A_1$  or  $A_R$ , have length comparable to  $|a - b|$  and  $|c - d|$  respectively, and all interior angles are bounded away from 0 and  $2\pi$  (the exact bound is unimportant, but we can take  $\pi/6$  to be specific). We say a polygon is  $\epsilon$ -thin if there is a Euclidean similarity to shape as described and if the extremal length between the two long sides in the polygon is less than  $\epsilon$  and there is no other pair of non-adjacent sides that are  $\frac{1}{100}$ -thin (again, the



exact constant is unimportant). Although the description is a bit wordy, a picture makes it much clearer, see Figure 45.

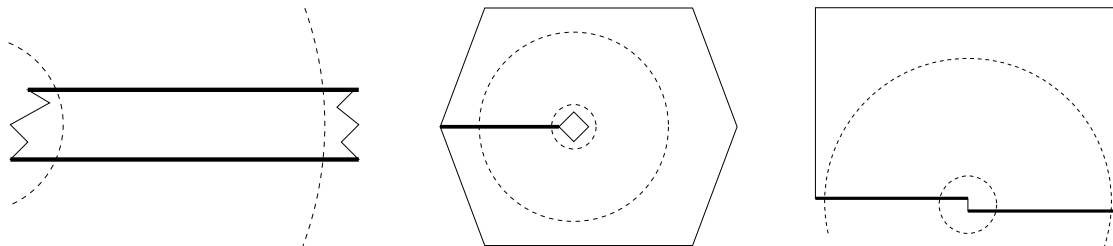


FIGURE 45. Examples of hyperbolic thin polygons. The long sides are emphasized and the dashed circles show outer boundary of  $A_1$  and the inner boundary of  $A_R$ .

The names of the two cases correspond to the thin parts that occur in Riemann surfaces. An  $\epsilon$ -thin parts of a hyperbolic manifold are the connected components of the set where the injectivity radius of the surface is  $< \epsilon$ . In the surface case, parabolic thin parts (also called “cusps”) are non-compact and have a single (finite) boundary component, whereas hyperbolic thin parts are compact and have two boundary components.

**Lemma 23.** *There is an  $\epsilon_0 > 0$  and  $0 < C < \infty$  so that if  $\epsilon < \epsilon_0$  then the following holds. Given a simply connected, polygonal domain  $\Omega$  we can write  $\Omega$  is a union of subdomains  $\{\Omega_j\}$  belonging to two families  $\mathcal{N}$  and  $\mathcal{K}$ . The elements of  $\mathcal{N}$  are  $O(\epsilon)$ -thin polygons and the elements of  $\mathcal{K}$  are  $\epsilon$ -thick. The number of edges in all the pieces put together is  $O(n)$  and all the pieces can be computed in time  $O(n)$  (constant depends on  $\epsilon$ ). We can either choose the pieces to be disjoint except for common boundaries, or given  $\epsilon_0 > \delta > 4\epsilon$ , we can choose them so that pieces of each type only intersect pieces of the other type and that the intersection is a  $\delta$ -thin polygon.*

*Proof.* All we have to do is choose polygons that approximate the images of the regions in  $\mathcal{N}$  and  $\mathcal{K}$  associated to the Carleson-Whitney decomposition in Section 10 (see the discussion preceding Lemma 17). Suppose  $E$  is a boundary component of a Carleson arch. Then the Euclidean distance of  $E$  to the nearest prevertex point is at least  $\frac{1}{2}\text{diam}(E)$  and hence we can use Schwarz reflection to show that  $f$  extends to be conformal in a ball of radius  $\frac{1}{2}\text{diam}(E)$  around every point of  $E$ . Then the Koebe distortion theorem implies there is a  $P < \infty$  so that if we take  $P$  equally spaced

points along  $E$  (including its endpoints on  $\mathbb{R}$ ) and connect the  $f$  images of these by line segments, the resulting polygonal curve is simple and hence divides  $\Omega$  into two polygonal subdomains.

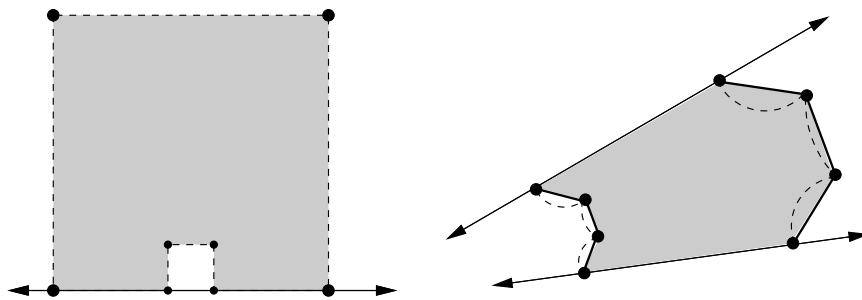


FIGURE 46. The intersection of a thin and thick piece is approximately the image of a Carleson arch whose width may be chosen.

When we do this for every domain in  $\mathcal{N}$  and  $\mathcal{K}$  we get the desired decomposition with the desired overlaps (if the parameter  $A$  is chosen correctly). The thin pieces have at most  $2P$  edges. To check that the thick pieces are really thick, we have to show that no two non-adjacent edges have modulus in the piece less than  $1/\epsilon$ . If both edges were new ones introduced (e.g., subarcs of a crosscut or a subarc of an original edge created by an endpoint of a crosscut) then this is clear from construction. A similar proof works if one edge is new and the other was an original edge. Finally, if both edges are original, then the modulus in the piece is smaller than it is in the whole polygon, and hence the pair is still thick, since it was thick before.  $\square$

The division of  $\Omega$  into thick and thin pieces is not unique, because parabolic thin pieces at the vertices either may or may not be included. However,  $\mathcal{N}$  must contain all the thin parts corresponding to all the Carleson arches in the decomposition corresponding to  $\Omega$ . It is easy to estimate the conformal map to thin polygons, at least if we stay near the long edges and away from the other edges.

**Lemma 24.** *Suppose  $R$  is the rectangle  $[0, L] \times [0, 1]$  and  $\Omega$  is a simply connected domain containing  $R$  that is formed by replacing the two vertical sides of  $R$  by curves. Let  $f : R \rightarrow \Omega$  be the conformal map such that  $f(c) = c$  and  $f'(c) > 0$ , where  $c = \frac{L}{2} + i\frac{1}{2}$  denotes the center of  $R$ . Then  $|f(z) - z| \leq O(e^{-L/2\pi})$  for  $|z - c| < 2$ .*

*Proof.* Suppose  $g : \mathbb{D} \rightarrow R$  and  $h : \mathbb{D} \rightarrow \Omega$  are conformal, taking 0 to  $c$  with positive derivative at  $c$ . Then  $F = h^{-1} \circ g$  is a conformal map from the disk to  $W = h^{-1}(R)$  that fixes the origin and has positive derivative there. Since the extremal length of the path family connecting  $B(c, 2) \cap R$  to  $\partial\Omega \setminus \partial R$  in  $\Omega$  is  $\geq \frac{1}{2}L + O(1)$ , we get that  $\partial W \setminus \mathbb{T}$  has two components, each of Euclidean diameter  $\leq \delta$  where  $\delta = O(e^{-L/2\pi})$  by Lemma 43. See Figure 47. Thus  $|F(z)| \geq 1 - O(e^{-L/2})$ . So if  $\log \frac{F(z)}{z} = u(z) + iv(z)$ , then  $-\delta \leq u \leq 0$  on  $\mathbb{D}$  where  $\delta = O(\exp(-L/2))$ . By reflection  $u$  extends to be harmonic with  $|u| \leq \delta$  on  $\mathbb{R}^2 \setminus E$  where  $E = h^{-1}(\partial\Omega \setminus \partial R) \subset \mathbb{T}$  has two components. Thus

$$|\nabla v| = |\nabla u| = O(\delta/\text{dist}(z, E)),$$

which together with  $v(0) = 0$ , implies  $|u| + |v| = O(\delta)$  on  $\{z : \text{dist}(z, E) \geq \frac{1}{10}\}$ , which further implies  $|F(z) - z| = O(\delta)$  on the same set. Back on  $R$ , this means that  $|f(z) - z| = O(e^{-L/2\pi})$ , as desired.  $\square$

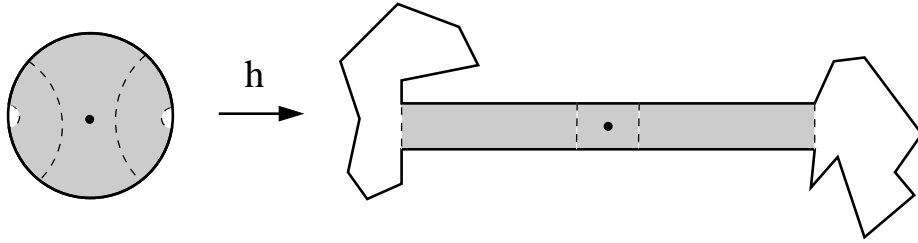


FIGURE 47. In the center of a thin polygon the conformal map is essentially independent of the region outside the center.

Given an  $\epsilon$ -thin polygonal domain  $\Omega$  with long edges connecting  $A_1$  and  $A_R$  as above, let  $\Omega' = \Omega \cap \{z : |z| < R\}$  if  $\Omega$  is parabolic and  $\Omega' = \Omega \cap \{z : 1 < |z| < R\}$  if  $\Omega$  is hyperbolic. We denote the “center” of  $\Omega$  as those points  $z$  so that the extremal distance of  $E_z = \{w \in \Omega : |w| = |z|\}$  to both  $A_1 \cap \partial\Omega$  and  $A_R \cap \partial\Omega$  is greater than  $\epsilon/2 + O(1)$  (in the hyperbolic case) or to just  $A_1 \cap \partial\Omega$  (in the parabolic case). Lemma 24 says that in the center of  $\Omega$ , the conformal map from  $\mathbb{H}$  to  $\Omega$  is essentially independent of the part of the boundary outside  $\Omega'$ . In particular, we can choose an elementary mapping from  $\mathcal{E}$  (see Section 11) that agrees with the conformal mapping onto  $\Omega$  up to order  $O(e^{-2\pi/\epsilon})$  in the center of  $\Omega$ .

In Lemma 23 we saw how to break a polygon into thick and thin pieces. Next we observe that we can reconstruct a representation for the whole domain from representations of the thick pieces (since we know maps onto the thin pieces automatically).

**Lemma 25.** *Suppose we are given a decomposition of a  $n$ -gon into thick and thin pieces (of either parabolic or hyperbolic type) with  $\eta$ -thin overlaps and we are given a normalized  $\epsilon$ -representation of each thick piece. Then in time  $O(n)$  (constant depending only on  $\eta$  and  $\epsilon$ ) we can compute a  $\delta$ -representation of  $\Omega$  where  $\delta = O(\epsilon + e^{-c\eta})$  for some  $c > 0$ .*

*Proof.* Choose a thick part  $\Omega_0$  and think of it as the “root” of a tree where the thick pieces are the vertices and are adjacent iff they are connected by a thin part. In a representation, a thin part corresponds to an arch. This arch has two complementary components; a bounded one and an unbounded one. A normalized representation for each thick part is one where the root lies in the unbounded complementary components of its adjacent hyperbolic thin arches, and the other thick parts lie in the bounded complementary components of the hyperbolic thin part that connects each to its parent.

By choice, the overlap of a thick piece  $\Omega_0$  and a thin piece  $\Omega_1$  corresponds to an  $\eta$ -thin piece. Thus in the decomposition of  $\mathbb{H}$  for  $\Omega_0$ , we can find a collection of Whitney boxes and Carleson squares whose union is an  $\eta$ -Carleson arch. Similarly, if  $\Omega_1$  is  $\epsilon$ -thin we have a map of an  $\epsilon$ -arch to  $\Omega_1$ . Moreover, we can choose a  $\eta$ -subarch that maps to the same region. We can renormalize the  $\epsilon$ -arch by linear transformations so that the two  $\eta$ -arches agree. Then remove the part of the decomposition for  $\Omega_0$  that lies below the  $\eta$ -arch corresponding to  $\Omega_1$  and replace it by an  $\epsilon$ -arch and the representing function for  $\Omega_1$ . See Figure 48.

Now repeat this for the other thin parts adjacent to  $\Omega$ . If any of these thin parts is adjacent to a second thick part  $\Omega_2$ , then we renormalize the decomposition for  $\Omega_2$  and insert a copy of the renormalized decomposition for  $\Omega_2$  below the  $\epsilon$ -arch of  $\Omega_1$ . Continuing in this way, we eventually insert all the pieces and obtain a  $O(\epsilon + e^{-2\pi/\eta})$ -representation of the whole polygon.  $\square$

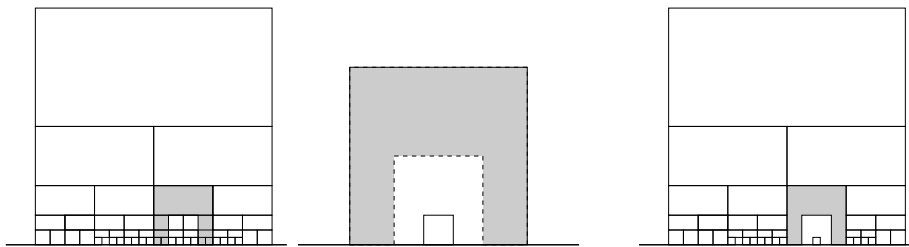


FIGURE 48. Combining a representation of a thick piece with an arch from a thin piece.

### 13. REPRESENTATIONS OF FINITELY BENT DOMAINS

One of the main ideas of the algorithm is to connect the given polygonal domain  $\Omega$  to the unit disk by a chain of intermediate domains  $\Omega_0 = \mathbb{D}, \Omega_1, \dots, \Omega_N = \Omega$  so that each is mapped to the next by an explicit quasiconformal map with small constant. For each domain  $\Omega_k$  we have to know how to improve a  $\epsilon$ -representation to any desired accuracy and we have to know how to take a representation for  $\Omega_k$  and create one for  $\Omega_{k+1}$ . The improvement step will be discussed in later sections; in this section we discuss the the creation of chain and passing representations from one step to the next.

The conformal maps onto the finitely bent elements on our chain are only computed to a fixed accuracy  $\epsilon_0$ ; just enough to allow us to compute the map onto the next element. Thus the precise timing of these steps is not crucial (as long as it is linear in  $n$  with a constant depending on  $\epsilon_0$ ). This gives us an  $\epsilon_0$ -representation of  $\Omega$  in time  $O(n)$ . The time dependence on  $\epsilon$  in Theorems 1 and 2 comes from only from iterating Lemma 31 for the domain  $\Omega$  in order to improve  $\epsilon_0$  to  $\epsilon$ .

If  $\Omega$  is finitely bent, we have seen how to create the chain with angle scaling. For a polygonal domain, we will approximate by a finitely bent domain and then use angle scaling on this. At this point we have a choice. One possibility is to replace the chain of finitely bent domains by a chain of inscribed polygons and describe how to pass representations of these polygons from one to the next. The other possibility is to deal directly with the finitely bent chain, but this requires extending the definition of  $\epsilon$ -representations to such domains (which causes some difficulties as was pointed out earlier). Both approaches involve a similar number of technicalities, but we will take

the second one since it seems cleaner and shows how our method can be adapted to certain domains with curved boundaries.

Suppose  $\Omega$  is a finitely bent domain with  $n$  vertices. As before, an  $\epsilon$  representation is a triple  $(S, \mathcal{W}, \mathcal{F})$  where  $S$  is a set of  $n$  points,  $\mathcal{W}$  is the Carleson-Whitney decomposition associated to  $S$  and  $\mathcal{F}$  consists of a power or Laurent series for each piece and a boundary map for each boundary piece. Each boundary map sends an interval on  $\mathbb{R}$  to an subarc of  $\partial\Omega$  and each is power function (possibly the identity) followed by a Möbius transformation. See Figure 49. These maps clearly suffice for Carleson squares and degenerate Carleson arches. However, for such maps to suffice for Carleson arches we have to make an assumption about  $\Omega$ : there is a  $\delta_0 > 0$ , so that whenever two sides of  $\partial\Omega$  have extremal distance  $< \delta_0$  in  $\Omega$ , the sides lie on intersecting circles. In this case, a power function, followed by a Möbius transformation can be used to map the base intervals of the arch into the sides of  $\Omega$ . We will call a finitely bent domain with this property simple. It is straight forward to check that this property is preserved by any angle scaling which decreases angles.

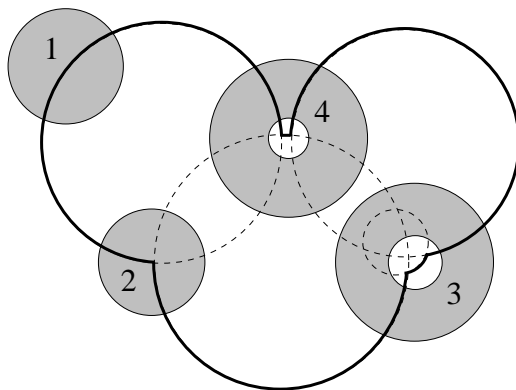


FIGURE 49. In region 1 we use a Möbius transform and in region 2 we can use a power function followed by a Möbius transformation. The same type of function works in the arch 3, since the corresponding circles intersect. However, arches of type 4 are not allowed since it is not clear how to explicitly map the boundary arcs into a single line by a conformal map.

Given an  $\epsilon$ -representation of a simple finitely bent domain, we can define a quasi-conformal map  $F$  from  $\mathbb{H}$  into  $\Omega$  using a partition of unity as in formula (5). However, this map is not onto  $\Omega$ . The problem is that when we take a convex combination of

two points on a circular arc, the result is not on the circle (unless the points coincide). However, if the circle has radius 1 and the points are only  $\epsilon$  apart, then it is clear that any convex combination is within  $O(\epsilon^2)$  of the boundary. We claim that the domain  $F(\mathbb{H}) \subset \Omega$  can be mapped to  $\Omega$  by a  $1 + O(\epsilon^2)$  quasiconformal map whose boundary values agree with radial projection on each arc of  $\partial\Omega$ . However, to prove this, it is not enough to know that the two boundaries are within  $O(\epsilon^2)$  of each other; we also need to know that the tangent directions agree to order  $O(\epsilon^2)$ .

Lemmas 47 and 48 in Appendix A give precise estimates bounding the quasiconformal “cost” of pushing the boundary in this way. We will use the latter to show that  $F(\mathbb{H})$  can be mapped to  $\Omega$  by a  $(1 + O(\epsilon^2))$ -quasiconformal map. After rescaling by linear maps, we may assume the base interval of the boundary piece is  $[0, 1]$  and the image arc lies on the unit circle. Suppose  $x \rightarrow (u, v)$  and  $x \rightarrow (a, b)$  are two maps sending  $[0, 1]$  to an arc of the unit circle with  $|u - a|, |v - b|, |u' - a'|, |v' - b'| = O(\epsilon)$  and suppose  $\varphi$  is a partition of unity. Write  $F = (\varphi)(u + iv) + (1 - \varphi)(a + ib)$  and  $g(z) = |F|^2 = F \cdot \bar{F} = |\varphi(u + iv) + (1 - \varphi)(a + ib)|^2$ . So to apply Lemma 48 to  $F$  it is enough to estimate the derivative of  $g$ . We begin by rewriting  $g$  as follows:

$$\begin{aligned}
g(x) &= (u\varphi + a(1 - \varphi))^2 + (v\varphi + b(1 - \varphi))^2 \\
&= ((u - a)\varphi + a)^2 + ((v - b)\varphi + b)^2 \\
&= a^2 + b^2 + 2(u - a)a\varphi + (u - a)^2\varphi^2 + 2(v - b)b\varphi + (v - b)^2\varphi^2 \\
&= 1 + 2(u - a)a\varphi + (u - a)^2\varphi^2 + 2(v - b)b\varphi + (v - b)^2\varphi^2 \\
&= 1 + 2(ua - a^2 + vb - b^2)\varphi + (u - a)^2\varphi^2 + (v - b)^2\varphi^2 \\
&= 1 + 2((u, v) \cdot (a, b) - 1)\varphi + (u - a)^2\varphi^2 + (v - b)^2\varphi^2 \\
&= 1 + 2(\cos \theta - 1)\varphi + (u - a)^2\varphi^2 + (v - b)^2\varphi^2,
\end{aligned}$$

where  $\theta$  is the angle between the vectors  $(u, v)$  and  $(a, b)$ , which by assumption is  $O(\epsilon)$ , as is its derivative  $\theta'$  (by the Cauchy estimates). If we differentiate  $g$ , the constant term drops out. The second term is bounded by

$$2 \sin \theta \cdot \theta' \varphi + O(\theta^2) \varphi' = O(\epsilon^2),$$

and the third term is bounded by

$$[(u - a)^2 \varphi^2]' = 2(u - a)(u' - a')\varphi^2 + (u - a)2\varphi\varphi',$$

and each term is  $O(\epsilon^2)$ . The same estimate holds for the last term. Thus the map  $F$  sends  $\mathbb{H}$  onto a small quasiconformal perturbation of  $\Omega$  (a subset, because of the convexity of disks). Later, in Lemma 31, when we solve the Beltrami equation using the dilatation of  $F$  as data, this data differs by  $O(\epsilon^2)$  from the dilatation of a quasiconformal map  $\tilde{F}$  that sends  $\mathbb{H}$  onto  $\Omega$ . However, the error given by that lemma is also  $O(\epsilon^2)$ , so using the dilatation of  $F$  in place of the dilatation of  $\tilde{F}$  gives an error which can be absorbed into this estimate.

Next we wish to approximate a thick polygonal domain  $\Omega$  with  $n$  sides by a finitely bent domain  $\Omega^{\text{fb}} \subset \Omega$  that has  $O(n)$  sides. We assume  $\Omega$  is thick for otherwise  $\Omega^{\text{fb}}$  may require  $\gg n$  disks; consider a  $1 \times r$  rectangle,  $r \gg 1$ . The problem is that the medial axis of this polygon has an edge-edge bisector that is very long in the hyperbolic metric. However, if we assume  $\Omega$  is  $\delta$ -thick, then there is an upper bound  $A$  on the hyperbolic length of any edge-edge bisector (and  $A \simeq \delta^{-1}$ ). This is the only property of thickness that we will use at present.

Fix some  $\eta > 0$ . We say  $\Omega^{\text{fb}}$  is an  $\eta$ -approximation to  $\Omega$  if it is the union of the medial axis disks corresponding to all the vertices of the medial axis and also corresponding to certain points chosen along the edges of the medial axis as follows:

**Case 1:** First suppose  $e$  is a point-point bisector. Then we simply choose the two endpoints of  $e$ . The union of the two corresponding maximal disks is the same as the union of all the maximal disks corresponding to  $e$ .

**Case 2a:** Next suppose  $e$  is an edge-edge bisector connecting two vertices of the medial axis in the interior of  $\Omega$ ). Then by the thickness assumption its hyperbolic length is  $\leq A$ . Thus given  $\eta$ , we can choose a collection of points on that edge that include the two endpoints and has the property that no point of the edge is more than hyperbolic distance  $\eta$  from some point of the collection. We call this being  $\eta$ -dense. Clearly we need at most  $1 + A/\eta$  points per edge. See left side of Figure 50.

**Case 2b:** Now suppose  $e$  is an edge-edge bisector with one endpoint a convex vertex of  $\Omega$ . Choose the segment of hyperbolic length  $A$  starting at the interior vertex and place points that are  $\eta$ -dense along it. Clearly we need at most  $1 + A/\eta$  points per edge. Note that the finite union of disks has one,  $D$ , closest to the corresponding convex vertex of  $\Omega$ . The arc  $\partial D \cap \Omega$  closest to the vertex will also be a boundary arc of  $\Omega^{\text{fb}}$ , and we will call it a “ending arc” of  $\Omega^{\text{fb}}$ . We place  $\eta^{-1}$  equally spaced vertices



along the arc to split it into smaller ending arcs. These have the property that the extremal distance to any non-adjacent arc is bounded away from zero (independent of  $\eta$ ), a property we will use later.

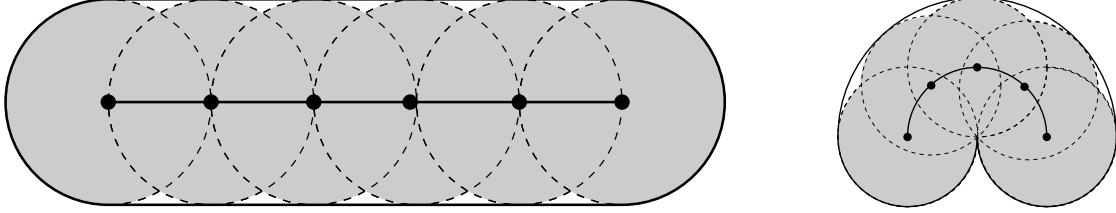


FIGURE 50. The finitely bent approximation for a edge-edge bisector and a point-edge bisector (the edge has been mapped to a circular arc).

**Case 3:** Finally suppose  $e$  is a point-edge bisector. Renormalizing by a Möbius transformation, assume the point is 0 and the edge is a subarc of the unit circle (such a transformation preserves the collection of medial axis disks, but does not preserve the medial axis itself since Euclidean centers of a circle need not be preserved by Möbius transformations). In this new region the medial axis is an arc of the circle of radius  $1/2$  and we take a collection of points that includes the endpoints, and so that the angular separation between points (when viewed from 0) is  $\leq \eta$ . Clearly at most  $1 + 2\pi/\eta$  suffice. Now map this collection of maximal disks back to the original domain to get a collection of disks centered on  $e$ . See the right side of Figure 50.

We have shown:

**Lemma 26.** *Suppose  $\Omega$  is a  $\delta$ -thick polygonal domain with  $n$  sides and  $\Omega^{\text{fb}}$  is an  $\eta$ -approximation of it. Then  $\Omega^{\text{fb}}$  has  $O(n/(\delta\eta))$  boundary arcs.*

Also note that by construction, each non-ending arc of  $\partial\Omega^{\text{fb}}$  is tangent to an edge of  $\partial\Omega$ , projects orthogonally onto a subsegment of that edge, and makes at most angle  $O(\eta)$  with lines parallel to that edge. Using Lemma 47 this means that there is a  $1 + O(\eta)$  quasiconformal map from  $\Omega^{\text{fb}}$  into a subdomain  $\Omega^{\text{rc}}$  ( $\text{rc}$  is for “rounded corners”) of  $\Omega$  bounded by the the ending edges of  $\Omega^{\text{fb}}$  and the projections onto  $\partial\Omega$  of the non-ending edges.

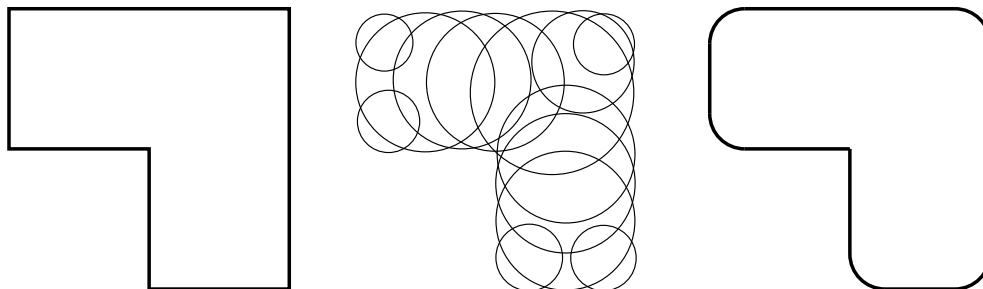


FIGURE 51. A polygon  $\Omega$ , a union of medial axis disks defining a finitely bent approximation  $\Omega^{\text{fb}}$  and the corresponding domain with rounded corners,  $\Omega^{\text{rc}}$ .

14. REALLY THICK AND ALMOST THICK PIECES

It would be very convenient if the finitely bent approximation of a thick polygon was also thick, for then the representation of  $\Omega^{\text{fb}}$  would not require any arches. This is not the case (see Figure 52), but there is a substitute that will be sufficient for our purposes. We shall show that if a polygon satisfies a stronger version of thickness, then its finitely bent approximation satisfies a weaker version of thickness. We make this precise with two new definitions.

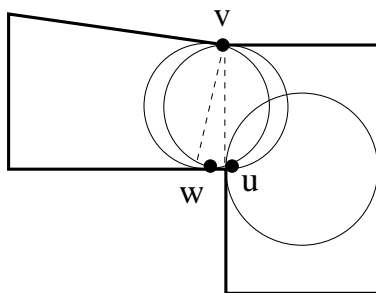


FIGURE 52. The polygon is clearly thick, but has interior angle  $\pi + \epsilon$  at the vertex  $v$ . This creates two medial axis vertices whose circles intersect at  $w$  which is only  $O(\epsilon)$  away from  $u$ , which must also be a vertex of the finitely bent approximation. Since  $\Omega^{\text{fb}}$  has  $O(1)$  sides and at least one side shorter than  $O(\epsilon)$ , it can't be  $\delta$ -thick if  $\epsilon \ll \delta$ .

Suppose  $e$  is an edge of a polygonal domain  $\Omega$ . We call a point  $x \in e \subset \partial\Omega$  “exposed” if there is a medial axis disk  $D$  with  $x \in \partial D$  and so that  $\partial D$  also contains a point of an edge that is not adjacent to  $e$ . See Figure 53. We say the edge  $e$  is exposed if it contains an exposed point in its interior. We will say that  $\Omega$  is “really

$\delta$ -thick" if it is  $\delta$ -thick and vertices with interior angle  $> \pi/2$  are never endpoints of exposed edges.

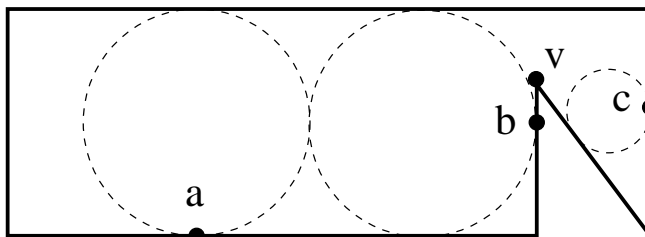


FIGURE 53. The points  $a, b$  are exposed but the point  $c$  is not (nor is the edge containing it). The polygon is thick, but not really thick, because the vertex  $v$  has large interior angle and bounds an exposed edge (the one containing  $b$ ).

Given a  $\delta$  thick polygonal domain  $\Omega$ , we can always modify it to be really  $\delta$ -thick by adding a bounded number of edges per vertex (thus  $O(n)$  overall). Compute the iota map, and the corresponding Carleson-Whitney decomposition. At each vertex with angle  $\theta > \pi/2$  compute the diameter,  $d$ , of the image of the corresponding degenerate arch, and let  $r = \beta d$ . The constant  $\beta$  is chosen small enough so that  $\Omega$  contains a sector of radius  $4r$  and angle  $\theta$ . On the other hand,  $\Omega$  does not contain a sector of angle  $\theta$  and radius  $> C(\beta)r$ , for this would violate the choice of the degenerate arch.

Draw circles of radius  $r, 2r$  around the vertex and replace the part of the edges adjacent to  $v$  inside the smaller circle by the polygonal arc as shown in Figure 54. The new arcs are chosen so that any medial axis disk that hits an interior point has radius  $< 2r$ , and hence does not hit a third edge of  $\partial\Omega$ . Thus all these new edges are unexposed. When we finish making this construction at every vertex, the resulting domain is really  $\delta$ -thick, for all the new edges are unexposed and none of the old adjacent pairs of edges have small extremal distance (if they were separated by a modified vertex).

In particular, given a  $\delta$ -thick polygonal domain  $\Omega$ , we can perform a thick/thin decomposition to remove a thin neighborhood of each vertex. Using the construction above we can arrange for the thick component (there is only one since  $\Omega$  is thick to being with) to be really thick. If we can construct an  $\epsilon$ -representation for this really thick domain, then we can use Lemma 25 to obtain a  $\delta$ -representation of  $\Omega$ . Thus it suffices to assume that  $\Omega$  is really thick.

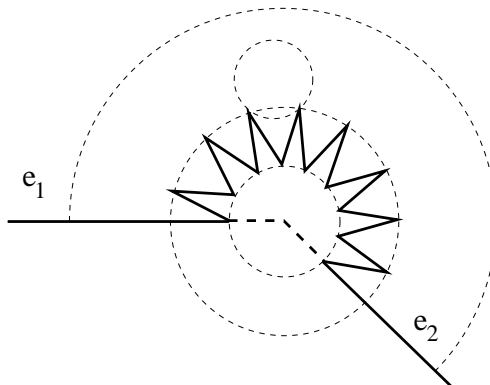


FIGURE 54. We replace the boundary of  $\partial\Omega$  by a polygonal arc near each concave vertex and at a scaled comparable to the largest sector in  $\Omega$  around this point. If the original domain is thick, then the new domain is really thick.

We say that a finitely bent approximation  $\Omega^{\text{fb}}$  of a polygonal domain  $\Omega$  is “almost  $\delta$ -thick” if whenever two non-adjacent arcs  $I_1, I_2$  have extremal distance  $\leq \delta$  in  $\Omega^{\text{fb}}$ , then these arcs are not ending arcs and they both project onto the same edge of  $\Omega$ . Thus any arch that occurs in a Carleson-Whitney decomposition corresponding to  $\Omega^{\text{fb}}$  has base intervals that map to arcs projecting onto the same edge of  $\Omega$ .

We defined the normalized separation between  $I_1$  and  $I_2$  as

$$\alpha = \text{dist}(I_1, I_2) / \min(\text{diam}(I_1), \text{diam}(I_2)).$$

Since both arcs are tangent to the same line and project orthogonally onto disjoint segments, its easy to see that the circles containing these arcs intersect at angle  $O(\alpha)$ . See Figure 55.

The main fact we will use concerns the conformal map  $f$  from  $D_1$  to  $D_1 \cup D_2$ .

**Lemma 27.** *Suppose  $D_1, D_2$  are disks of comparable size which intersect at angle  $\alpha$  and  $f : D_1 \rightarrow D_1 \cup D_2$  is conformal and chosen to fix the two intersection points,  $a, b$ , and and the point  $c \in \partial D_1 \setminus D_2$  on the bisector of  $a, b$ . Then  $|f(z) - z| = O(\alpha)\text{diam}(D_1)$  for every  $z \in D_1$ .*

*Proof.* This can be proven by an explicit calculation. Note that  $f = \tau^{-1}(\lambda\tau(z)^{1+\alpha})$  where  $\tau(z) = (a - z)/(z - b)$  and  $\lambda$  is an appropriately chosen constant of modulus 1 so that  $\tau(c) = i$ . See Figure 56. Suppose  $z \in D_1$ ,  $w = \tau(z)$  and  $x = |w|$ . If  $0 \leq x \leq 1$ , then  $x - x^{1+\alpha}$  attains its maximum at its critical points, i.e., at  $x = (1 + \alpha)^{1/\alpha}$  which

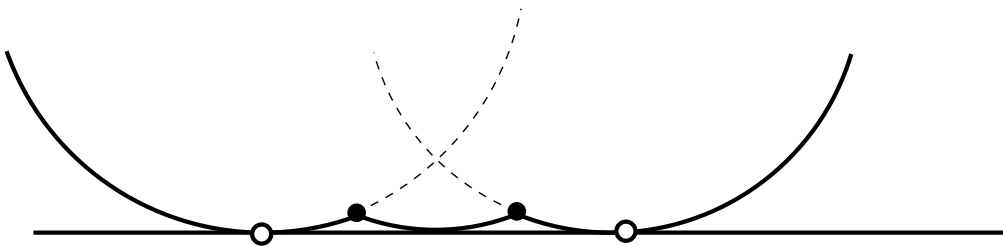


FIGURE 55. We have two circular arcs of diameter  $\geq 1$ , which are distance  $\alpha$  apart and both tangent to the same line. Moreover, the endpoints (shown black) are connected by a path of circular arcs of similar radius and tangent to the same line, which implies the distance from the line is  $O(\alpha^2)$ . Thus the tangent points of the arcs on the line (shown white) are only  $O(\alpha)$  apart and the corresponding circles intersect with angle  $O(\alpha)$ .

close to  $1/e$  for small  $\alpha$ . Thus the maximum is  $O(\alpha)$  which proves the estimate for such  $z$  (because  $\tau$  and  $\tau^{-1}$  have bounded derivative at such points). The case of  $x > 1$  is similar using  $1/\tau$ .  $\square$

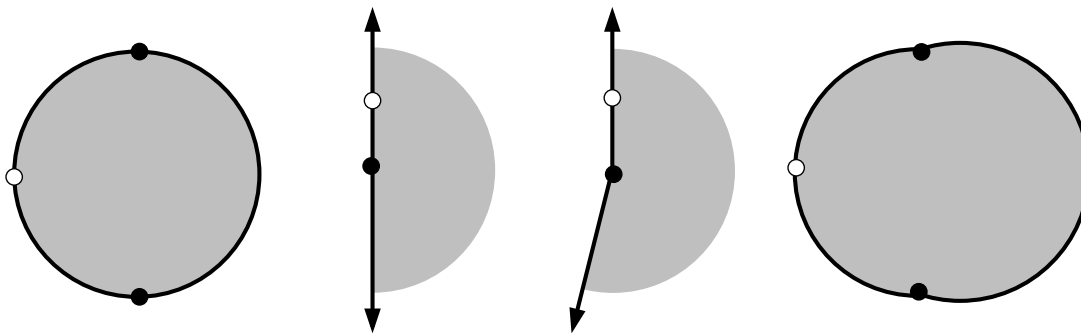


FIGURE 56. The disk  $D_1$  mapped by  $\tau$ ,  $z^{1+\alpha}$  and  $\tau^{-1}$ . The Möbius transformation  $\tau$  sends  $a, b, c$  to  $0, \infty, i$ .

**Lemma 28.** *If  $\delta$  and  $\eta$  are small enough the following holds. If  $\Omega$  is a really  $\delta$ -thick polygon, then the finitely bent  $\eta$ -approximation,  $\Omega^{\text{fb}}$ , is almost  $\delta/2$ -thick.*

*Proof.* Suppose we have two non-adjacent arcs,  $I_1, I_2$  in the boundary of  $\Omega^{\text{fb}}$ . By construction, the extremal distance of an ending arc to any non-adjacent arc is bounded away from zero (independent of  $\eta$ ). So we may assume neither of these is an ending

arc. Thus they are mapped to line segments  $J_1, J_2 \subset \partial\Omega$ , under the  $(1 + O(\eta))$ -quasiconformal map  $\Omega^{\text{fb}} \rightarrow \Omega^{\text{rc}}$  discussed above. Since  $K$ -quasiconformal maps change extremal length by a factor of at most  $K$ , the extremal distance between  $J_1$  and  $J_2$  is  $\geq (1 + O(\eta))(\delta/2) \leq \delta$  if  $\eta$  is small enough. Hence the extremal distance between the edges of  $\Omega$  containing them is also  $\leq \delta$ . Since  $\Omega$  is  $\delta$ -thick, the edges containing  $J_1$  and  $J_2$  must be the same or adjacent. If they are adjacent edges, then the common endpoint  $v$  must be  $\leq \pi/2$  by the really thick condition. But the arc  $I_1$  has a tangent point within distance  $\alpha \cdot \text{diam}(I_1)$  of the common vertex for a small  $\alpha$  (depending on  $\eta$ ), which means the circle containing  $I_1$  can't bound a disk in  $\Omega$  (it would hit the other edge hitting  $v$ ). This contradiction means  $I_1, I_2$  project onto the same edge of  $\partial\Omega$ , a.s desired.  $\square$

**Lemma 29.** *For any  $\epsilon > 0$  there is an  $N < \infty$  so that the following holds. Suppose  $\{\Omega_k\}_0^N$  is the angle scaling family constructed from an almost  $\delta$ -thick finitely bent domain  $\Omega^{\text{fb}} = \Omega_N$  and suppose  $0 \leq k < N$ . Then given an  $\epsilon$ -representation of  $\Omega_k$ , we can construct an  $2\epsilon$ -representation of  $\Omega_{k+1}$  in time  $O(n)$  (constant depends on  $\epsilon, N$ ).*

*Proof.* The representation of  $\Omega_{k+1}$  uses the same set  $S \subset \mathbb{R}$  and the same Carleson-Whitney decomposition  $\mathcal{W}$  as is given for  $\Omega_k$ ; only the functions will change by composing with a conformal map that sends the image from  $\Omega_k$  to  $\Omega_{k+1}$ . (This simplicity is why we have gone through the effort of defining almost thick domains; if we allowed more general arches, we would have to update  $S$  and  $\mathcal{W}$  as well.)

For each Whitney box  $Q$  let  $f$  be the map defined on  $Q$  and choose a gap  $G$  in the gap/crescent decomposition of  $\Omega_k$  which hits  $f(Q)$  (or so that an adjacent crescent hits  $f(Q)$ ). This gap is the image under Möbius transformation  $\sigma_k$ , of an ideal triangle in the complement of the bending lamination. The corresponding gap in  $\Omega_{k+1}$  is the image of the same triangle under a transformation  $\sigma_{k+1}$ . We modify the function  $f$  associated to  $Q$  by post composing by  $\sigma_{k+1} \circ \sigma_k^{-1}$ .

In the previous paragraph we claimed that for each box  $Q$  we could find a gap or crescent that intersects  $f(Q)$ . We should verify that we can do this for all  $O(n)$  boxes in time  $O(n)$ . This is not immediately clear since arbitrarily many gaps and crescents may hit a particular  $f(Q)$ , so there is not a constant amount of work to do per box. However, both the Whitney boxes and the gap/crescent decomposition come with tree structures. In time  $O(n)$  we can search both trees to find some box and some

gap/crescent that intersect. Treating these as roots of their respective trees, we can then search outwards finding the desired intersecting pieces and visiting each vertex of each tree only once (the process is analogous to merging two sorted lists in linear time). The details are given at the end of Appendix A following Lemma 51.

For each of the three kinds of boundary pieces,  $Q$ , we associate conformal maps  $\tau_k, \tau_{k+1}$  onto corresponding part of  $\Omega_k, \Omega_{k+1}$  and form the updated map by composing with  $\sigma_k = \tau_{k+1} \circ \tau_k^{-1}$ . We just have to specify the maps  $\tau_k$  for each type of piece.

If  $Q$  is a Carleson square, then it hits a boundary crescent and  $\tau_k$  is the associated Möbius transformation. For a degenerate arch, the base is an interval containing a point  $v$  of  $S$  which divides it into two subintervals whose images lie on intersecting circles. We take the map  $\tau_k$  to be the composition of a power function (determined by the angle of intersection of the circles) and Möbius transformation chosen send  $v, \infty$  to the two intersection points of the circles. For an arch  $Q$ , the base consists of two intervals which are mapped onto two arcs in boundary of the corresponding domain. By construction,  $\Omega^{\text{fb}}$  is almost thick, so these two arcs lie on circles which intersect at angle  $O(\eta)$  where  $\eta$  is the normalized separation between them. The map  $\tau_k$  is a Möbius transformation of the upper half-plane to  $D_1$ , followed by the conformal map given in Lemma 27.

To estimate the norm of the new collection, we use Lemma 11 (for Whitney boxes and Carleson squares), Lemma 10 (for degenerate arches) and Lemma 27 (for arches). Each result says that the maps  $\tau_{k+1} \circ \tau_k^{-1}$  are close to the angle scaling map  $\psi_k : \Omega_k \rightarrow \Omega_{k+1}$  which is a quasi-isometry with constants as close to 0 as we wish by taking  $N$  large. Thus for any point in overlapping neighborhoods of adjacent pieces  $Q_i, Q_j$

$$\begin{aligned} |f_i^{k+1}(z) - f_j^{k+1}(z)| &\leq |f_i^{k+1}(z) - \psi_k(f_i^k(z))| + |\psi_k(f_i^k(z)) - \psi_k(f_j^k(z))| \\ &\quad |\psi_k(f_j^k(z)) - f_j^{k+1}(z)|. \end{aligned}$$

The middle term is small if  $\mathcal{F} = \{f^k\}$  has small norm and  $\psi_k$  has quasi-isometry constant close to 0. The first and last terms are small since  $\sigma_j^k$  is close to  $\psi_k$ .  $\square$

**Lemma 30.** *Given an  $\epsilon$ -representation of  $\Omega^{\text{fb}}$  (the finitely bent  $\eta$ -approximation to a really thick polygonal domain  $\Omega$ ) we can construct an  $2\epsilon$ -representation of  $\Omega$  in time  $O(n)$ , assuming  $\eta$  is chosen small enough (depending on  $\epsilon$ , but not on  $n$  or the geometry of  $\Omega$ ).*

*Proof.* The proof is similar to the previous proof. As above, we leave the set  $S$  and the decomposition the same, and only change the maps. For Whitney boxes, we compose with the identity (i.e., use the same map). We do the same for boundary pieces corresponding to ending arcs. For Carleson squares corresponding to non ending arcs, we compose by the Möbius transformations that maps the boundary arc onto its orthogonal projection on  $\partial\Omega$  (with the tangent point going to itself). For degenerate arches we use the power function composed with Möbius transformation that sends the boundary arc into its orthogonal projection with the vertex going to its projection. For arches we use the conformal map of  $D_1 \cup D_2$  onto the half-plane bounded by the line containing the corresponding boundary edge. Since the diameter of the boundary pieces  $W$  are comparable to the lengths of the boundary arcs they hit, each type of maps moves points by less than  $O(\delta)\text{diam}(W)$ . Thus an  $\epsilon$ -representation is converted to a  $(\epsilon + O(\delta))$ -representation by taking  $\delta$  small enough.  $\square$

So given any polygonal domain, we perform a thick/thin decomposition to remove the hyperbolic thin parts. For each resulting thick part we decompose it into a really thick part and its parabolic thin parts. We then take a finitely bent approximation of each really thick components, and using angle scaling chains to inductively construct representations of the really thick components. We then combine these with the explicit representations of the thin components to get a representation of the original domain using Lemma 25. This completes proof of Theorems 1 and 2 except for the proof of Lemma 31.

## 15. ITERATING TO THE SOLUTION

In this section we will show how to improve a partial  $\epsilon$ -representation quickly assuming a certain  $\bar{\partial}$ -problem can be solved quickly. The following is our Newton type iteration for improving an  $\epsilon$ -representation. The fact that  $\epsilon_0$  does not depend on  $\Omega$  is one of the pillars upon which the whole proof rests.

**Lemma 31.** *There is an  $\epsilon_0 > 0$  so that if  $0 < \epsilon < \epsilon_0$  then the following holds. Given a partial  $\epsilon$ -representation of a polygonal region  $\Omega$  we can construct a partial  $\epsilon^2$ -representation in time  $O(n \log \frac{1}{\epsilon} \log \log \frac{1}{\epsilon})$ .*

Recall the notation  $\bar{\partial}f = f_{\bar{z}} = \frac{1}{2}(f_x + if_y)$ ,  $\partial f = f_z = \frac{1}{2}(f_x - if_y)$ . The Beltrami dilatation of a map is given by  $\mu_f = f_{\bar{z}}/f_z = \bar{\partial}f/\partial f$ .



Suppose  $(S_0, \mathcal{B}_0, \mathcal{G}_0)$  is a partial  $\epsilon$ -representation of the domain (recall this means  $S$  is a set of  $n$  points giving our current guess of the prevertices,  $\mathcal{B}$  is the covering of the corresponding decomposition, and  $\mathcal{G}$  is a function defined on each decomposition piece). Let  $F$  denote the quasiconformal map associated to this  $\epsilon$  approximation by (5). Then  $\mu_F$  is a piecewise rational function bounded by  $\epsilon$  and we can estimate it to within  $\epsilon^2$  by a polynomial on each piece with at most  $O(p)$  terms (using the geometric sum formula). More precisely, if  $Q_k$  is a decomposition piece and  $z \in N_s(Q_k)$ , then

$$\mu_F(z) = \frac{\sum f_j(z) \bar{\partial} \varphi_j(z)}{\sum \partial f_j(z) \cdot \varphi_j(z) + f_j(z) \cdot \partial \varphi_j(z)}.$$

Let  $\mu$  be the symmetrized version (with respect to the real axis) of this approximation, i.e.  $\mu$  is extended to the lower half-plane by  $\mu(\bar{z}) = \overline{\mu(z)}$ . Any solution of the Beltrami equation with this data is also symmetric, so maps the real line to itself. Note that  $\|\mu\|_\infty = O(\epsilon)$  and is supported on the  $O(n)$  squares that cover the boundary of our Carleson-Whitney decomposition (and its reflection in the lower half-plane). If  $\|\mu\|_\infty \leq \epsilon$ , we wish to find a quasiconformal map  $H$  of  $\mathbb{H}$  to itself that satisfies

$$(9) \quad \mu_H = \mu + O(\epsilon^2).$$

Then  $G = F \circ H^{-1}$  is a quasiconformal map of  $\mathbb{H}$  to  $\Omega$  with quasiconformal constant  $1 + O(\epsilon^2)$ .

Let  $p = O(|\log \epsilon|)$ . Suppose we can find a  $p$ -term series expansion for  $H$  in each empty piece of the decomposition. Then we could compose  $H^{-1}$  with our existing representation for  $F$  to get the  $p$  first terms of series approximating  $F \circ H^{-1}$  on the empty pieces of the Carleson-Whitney decomposition associated to  $H(S_0)$ , and this series is accurate to within  $\tilde{\rho}_\Omega$ -distance  $O(\epsilon^2)$ . We can then apply Lemma 21 to obtain a  $O(\epsilon^\alpha)$  representation for some  $\alpha > 1$ . Iterating this a fixed number of times (depending on  $\alpha$  and the constant in the “ $O$ ”) gives a  $\epsilon^2$ -representation.

In the remainder of this section we show how to define the new representation of  $\Omega$ , given the expansions for  $H$ . In the next section we show how to define  $H$ , assuming we can solve a certain  $\bar{\partial}$  problem, and in Section 17 we show how to solve this  $\bar{\partial}$  problem.

How do we define the new representation for  $\Omega$ ? Suppose  $(S_0, \mathcal{B}_0, \mathcal{G}_0)$  is the previous partial  $\epsilon$ -representation with dilatation  $\mu$  and that  $H$  is a  $(1 + O(\epsilon))$ -quasiconformal map of  $\mathbb{H}$  to itself that solves  $\mu_H = \mu + O(\epsilon^2)$ . Moreover,  $H$  is conformal on the

empty pieces of our decomposition and we have power series on each empty piece  $D$  that agree with  $H$  to within  $O(\epsilon^2 \text{diam}(f_k(E)))$  on  $N_s(E)$  where  $E$  is a boundary component of  $Q_k$ .

The points  $S = H(S_0)$  are known, and we take these to be the first part of our new triple. In time  $O(n)$  we can compute a covering of the hyperbolic convex hull of  $S$  and extend this to a decomposition of  $\mathbb{H}$ . This will be our new  $\mathcal{B}$ . For each Whitney square  $Q$  in  $\mathcal{B}$ , choose a Whitney square  $Q_0 \in \mathcal{B}_0$  so that  $H(Q_0)$  hits  $Q$  (we can do this in bounded time since  $H$  is almost an isometry and we need only search a uniformly bounded number of possible squares). Then there is a ball  $B$  so that  $Q \subset B \subset H(5Q_0)$  and we can compute the inverse  $h_Q$  of the power series of  $H$  on  $B$  in and then compute the composition of that series followed by the series for  $Q_0$  (which converges on  $10Q$ ). This gives the element of  $\mathcal{F}$  corresponding to  $Q$ . This computation takes time  $O(p \log p)$ ,  $p = \log \frac{1}{\epsilon}$  (see Lemma 52 of Appendix B). A truncation of this series, as given by Lemma 21, will give the desired element of  $\mathcal{F}$ . To see how, we use the following result.

**Lemma 32.** *Suppose  $f : \mathbb{D} \rightarrow \mathbb{D}$  is  $(1 + \epsilon^2)$ -quasiconformal and is conformal on the disk  $D(0, 1/M)$  and maps 0 to 0. Then there is a truncation  $g$  of the power series of  $f$  at 0, such that  $|g(z) - f(z)| \leq O(\epsilon^{2(1-\beta)})$  on  $D(0, M^{\beta-1})$ .*

*Proof.* Since  $f$  is  $(1 + \epsilon^2)$ -quasiconformal and fixes the origin, it agrees with a rotation  $\tau$  to within  $O(\epsilon)$ . Apply Lemma 21 to deduce the result.  $\square$

Our previous remarks prove:

**Lemma 33.** *If  $\|\mu\|_\infty = \epsilon < \epsilon_0$  then  $\|\mathcal{G}\| \leq O(\epsilon^{2(1-\beta)})$ .*

Thus if  $\beta < 1/2$  and  $\epsilon_0$  is small enough we get a definite improvement, and a bounded number of iterations will improve it below  $\epsilon^2$ . This choice of  $\beta$  determines the choice of  $M$  in the construction of the decomposition in Section 10.

## 16. REDUCING THE BELTRAMI PROBLEM TO A $\bar{\partial}$ PROBLEM

In Appendix A we recall that the Beltrami equation  $\bar{\partial}f = \mu\partial f$  can be solved using an infinite series of the form  $T\mu + T\mu T\mu + \dots$ , where  $T$  is the Beurling transform. The method we describe below might be adapted to use several terms of this series, but we shall use only the leading term.

We will replace the Beltrami equation  $\bar{\partial}H = \mu\partial H$  with the easier equation  $\bar{\partial}H = \mu$ . For  $\epsilon$  small, we will show  $\partial H$  is close to a constant on each piece of our decomposition, which means the solution of the Beltrami problem is close to a constant multiple of the solution of the  $\bar{\partial}$ -problem. Since  $\mu$  has compact support, the  $\bar{\partial}$ -problem can be exactly solved by the convolution

$$G_1(z) = \frac{1}{2\pi i} \iint \frac{\mu(w)dx dy}{z-w}.$$

It will actually be slightly more convenient to deal with  $\partial G_1$ , which is given by the Beurling transform  $T\mu$ ,

$$\partial G_1(z) = T\mu(w) = \lim_{r \rightarrow 0} \frac{1}{2\pi i} \iint_{|z-w|>r} \frac{\mu(z)}{(z-w)^2} dx dy.$$

This convolution gives a solution of  $\bar{\partial}G_1 = \mu$ , but we cannot compute  $\partial G_1$  exactly in finite time. However, we can compute  $p$  terms of a power or Laurent series that approximates  $\partial G_1$  in each of the empty pieces of our decomposition (where  $G_1$  is holomorphic). We will refer to the expansion on a piece  $Q$  as  $G_Q$ . We will see later that for each piece  $Q$  of our decomposition we can compute an expansion  $G_Q$  so that

$$(10) \quad |\partial^2 G_1(z) - \partial^2 G_Q(z)| \leq \frac{C\epsilon^2}{\text{diam}(D_Q)}, z \in D,$$

where  $D$  denotes the empty region of  $Q$ . (The  $\epsilon^2$  could be replaced by a higher power of  $\epsilon$ , if necessary, by simply taking more terms in  $G_Q$ ).

It will also be convenient to consider a function  $G_2$  on  $\mathbb{H}$  so that (1)  $G_2 = G_1$  on  $N_s$  (recall this is the union of  $N_s(E)$  over all boundary components of all pieces), (2)  $G_2 = G_Q$  on  $D_Q$  and (3)  $\bar{\partial}G_2 = \bar{\partial}G_1 + O(\epsilon^2)$ . This can easily be obtained by combining  $G_1$  and the  $G_Q$ 's using a partition of unity whose gradient is supported in  $N_s(D) \setminus D$ , whose gradient is bounded by  $O(\text{diam}(E)^{-1})$  and whose second gradient is bounded by  $O(\text{diam}(E)^{-2})$  on  $N_s(E)$ , when  $E$  a boundary component of  $D$ . Note that this implies

$$(11) \quad |\partial G_1(z) - \partial G_2(z)| \leq C\epsilon^2.$$

The algorithm only requires the computation of  $\partial G_Q$ , not of  $\partial G_2$ ; the latter function will only be used in the proof that the algorithm gives the desired accuracy.

**Lemma 34.** *Suppose  $E$  is a boundary component of a piece  $Q$ . Then  $|\partial^2 G_1(z)| \leq C\epsilon/\text{diam}(E)$ ,  $z \in N_s(E)$ . The same estimate also holds for  $G_2$ .*

*Proof.* Assume  $z \in N_s(E)$ . Let  $D$  be a Euclidean disk of radius  $r \simeq \text{diam}(E)$  around  $z$  and let  $\chi_D$  denote its characteristic function ( $= 1$  on  $D$  and  $0$  off  $D$ ). Let  $L(w)$  be the linear function such that  $|\mu(w) - L(w)| \leq C\epsilon|z - w|^2/r^2$  for  $w \in D$  (there is such a function because we constructed  $\mu$  to have second derivative bounded by  $C\epsilon/r^2$ ). Then,

$$\begin{aligned} |\partial^2 G_1(z)| &\simeq \left| \iint \frac{\mu(w) dx dy}{(z - w)^3} \right| \\ &\lesssim \iint \frac{|\mu(w) - L(w)\chi_D(w)| dx dy}{|z - w|^3} + \left| \iint_D \frac{L(w) dx dy}{(z - w)^3} \right| + \iint_{D^c} \frac{\epsilon dx dy}{|z - w|^3} \\ &\lesssim C\epsilon \iint_D \frac{dx dy}{r^2|z - w|} + 0 + C\epsilon/r \\ &\leq C\epsilon/r. \end{aligned}$$

The final claim holds because  $G_1 = G_2$  on  $N_s(E)$ . □

**Corollary 35.** *Suppose  $Q$  is a piece of our decomposition. Then  $|\partial G_2(z) - \partial G_2(z_Q)| \leq C\epsilon$  for every  $z \in Q$ .*

*Proof.* Recall the definition of  $z_Q$  (see Figure 34). For Whitney type squares and Carleson squares, there is only one boundary component and the proof of Lemma 34 actually applies to any point in  $Q$  and then we integrate along a segment connecting  $z$  and  $z_Q$  and note that the length of the segment at most  $O(\text{diam}(E))$ .

For arches, it is slightly more involved since there is a boundary component that is much smaller than the diameter of the whole piece. Since  $\partial G_2$  is holomorphic in the empty part of the piece, the maximum principle implies it is enough to check the inequality near the boundary components. The proof for the “big” boundary component is just like the case of Whitney squares and Carleson boxes. For the ‘small’ boundary component it suffices to check the estimate at one point near that component, say the one directly underneath  $z_Q$  and distance  $2s \cdot \text{diam}(E)$  above  $E$ . Then

$$\partial^2 G_1 = O\left(\iint \frac{|\mu(w)|}{|z - w|^3} dx dy\right),$$

and we can break the integral into two parts corresponding to the two complementary components of the annulus. The unbounded part is bounded by  $O(\epsilon \text{diam}(Q)^{-1})$  and the other is bounded by  $O(\epsilon t^{-3} \text{diam}(E)^2)$  for a point at height  $t$ . Integrating both estimates from  $t = \text{diam}(E)$  to  $t = \text{diam}(Q)$ , gives  $O(\epsilon) + O(\epsilon)$  and is an upper bound

for the variation of  $\partial G_1$  along the vertical line segment connecting the two boundary components. This proves the desired estimate for  $G_1$ . It follows for  $G_2$  by (11).  $\square$

Given the function  $G_2$ , which is an approximate solution of the  $\bar{\partial}$ -problem, we can define a quasiconformal mapping on each piece of our decomposition. Assume for the moment that  $z_Q$  maps to  $w_Q$  and let  $d_Q = \text{Im}(w_Q)/\text{Im}(z_Q)$ . Define

$$H_Q(z) = L_0(z) + d_Q(G_2(z) - L_1(z)),$$

where  $L_0$  is the unique conformal linear map of  $\mathbb{H}$  to itself that maps  $z_Q$  to  $w_Q$ , and  $L_1$  is the unique conformal linear map that agrees with  $G_2$  at  $z_Q$ . Note that  $H_Q(z_Q) = w_Q$  and  $\partial L_0 = d_Q$  and that we only need to know the difference  $G_Q(z) - G_Q(z_Q)$  in order to define  $H_Q(z)$ .

By Corollary 35  $|\partial G_2 - \partial L_1| \leq O(\epsilon)$  on  $N_s(Q)$ . Thus for  $z \in N_s(Q)$ ,

$$\partial H_Q = d_Q + d_Q O(\epsilon) = d_Q(1 + O(\epsilon)),$$

and using this we get

$$\bar{\partial} H_Q = d_Q \bar{\partial} G_2 = d_Q \mu + O(d_Q \epsilon^2) = (\mu + O(\epsilon^2)) \partial H_Q$$

$$(12) \quad \mu_{H_Q} = (\mu + \epsilon^2)$$

for  $z \in Q$ . Thus  $H_Q$  is a quasiconformal map on  $N_s(Q)$  with dilatation  $\mu + O(\epsilon^2)$ .

So far we have assumed that we know the images  $w_Q$  of  $z_Q$ . We now describe how to find  $w_Q$ . We proceed in a “top-down” manner, by starting at the root piece  $Q_0$  and assuming  $H(z_{Q_0}) = z_{Q_0}$  is fixed. Then if  $Q$  is a child of  $Q_0$  let  $w_Q = H_{Q_0}(z_Q)$ , i.e., use the quasiconformal map for the parent piece to define where the center point of the child maps to. In this way we can proceed inductively down the tree of pieces and define  $H_Q$  for every piece.

In each step of this procedure, we might introduce an error of size  $O(\epsilon^2)$  in the definition of  $w_Q$ . This is not a problem by itself since we are only trying to compute a map with this accuracy. However, it is possible to have two adjacent pieces  $Q, Q'$  of our decomposition that have no common ancestor for a very large number of generations, and in such a situation the definitions of  $w_Q$  and  $w_{Q'}$  might begin to diverge to an unacceptable degree. In order to avoid this problem, we modify the “top-down” induction described above for Whitney type pieces. If the current piece is a Whitney type piece  $Q$  and it is adjacent to a Whitney type piece  $Q'$  of the same

height and they have 3rd generation descendants that are Whitney type and adjacent, then we modify the definitions of  $w$  for the 3rd generation descendants as follows. For the descendants of  $Q$  and  $Q'$  that are adjacent we define  $w$  using the average of the values we would get using  $H_Q$  and  $H_{Q'}$ . For the descendant next to the center of  $Q$  we use the value of  $Q$  alone and for the intermediate values we take weighted averages that linearly interpolate between the endpoint cases. This step insures that adjacent pieces have  $d_Q$  values that are within  $1 + O(\epsilon)$  of each other, i.e.,

**Corollary 36.** *If  $Q$  and  $Q'$  are adjacent pieces of the decomposition then  $d_Q/d_{Q'} = 1 + O(\epsilon)$ .*

Suppose  $Q$  and  $Q'$  are adjacent pieces. How close are the functions  $H_Q$  and  $H_{Q'}$  along the common boundary? Note that both maps are quasiconformal on a Carleson square containing both  $Q$  and  $Q'$  and that  $H_{Q'}$  was chosen to agree with  $H_Q$  at the point  $z_{Q'}$ . Thus the maps also agree at the reflection of this point in the lower half-plane and both maps take  $\infty$  to  $\infty$ . Moreover, by Corollary 36 and (12) the dilatations of these maps agree to within  $\epsilon^2$  and hence it follows from Lemma 45 of Appendix A that the maps agree to within  $d_Q\epsilon^2$ , i.e.,

$$(13) \quad |H_Q(z) - H_{Q'}(z)| = O(d_Q\epsilon^2),$$

for  $z$  in  $N_s(Q) \cap N_s(Q')$ .

Given the approximate solutions  $H_Q$  on each piece we can combine them using a partition of unity to get a single approximate solution on the whole upper half-plane (again, we only do this to estimate the error; it is not necessary to do so as part of the algorithm). Define a mapping of  $\mathbb{H}$  to itself by

$$H = \sum_Q \varphi_Q H_Q$$

where  $\{\varphi\}$  is a partition of unity as in Section 11. If  $Q$  and  $Q'$  are adjacent squares and  $z$  is in the  $s$  neighborhood of the common boundary, then

$$|d_H(z_Q) - d_H(z_{Q'})| \leq C d_H(z_Q)\epsilon.$$

$$|H_Q(z) - H_{Q'}(z)| \leq \epsilon d_H(z_Q)\text{Im}(z_Q)$$

Also,

$$\bar{\partial}H = \sum_Q \bar{\partial}\varphi_Q \cdot H_Q + \sum_Q \varphi_Q \cdot \bar{\partial}H_Q = I + II.$$

Since  $\sum_Q \bar{\partial}\varphi_Q = 0$ ,  $\sum |\bar{\partial}\varphi_Q| \leq C/\text{Im}(z)$ , the estimate (13) implies that I is bounded by  $O(d_Q\epsilon^2)$ . Since  $\sum_Q \varphi_Q = 1$ , the estimate (12) shows that second sum is  $d_Q\mu + O(d_Q\epsilon^2)$ . Similarly,

$$\partial H = \sum_Q \partial\varphi_Q H_Q + \sum_Q \varphi_Q \partial H_Q.$$

As above, the first sum is  $O(\epsilon^2 d_H(z))$  and the second sum is

$$d_H(z_Q)(1 + O(\max |d_H(z_Q) - d_H(z_{Q'})| + \epsilon))$$

where the maximum is over all pieces  $Q'$  that are adjacent to  $Q$ . This maximum is  $O(\epsilon)$ , so we have  $\partial H = d_H(z_Q)(1 + O(\epsilon))$  if  $z \in Q$ . Thus

$$\mu_H(z) = \frac{\bar{\partial}H(z)}{\partial H(z)} = \frac{d_H(z_Q)(\mu + O(\epsilon^2))}{d_H(z_Q)(1 + O(\epsilon))} = \mu + O(\epsilon^2).$$

Thus in the empty regions (where only one partition of unity function is non-zero) our piecewise solutions  $H_Q$  agree with a global solution  $H$ . On the empty regions of the decomposition  $H_Q$  agrees with a function defined using only  $G_Q$ , which we can compute. Thus the truncated expansions that we can actually compute, agree (on the empty regions) with a globally defined quasiconformal map whose dilatation is  $\mu + O(\epsilon^2)$ .

## 17. FAST COMPUTATION OF THE BEURLING TRANSFORM

Now it only remains to compute  $\partial G_Q(z) - G_Q(z_Q) \approx T\mu$  as quickly and as accurately as we claimed. Since we only need to compute this difference in regions where  $T\mu$  is holomorphic, we will compute a series expansion for

$$\partial T\mu(w) = \lim_{r \rightarrow 0} \frac{-1}{\pi i} \iint_{|z-w|>r} \frac{\mu(z)}{(z-w)^3} dx dy$$

and then simply integrate the series term-by-term. We need to compute this with error at most

$$\frac{C\epsilon^2}{\text{diam}(Q_j)},$$

on a Whitney square  $Q_j$ .

We shall use the fast multipole algorithm of Rokhlin and Greengard [70] (named one of the top ten algorithms of the 20th century in [39]). The basic idea is that we have  $n$  empty regions where we want to compute a series expansion, each of which is influenced by the  $n$  regions where the data is supported. This is  $n^2$  interactions to

compute in only time  $O(n)$ . The multipole method takes advantage of the fact that pieces of data that are close together affect distant outputs in similar ways. Thus the data can be grouped together and the combined effects computed simultaneously. By way of review, we first describe how the method works in an easier setting: binary trees.

Suppose  $T$  is a binary tree with vertex set  $V$  of size  $n$ ,  $f : V \rightarrow \mathbb{R}$  is given, and we want to evaluate the sum

$$F(v) = \sum_{w \in V \setminus \{v\}} K(v, w) f(w),$$

at every  $v \in V$  where  $K(v, w) = a^{\rho_T(v, w)}$  and  $\rho_T$  is the path distance in the tree. There are  $n$  inputs and  $n$  outputs and each input affects the evaluation of every output, so naively it seems that  $n^2$  operations are required. However, all  $n$  values of  $F$  can be computed in  $O(n)$  steps as follows. Choose a root  $v_0 \in V$  and for any  $v \in V$  let  $D(v) \subset V$  be the vertices that are separated from the root by  $v$ , not including  $v$ . (i.e., its descendants). Let  $\tilde{D}(v) = V \setminus (\{v\} \cup D(v))$ . Let

$$F_1(v) = \sum_{w \in D(v)} K(v, w) f(w), \quad F_2(v) = \sum_{w \in \tilde{D}(v)} K(v, w) f(w).$$

We can compute each of these functions in one pass through the tree. For  $F_1$  start by setting  $F_1(v) = 0$  for each leaf of  $T$  and proceed from the leaves to the root by setting

$$F_1(v) = a \sum_{w \in C(v)} F_1(w),$$

where the sum is over the children of  $v$ . This is called the “up-pass” since we start at the leaves and work towards the root. Next, we transfer values from  $F_1$  to  $F_2$  using an “across-pass”. For each vertex where  $F_1$  has already been evaluated by the up-pass, add  $a^2 \cdot (f(v) + F_1(v))$  to  $F_2(w)$ , for each sibling  $w \in S(v)$  of  $v$  ( $w \neq v$  is a sibling of  $v$  if it has the same parent as  $v$ ). Lastly, we compute  $F_2$  using a “down-pass”, by setting  $F_2(v) = 0$  when  $v$  is the root (which has no sibling, so was not affected by the across-pass), and in general if  $F_2(v)$  has already been computed, then for each of its children  $w$  we set

$$F_2(w) = F_2(w) + a(F_2(v) + f(v)).$$



We get the desired output by noting

$$F(v) = (F_1(v) + F_2(v)),$$

for every  $v \in V$  (we can evaluate vertices in any order). Thus  $F$  has been evaluated at all  $n$  points in  $O(n)$  steps.

The same method works more generally. If we are given a rooted tree  $T$  with vertex set  $V$  we turn it into a directed graph  $G$  by taking two copies  $V_1, V_2$  of  $V$ , point all edges towards the root in  $V_1$  and away from the root in  $V_2$  and connect each vertex in  $V_1$  to the copies of its siblings in  $V_2$ . Assume we have linear space  $X_v^1, X_v^2$  for each vertex  $v \in V$  and a linear map from each  $X_v^1$  to its parent and from each  $X_v^2$  to each of its children. Assume we also have an ‘‘across map’’  $A_v : X_v^1 \rightarrow X_v^2$ . We define a linear map  $L(w, v) : X_w \rightarrow X_v$  by composing maps along the path from  $w$  to  $v$ . Given the  $n$  values  $x_v \in X_v^1, v \in V$  the method above evaluates all  $n$  values of

$$F(x_v) = \sum_{w \in V} L(w, v)x_w$$

in only  $O(n)$  steps.

In the previous example, the linear spaces were one dimensional and the edge maps were multiplication by  $a$ . For our application to computing a Beurling transform, the tree will be the tree of dyadic Whitney boxes that intersect the support of the dilatation  $\mu$ . To each Whitney box,  $Q$ , we will associate a finite set of regions  $\{W_j\}$ ; each will be either a disk or a disk complement (including  $\infty$ ). The linear spaces will be spaces of analytic functions on these regions. We will actually consider two situations: an infinite dimensional ideal model and a finite dimensional approximation that we actually compute.

In the idealized version we consider the space  $X_Q$  of all analytic functions on a region  $W$ . If  $W$  is a disk then every such function has a power series  $\sum_{k=0}^{\infty} a_n(z - a)^k$  converging in the disk and for the disk complements there is a Laurent series  $\sum_{k=0}^{\infty} a_n(z - a)^{-k}$ . The finite dimensional version of these spaces are the spaces  $X_Q^p$ . These consist of  $p$  term power series  $\sum_{k=0}^p a_n(z - a)^k$  (for disks) or Laurent series  $\sum_{k=0}^p a_n(z - a)^{-k}$  (for disk complements). There is an obvious truncation map  $T : X_Q \rightarrow X_Q^p$  and an inclusion map  $I : X_Q^p \rightarrow X_Q$ .

Given two regions, one of which is contained the other, we can restrict a function from the larger region to the smaller. This defines restriction maps  $R$  between the

infinite dimensional spaces  $X_Q$ . For the finite dimensional analog, we define maps  $R^p$  between the spaces  $X_Q^p$  by restricting and then truncating the series expansion. We will see how to compute the Beurling transform exactly using the restriction maps, and then check how much error is introduced when we replace these by the finite dimensional restriction/truncation maps.

When we allow infinite expansions, then restricting an analytic function to a subdomain introduces no errors and the method described above allows us to compute series expansion for the Beurling transform in time  $O(n)$  with no errors (except for filling in the initial values of the arrays). Similarly, if we restrict a power series to a smaller disk, there is no error introduced, since the restriction of a degree  $p$  polynomial is still a degree  $p$  polynomial. However, if we change the center of a Laurent expansion, then a finite expansion may become infinite and truncating to  $p$  terms causes an error (depending on  $p$  and the geometry of the regions). In this case, performing the restriction-truncation along a series of nested regions might not give the same result as restricting to the smallest domain in single step. Because of this, we have to estimate the errors at each step and show the total accumulated error along the whole path is still small.

We will now introduce the elements needed to apply these general ideas to the specific problem of computing  $\partial T\mu$ .

We start with a partial  $\epsilon$ -representation of a polygonal domain. As in Section 15, we use this to construct a dilatation  $\mu$  that is a sum  $\sum \mu_k$  of terms, each of which are supported in small squares whose union covers a neighborhood,  $N_s$ , of the boundary of our decomposition. We assume that  $\mu$  is defined by reflection on the lower half-plane, so that solutions of the Beltrami equation will be real on the real line. Each  $\mu_n$  is a polynomial in  $x$  and  $y$  of degree at most  $O(n)$  restricted to a small square. The terms of this polynomial are of the form  $z^k x^a y^b = (x + iy)^k x^a y^b$  with  $0 \leq k \leq p$  and  $0 \leq a, b \leq C$  where  $p$  grows depending of the desired accuracy, but  $C$  is fixed, depending only on the degrees of the piecewise polynomials used in our partition of unity associated to the decomposition  $\mathcal{W}$  of our representation. Thus there are only  $O(n)$  terms to consider, not  $O(n^2)$  as would be the case if all powers of  $x$  and  $y$  less than  $n$  had to be considered.

We take as our tree the collection of all Whitney squares in the upper half-plane that hit the support of  $\mu$ , i.e., which hit  $N_s$ . There are  $O(n)$  such, since there are  $O(n)$  boundary components in our decomposition and each only hits a bounded number of Whitney boxes (for arches we only need to cover the edges of the arch, not the interior). The adjacency relation is the usual one;  $Q$  is a child of  $Q^*$  if the base of  $Q^*$  contains the base of  $Q$  and  $Q$  is maximal with this property. A given Whitney square can have zero, one or two children. Those with no children are called “leaves” of the tree. Often a child is half the size of its parent and the top edge of the child is half the bottom edge of the parent, but because of arches, there are some cases where a child is much smaller than its parent. A neighbor of a dyadic Whitney square is a distinct dyadic Whitney square of the same size that touches along the boundary. The terms “descendant” and “ancestor” have the usual meanings for a rooted tree.

For any Whitney box  $Q$  in  $\mathbb{H}$  with base interval  $I$  (its vertical projection on  $\mathbb{R}$ ) let  $c_Q$  denote the center of this base and let  $c_Q^j$ ,  $j = 1, \dots, 8$  be 8 equally spaced points in  $I$  (including the right, but not the left endpoint of  $I$ ). Let  $A_Q = \{z : |z - c_Q| \geq \lambda|I|\}$  where we choose  $\frac{1}{2}\sqrt{5} < \lambda < \frac{5}{4}$ , and let  $D_Q^j = \{z : |z - c_Q^j| \leq \frac{1}{4}|I|\}$ . These will be called the type I and type II regions associated to  $Q$  respectively. See Figure 57. The number  $\lambda$  is chosen in this range so that the type I region does not intersect  $Q$ , but it does contain the type II regions of any  $Q'$  that is the same size as  $Q$ , but not adjacent to it. See Figure 58. A series expansion in terms of  $(z - c_Q)^{-1}$  or  $(z - c_Q^j)$  will be called type I and type II expansions respectively.

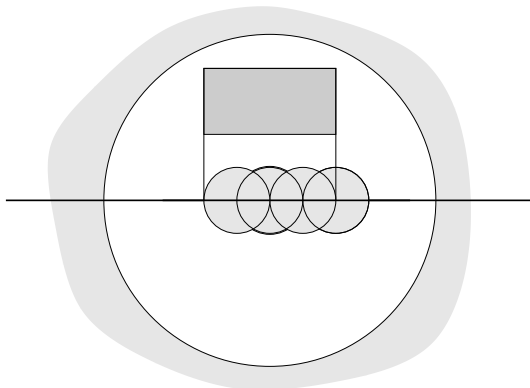


FIGURE 57. A Whitney box and its type I and type II regions.

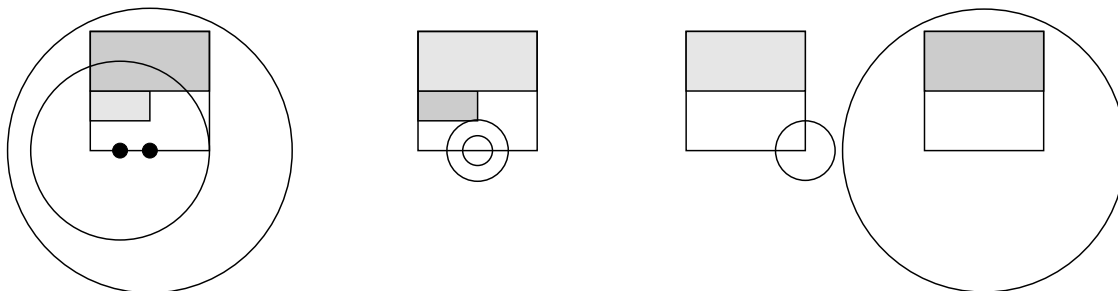


FIGURE 58. The three kinds of conversions: multipole-to-multipole, local-to-local and multipole-to-local. In each case the first Whitney square is shaded lighter than the second.

Given a Whitney box  $Q$  we can restrict  $\mu$  to  $Q$  and compute type I and type II expansions for  $\partial T\mu|_Q$ . Since  $\mu$  is a piecewise polynomial of degree  $O(p)$ , and there is an explicit formula for the expansion of each monomial, this can be done in time  $O(p \log p)$  by the remarks in Appendix B.

Given a Whitney box  $Q$  and its parent  $Q^*$ , the type I region for  $Q$  contains that for  $Q^*$  and so we can take the analytic function  $f$  defined by the type I expansion for  $Q$  and compute its Laurent expansion in the type I region for  $Q^*$ . Then truncate this (infinite) series to get a type I expansion for  $Q^*$ . This is called a I-to-I conversion or a multipole-to-multipole conversion. See Figure 58. This introduces an error of  $\epsilon M_f$ , where  $\epsilon = \lambda^p$ , where  $\lambda < 1$  and  $M_f$  is the maximum of  $f$  on the type I region of  $Q$ .

Similarly, we can take a type II expansion for  $Q$  and restrict it to one of the two type II regions for a child of  $Q$  whose center agrees with the first center or is immediately to the left of it. Changing the center of the expansion just gives another degree  $p$  polynomial and there is no error introduced, i.e.,  $R = R^p$ . This is a local-to-local conversion.

Finally, the type I region of a Whitney box  $Q$  contains the type II regions of a box  $Q'$  of the same size if  $Q'$  is in  $3Q^*$  but not in  $3Q$  (here  $Q^*$  denotes the parent of  $Q$ ). Therefore, we can restrict the type I expansion of  $Q$  to a type II region of  $Q'$  and do a I-to-II conversion (or multipole-to-local conversion), with an error of  $\epsilon M_f$ , as above.

For a given box  $Q$ , the associated regions cover the whole upper half plane, except for a region of bounded hyperbolic diameter around  $Q$ .

We think of the type I and type II expansions associated to each  $Q$  as defining two arrays indexed by the Whitney boxes. We next describe how to initialize and update these arrays:

**Initialize Type I array:** For each  $Q$  compute the initial type I expansion.

**Initialize Type II array:** For each  $Q$  compute the initial type II expansion for each type II disk.

**Modify Type II array:** Compute type II expansions for two neighbors and add to their initial expansions. Every type II expansion now has contributions from at most three boxes (its parent and the parent's neighbors)

**Perform the up-pass:** Starting with leaves of the tree, do I-to-I conversion of the current type I expansion and add it to the type I expansion of the parent. Continue until we reach the root.

**Perform the across-pass:** For each square  $Q$ , do I-to-II conversions taking the current type I expansion and obtaining type II conversions for regions corresponding to centers in  $3I^* \setminus 3I$  where  $I$  is the base of  $Q$  and  $I^*$  is the base of  $Q$ 's parent.

**Perform the down-pass:** Starting with root square, do II-to-II conversions, taking each type II expansion and restricting it to the two type II expansions of the children. Continue downward until we reach the leaves of the tree.

This is clearly  $O(n)$  steps and when we are finished, the type I expansion of a square  $Q$  contains the contribution of  $Q$  and every descendant of  $Q$  and the type II expansions of  $Q$  contain the contributions of every square that is not a (strict) descendant of  $Q$  or its two neighbors.

The third step (Modify the type II array) is necessary because the tree structure on Whitney squares does not completely reflect their actual placement in  $\mathbb{H}$ ; two squares that are far apart in the tree could be adjacent in  $\mathbb{H}$ . The type I region of a square does not contain the type II disks of its neighbors (they are too close), so we need this special step to pass the information to these regions (for other regions it is passed in the across-step).

Now suppose  $D$  is an empty piece of our decomposition and  $Q$  is the Whitney box containing  $D$ . If  $D$  is a disk, it is contained in a type II region of a grandparent of  $Q$  and is contained in the type I region of all grandchildren of  $Q$  and its two neighbors.

Therefore we can do series conversions and compute the expansion in  $D$  due to these expansions. There are only a finite number of Whitney boxes whose contributions have not been accounted for and all these lie within a uniformly bounded distance of  $Q$ . For each piece of  $\mu$  supported in one of these boxes, we compute the contribution to  $D$  directly.

Given any Whitney boxes  $Q'$  and  $Q$  there is a path in our directed graph that starts from an initial expansion for  $Q$  and goes to a terminal expansion for  $Q'$  or one of its neighbors. To see this we consider several cases.

- (1) If  $Q = Q'$  there is nothing to do.
- (2) If  $Q = Q_2$  is an ancestor of  $Q_1$  then the all “down” path works.
- (3) If  $Q_3$  is a neighbor of square  $Q_2$  in (1), then start with the special “Modify type II” step and follow by all downs.
- (4) If  $Q_4$  is a descendant of a case (2) square, then follow “up” paths until we hit a child of  $Q_3$  and then use a “across” step to bring us to an ancestor of  $Q'$  (this works because by the definition of the across step).
- (5) If  $Q$  is a descendant of  $Q'$ , then use all “up”’s.
- (6) The only remaining case is that  $Q$  is a neighbor of  $Q'$  or a descendant of a neighbor. Using an all “up” path works.

If  $D$  is an empty piece of our decomposition, we want to show that the desired expansion for  $\partial T\mu$  can be computed using a bounded number of type I and type II expansions, plus a bounded number of direct expansions of nearby squares. Fix such a  $D$  and suppose  $Q$  is any Whitney box, then  $D$  is a subset of one of the type I or II regions associated to  $Q$  or one of its neighbors, unless  $Q$  is within a uniformly bounded hyperbolic distance  $M$  of  $D$ . If  $D$  is a subset of one of these regions, then we can convert the series expansion on the region to one on  $D$ , the conversion being one of three types. First, we might have to convert a power series in  $(z - a)$  to one in  $(z - b)$ ; this happens when  $D$  is a disk or arch contained in a disk and involves no loss of accuracy. Second, converting an expansion in  $(z - a)^{-1}$  to one in  $(z - b)^{-1}$ ; this happens when  $D$  is an arch that contains  $Q$  in its bounded complementary component and there is a loss of accuracy (described in Lemma 37). Finally, in all other cases we must convert an expansion in  $(z - a)^{-1}$  to one in  $(z - b)$ ; this also involves a small loss of accuracy.

**Lemma 37.** *Suppose  $|a| \leq \frac{1}{4}$ ,  $|b| \leq \frac{1}{2}$  and  $f$  is analytic on  $\{z : |z - a| > 1\}$  and  $|f| \leq 1$  there. Also assume  $f(z)z^3$  is bounded as  $z \rightarrow \infty$ . Suppose  $A = \{z : |z - b| > 2\}$  and let  $f(z) = \sum_{j=0}^{\infty} a_j(z - b)^{-j}$  be the Laurent expansion for  $f$  in  $A$  and let  $g(z) = \sum_{j=0}^p a_j(z - b)^{-j}$ . Then there is  $0 < \lambda < 1$  so that for  $\epsilon = \lambda^p$ ,*

- (1)  $a_0 = a_1 = a_2 = 0$ ,
- (2)  $|g(z)| \leq (1 + \epsilon)|z|^{-3} \leq |z|^{5/2}$ , if  $p$  is large enough.
- (3)  $|f(z) - g(z)| \leq \epsilon|z|^{-3}$ .

The proof is just the standard estimates for Taylor series and left to the reader. If we start with an expansion  $f_0$  on the type I region of a box  $Q$  of size 1 and then restrict the expansion to get an expansion  $f_1$  for the type I region of its parent, then repeat this over and over, we accumulate an error each time. Suppose  $f_k$  is  $k$ th expansion on the  $k$ th region  $A_k$ . Then  $\sup_{A_k} |f_k| \leq |z|^{-5/2}$ , which means the maximum error between  $f_k(z)$  and  $f_{k+1}(z)$  on  $A_{k+1}$  is bounded by  $\epsilon|z|^{-5/2}$ . So the total error that is ever possible inside  $A_N$  is

$$\begin{aligned} &\leq \sum_{k=1}^N |f_k(z) - f_{k+1}(z)| \\ &\leq \sum_{k=1}^N \epsilon \text{diam}(\partial A_k)^{-5/2} (\text{diam}(\partial A_n) / \text{diam}(\partial A_k))^{-3} \\ &\leq O(\epsilon) \text{diam}(\partial A_N)^{-3} \sum_{k=1}^N \text{diam}(\partial A_k)^{1/2}. \end{aligned}$$

Since the regions grow by at least a factor of two at each stage, the final sum is dominated by its final term, and so the total error is less than  $O(\epsilon \text{diam}(\partial A_N)^{-2.5})$ .

Summarizing this argument gives:

**Lemma 38.** *Suppose  $f_0(z) = \sum_{k=3}^p a_k(z - c_Q)^{-k}$  is a type I expansion associated to a dyadic Whitney square  $Q_0$  and  $|f_0|$  is bounded by  $M$  on the type I region of  $Q_0$ . Suppose  $Q_1, \dots, Q_N$  are ancestors of  $Q$  and  $f_k$  is the result of applying a I-to-I conversion to  $f_{k-1}$  for  $k = 1, \dots, N$ . Then on the type I region of  $Q_N$ ,  $|f_0 - f_N| \leq O(\epsilon M (\text{diam}(Q_0) / \text{diam}(Q_N))^{2.5})$  with  $\epsilon = \lambda^p$  and a constant that is independent of  $N$ .*

**Corollary 39.** *Suppose  $Q_0$  is a Whitney square and for each  $Q$  that is a descendant of  $Q_0$ , let  $f_Q$  be the type I expansion of  $\partial T \mu$  for  $\mu$  restricted to  $Q$ . Let  $f_0$  be the type*

*I expansion for  $Q_0$  obtained by running the up-pass over all descendants of  $Q$  with initial data  $\{f_Q\}$ . Let  $F_0 = \sum_{Q \in D(Q_0)} f_Q$  be the exact sum of these initial expansion restricted to the type I region of  $Q_0$ . Then*

$$|f_0(z) - F_0(z)| = O\left(\epsilon \frac{\text{diam}(Q_0)^2}{|z - c_{Q_0}|^3} \|\mu\|_\infty\right).$$

*Proof.* The maximum of  $f_Q$  on the type I region of  $Q$  is clearly  $O(\|\mu\|_\infty/\text{diam}(Q))$ . Therefore, by the Lemma 38 the error of applying I-to-I conversions until we reach  $Q_0$  is

$$O(\epsilon \|\mu\|_\infty \text{diam}(Q)^{1.5} / \text{diam}(Q_0)^{2.5}).$$

There are at most  $2^k$  descendants of  $Q_0$  with  $\text{diam}(Q) = 2^{-k} \text{diam}(Q_0)$ , so the total error of all of these is

$$O(\epsilon \|\mu\|_\infty \text{diam}(Q)^{1.5} / \text{diam}(Q_0)^{2.5}) = O(\epsilon \|\mu\|_\infty 2^{-k/2} / \text{diam}(Q_0)).$$

We now sum  $k = 1, 2, \dots$  and see the total error over all descendants of  $Q_0$  is at most  $O(\epsilon \|\mu\|_\infty / \text{diam}(Q_0))$ . The error is an analytic function on the type I region of  $Q_0$  that decays like  $|z - c_{Q_0}|^{-3}$  near infinity (since it is a difference of functions which do), and this gives the estimate in the corollary.  $\square$

**Corollary 40.** *Let  $f$  be a type II expansion for a Whitney square  $Q$  that is obtained by starting with expansions of  $\partial T\mu$  and applying the up-pass, across-pass and down-pass. Then the total error between  $f$  and simply adding all the initial expansions that contribute to  $f$  is  $O(\epsilon \|\mu\|_\infty / \text{diam}(Q))$ .*

*Proof.* The contribution of the ancestors of  $Q$  are through II-to-II conversions, which introduce no error. The neighbors of ancestors contribute are direct computation of a type II expansion, followed by II-to-II expansions, so also contribute no error. Every other contribution comes from a sequence of I-to-I conversions (the up-pass), followed by a I-to-II conversion (the across-pass) and then II-to-II conversions (the down-pass). Fix a square  $Q_j$  to which the across-pass is applied. The errors due to all the descendants of  $Q_j$  is bounded by  $O(\epsilon \|\mu\|_\infty / \text{diam}(Q_j))$ . If  $\text{diam}(Q_j) = 2^j \text{diam}(Q)$ , then this is  $O(2^{-j} \epsilon \|\mu\|_\infty / \text{diam}(Q))$ . The across-pass adds an error with the same bound and the following down-pass adds no new error. Thus the total contribution of  $Q_j$  to the error is  $O(2^{-j} \epsilon \|\mu\|_\infty / \text{diam}(Q))$ . There are only a bounded number (at



most 4) of such  $Q_j$ 's of a given size, so summing over all possible  $j$ 's shows the total error is at most  $O(\epsilon\|\mu\|_\infty/\text{diam}(Q))$ .  $\square$

Now every expansion that contributes to the final expansion on an empty region is either directly computed from the data, or comes from an expansion created by the up-pass, across-pass and down-pass. By the corollary, the up-pass creates a small error, and we already know the across-pass creates a small error and the down-pass creates no errors. Thus the total error comes from a uniformly bounded number of terms, each of which has error bounded by  $O(\epsilon\|\mu\|_\infty/\text{diam}(Q))$ .

This completes the proof of Lemma 31 and hence of the theorem.

## APPENDIX A. BACKGROUND IN ANALYSIS

In this section will give various definitions and results from analysis. It is intended as a review or (very brief) introduction to ideas used in the paper.

**A.1. Möbius transformations.** A linear fractional (or Möbius) transformation is a map of the form  $z \rightarrow (az + b)/(cz + d)$ . This is a 1-1, onto, holomorphic map of the Riemann sphere  $\mathbb{S} = \mathbb{C} \cup \{\infty\}$  to itself. Such maps form a group under composition and are well known to map circles to circles (if we count straight lines as circles that pass through  $\infty$ ). Möbius transforms are conformal, so they preserve angles.

The non-identity Möbius transformations are divided into three classes. Parabolic transformations have a single fixed point on  $\mathbb{S}$  and are conjugate to the translation map  $z \rightarrow z + 1$ . Elliptic maps have two fixed points and are conjugate to the rotation  $z \rightarrow \lambda z$  for some  $|\lambda| = 1$ . The loxodromic transformations also have two fixed points and are conjugate to  $z \rightarrow \lambda z$  for some  $|\lambda| < 1$ . If, in addition,  $\lambda$  is real, then the map is called hyperbolic.

Given two sets of three distinct points  $\{z_1, z_2, z_3\}$  and  $\{w_1, w_2, w_3\}$  there is a unique Möbius transformation that sends  $w_k \rightarrow z_k$  for  $k = 1, 2, 3$ . A Möbius transformation sends the unit disk 1-1, onto itself iff it is of the form

$$z \rightarrow \lambda \frac{z - a}{1 - \bar{a}z},$$

for some  $a \in \mathbb{D}$  and  $|\lambda| = 1$ . Any loxodromic transformation of this form must actually be hyperbolic.

**A.2. Conformal maps:** A conformal mapping is a diffeomorphism that preserves angles. We will only consider orientation preserving maps here, in which case a conformal map between planar domains is the same as a 1-1 holomorphic mapping. The Riemann mapping theorem states that given any simply connected, proper subdomain  $\Omega$  of the plane there is a one-to-one, onto holomorphic map  $f : \mathbb{D} = \{z : |z| < 1\} \rightarrow \Omega$ . If  $\partial\Omega$  is locally connected then this map extends continuously to the boundary. Moreover, we can always take  $f(0)$  to be any given point of  $\Omega$  and  $f'(0)$  to have any argument we want. If  $\partial\Omega$  is Jordan curve we can also normalize by making any three points on the unit circle map to any three points on  $\partial\Omega$  (as long as they have the same orientation).

The Schwarz-Christoffel formula gives a formula for the Riemann map of the disk onto a polygonal region  $\Omega$ : if the interior angles of  $P$  are  $\alpha\pi = \{\alpha_1\pi, \dots, \alpha_n\pi\}$ , then

$$f(z) = A + C \int^z \prod_{k=1}^n \left(1 - \frac{w}{z_k}\right)^{\alpha_k-1} dw.$$

See e.g., [48], [98], [126]. On the half-plane the formula is

$$f(z) = A + C \int \prod_{k=1}^{n-1} (w - z_k)^{\alpha_k-1} dw.$$

The formula was discovered independently by Christoffel in 1867 [38] and Schwarz in 1869 [110], [109]. For other references and a brief history see Section 1.2 of [48]. It is also possible to formulate it with other base domains, such as an infinite strip (see [48]). See [82] for a version involving doubly connected polygonal regions. There are also versions for domains other than polygons, e.g., circular arc polygons as in [81], [98]. In this case, we get a simple formula for the Schwarzian derivative of the conformal map, but it involves unknown parameters with no obvious geometric interpretation.

One particular case of the Schwarz-Christoffel formula we need (see Section 11) is for the map of the upper half-plane to a triangle with one vertex at  $\infty$  (i.e., a region bounded by two half-infinite rays and a finite segment). Since there are only two finite vertices, there is no parameter problem to solve; they can be chosen to be any two points we want, say  $\pm 1$ , so the formula becomes

$$(14) \quad f(z) = A + C \int (w - 1)^{\alpha_1-1} (w + 1)^{\alpha_2-1} dw.$$

Note that using the general form of the binomial theorem,

$$(1+z)^p = \sum_{k=0}^{\infty} \frac{p(p-1)\cdots(p-k+1)}{k!} z^k,$$

we can easily compute power series for these functions in disks away from the singularities.

The problem in applying the Schwarz-Christoffel formula with  $n > 3$  vertices is that the points  $\mathbf{z} = \{z_1, \dots, z_n\}$  are unknown to us until we know  $f$ , so the formula seems circular. However, there are various iterative methods for finding the points  $\mathbf{z}$  starting from an initial guess (often taken to be  $n$  uniformly distributed points on  $\mathbb{T}$ ), e.g., see [48], [87]. For example, the method of Davis [45] takes an  $n$ -tuple of points  $\{z_1, \dots, z_n\}$  on the unit circle, computes an image polygon using the Schwarz-Christoffel formula with these parameters (and the known angles) and compares the side lengths of this polygon with the desired polygon. If a side is too short, the corresponding parameter values are moved apart in the next iteration and conversely. More precisely, if  $\{z_1^k, \dots, z_n^k\}$  is the current guess, and the image polygon has vertices  $\{v_1^k, \dots, v_n^k\}$  we define the next set of parameter guesses as

$$|z_k^{j+1} - z_{j-1}^{k+1}| = k|z_j^k - z_{j-1}^k| \frac{|v_j - v_{j-1}|}{|v_j^k - v_{j-1}^k|},$$

for  $j = 0, \dots, n$  where  $k$  is a normalizing constant and  $\mathbf{v} = \{v_0, \dots, v_n\}$  are the vertices of the target polygon. The method works in practice in many cases but is not known to converge.

Davis' method is used in [7] by Banjai and Trefethen to give a  $O(n)$  method for finding the prevertices that is practical for tens of thousands of vertices (the bound, however is an average case analysis, not a uniform estimate for all polygons). Many other methods exist for computing conformal mappings including integral equation methods that are very effective. For example, in [99] Rokhlin and O'Donnell compute conformal maps using the fast multipole method to solve an integral equation arising from the Kerzman-Stein formula. Marshall has a fast method called "zipper" based on iterating simple maps (see [93]). For surveys of different numerical conformal mapping techniques see, e.g., [46], [63], [75], [83], [101], [125], [129], [132].

A circle packing of a domain is a collection of disjoint (except for tangencies) disks in the domain. The Andreev-Thurston theorem says that given such a packing one can

find a packing of the disk with the same tangency relations and that if the circles are small enough the mapping between the packings is an approximation to the Riemann map [108], [72], [73], [117], [118], [119]. A polynomial time algorithm for computing conformal mappings is described in [115] using a polynomial time algorithm for finding circle packings, but no details are provided about how to choose a packing of a domain in time independent of the geometry. A polynomial time algorithm for circle packings is also described in [96], [97]. Software for computing conformal maps via circle packings is available from Ken Stephenson [116].

An alternate approach to the computational complexity of conformal mapping is considered by Binder, Braverman and Yampolsky in [10]. They consider domains with complicated boundaries (such as fractals) and assume an oracle is given that will decide whether a given point is within  $\epsilon$  of the boundary. The complexity of a domain is determined by how quickly such an oracle works (as a function of  $\epsilon$ ). Given such an oracle they show the Riemann mapping at a point can be computed to accuracy  $\epsilon^a$  using  $b \log^2 \epsilon$  space and  $\epsilon^{-c}$  time for some positive constants  $a, b, c$  (their method solves a Dirichlet problem using a random walk on an  $\epsilon$ -grid stopped by the oracle). This is related to other notions of the computability of conformal maps, such as constructibility in the sense of Brouwer and Errett Bishop, e.g., see [18], [31], [76], [138].

**A.3. Hyperbolic geometry.** On the unit ball,  $\mathbb{B}$ , the hyperbolic metric is given by

$$|d\rho| = \frac{2|dz|}{1 - |z|^2}.$$

More explicitly, it can be written as

$$\rho(z_1, z_2) = \frac{1}{2} \log \frac{1 + |\sigma(z_2, z_1)|}{1 - |\sigma(z_2, z_1)|},$$

where  $\sigma(z_1, z_2) = (z_2 - z_1)/(1 - \bar{z}_1 z_2)$ . In the upper half space model,  $\mathbb{R}_+^3$ , it is given by

$$|d\rho| = \frac{|dz|}{\text{dist}(z, \partial\mathbb{R}^2)}.$$

For the ball and upper half-space models, hyperbolic geodesics are circular arcs that are orthogonal to the boundary (also vertical lines in the case of the half-space).

Hyperbolic area on  $\mathbb{D}$  is defined as  $dx dy/(1 - |z|^2)^2$  and on  $\mathbb{H}$  as  $dx dy/y^2$ . The disk and half-plane have infinite area; indeed, each Whitney square (Section 9) has

area  $\simeq 1$  and the area of a hyperbolic  $r$ -ball is grows exponentially with  $r$ . A striking feature of hyperbolic geometry is that the area of a triangle is determined by its three angles, namely  $\text{area}(T) = \pi - (\alpha + \beta + \gamma)$ . Thus an ideal triangle (one with all three vertices on the boundary) has area  $\pi$  and all other triangles have smaller area.

Simply connected, proper subdomains of the plane inherit a hyperbolic metric from the unit disk via the Riemann map. If  $\varphi : \mathbb{D} \rightarrow \Omega$  is conformal and  $w = \varphi(z)$  then  $\rho_\Omega(w_1, w_2) = \rho_{\mathbb{D}}(z_1, z_2)$  defines the hyperbolic metric on  $\Omega$  and is independent of the particular choice of  $\varphi$ . It is often convenient to estimate  $\rho_\Omega$  in terms of the more geometric “quasi-hyperbolic” metric on  $\Omega$  that is defined as

$$\tilde{\rho}(w_1, w_2) = \inf \int_{w_1}^{w_2} \frac{|dw|}{\text{dist}(w, \partial\Omega)},$$

where the infimum is over all arcs in  $\Omega$  joining  $w_1$  to  $w_2$ .

**Theorem 41** (Koebe’s distortion theorem). *Suppose  $\varphi : \mathbb{D} \rightarrow \Omega$  is a conformal map of the disk to a simply connected domain. Then for all  $z \in \mathbb{D}$ ,*

$$\frac{1}{4}|\varphi'(z)|(1 - |z|^2) \leq \text{dist}(\varphi(z), \partial\Omega) \leq |\varphi'(z)|(1 - |z|^2).$$

Because of Koebe’s distortion theorem we have

$$(15) \quad d\rho_\Omega \leq d\tilde{\rho}_\Omega \leq 4d\rho_\Omega.$$

**Lemma 42.** *Suppose  $\Omega$  is simply connected and  $z \in \Omega$  satisfies  $\text{dist}(z, \partial\Omega) = 1$ . If either  $|w - z| > R$  or  $\text{dist}(w, \partial\Omega) < 1/R$ , then  $\rho_\Omega(z, w) \geq \frac{1}{4} \log R$ .*

*Proof.* Recall that  $\rho_\Omega \geq \frac{1}{4}\tilde{\rho}$  where  $\tilde{\rho}$  denotes the quasi-hyperbolic metric on  $\Omega$ , defined by  $d\tilde{\rho} = |dz|/\text{dist}(z, \partial\Omega)$ . If  $\text{dist}(w, \partial\Omega) \leq 1/R$  then  $\tilde{\rho}(z, w) \geq \int_{1/R}^1 \frac{1}{t} dt = \log R$ . If  $|w - z| \geq R$ , then  $\tilde{\rho}(z, w) \geq \int_1^R \frac{1}{t} dt \geq \log R$ .  $\square$

Möbius transformations are the only 1-1, onto holomorphic maps of the Riemann sphere to itself. In the complex plane we write these maps as  $z \rightarrow (az + b)/(cz + d)$ . Every such map extends uniquely to be a hyperbolic isometry of the upper half-space,  $\mathbb{R}_+^3$ , and every orientation preserving isometry on  $\mathbb{R}_+^3$  is of this form.

**A.4. Conformal modulus:** Suppose  $\Gamma$  is a family of locally rectifiable paths in a planar domain  $\Omega$  and  $\rho$  is a non-negative Borel function on  $\Omega$ . We say  $\rho$  is admissible

for  $\Gamma$  if

$$\ell(\Gamma) = \inf_{\gamma \in \Gamma} \int_{\gamma} \rho ds \geq 1,$$

and define the modulus of  $\Gamma$  as

$$\text{Mod}(\Gamma) = \inf_{\rho} \int_{\Omega} \rho^2 dx dy,$$

where the infimum is over all admissible  $\rho$  for  $\Gamma$ . The reciprocal of the modulus is called the extremal length of the path family. These are important conformal invariants whose basic properties are discussed in many sources such [2]. A simple result we used in this paper is:

**Lemma 43.** *Suppose  $\gamma \subset \mathbb{D}$  is a Jordan arc with one endpoint on  $\partial\mathbb{D}$  and has diameter  $\leq \frac{1}{4}$ . Then the modulus of the path family separating  $\gamma$  from  $B(0, \frac{1}{2})$  in  $\mathbb{D}$  is  $\pi/\log(\text{diam}(\gamma)) + O(1)$ .*

A generalized quadrilateral  $Q$  is a Jordan domain in the plane with four specified boundary points  $x_1, x_2, x_3, x_4$  (in counterclockwise order). We define the modulus of  $Q$ ,  $M_Q(x_1, x_2, x_3, x_4)$  (or just  $M_Q$  or  $M(Q)$  if the points are clear from context), as the modulus of the path family in  $Q$  that connects the arc  $(x_1, x_2)$  to the arc  $(x_3, x_4)$ . This is also the unique positive real number  $M$  such that  $Q$  can be conformally mapped to a  $1 \times M$  rectangle with the arcs  $(x_1, x_2), (x_3, x_4)$  mapping to the opposite sides of length 1. Given a generalized quadrilateral  $Q$  with four boundary points  $x_1, x_2, x_3, x_4$ , the quadrilateral  $Q'$  with vertices  $x_2, x_3, x_4, x_1$  is called the reciprocal of  $Q$  and it is easy to see that  $\text{Mod}(Q') = 1/\text{Mod}(Q)$ . We also call  $\text{Mod}(Q')$  the “extremal distance” from  $(x_1, x_2)$  to the arc  $(x_3, x_4)$  in  $Q$ .

**A.5. Cross ratio:** Given four distinct points  $a, b, c, d$  in the plane we define their cross ratio as

$$\text{cr}(a, b, c, d) = \frac{(d-a)(b-c)}{(c-d)(a-b)}.$$

Note that  $\text{cr}(a, b, c, z)$  is the unique Möbius transformation that sends  $a$  to 0,  $b$  to 1 and  $c$  to  $\infty$ . This makes it clear that cross ratios are invariant under Möbius transformations; that  $\text{cr}(a, b, c, d)$  is real valued iff the four points lie on a circle; and is negative iff in addition the points are labeled in counterclockwise order on the circle. If the four points lie on  $\mathbb{T}$ , then since  $\text{cr}$  and  $M_{\mathbb{D}}$  are both invariant under

Möbius transformations of the disk to itself, each must be a function of the other in this case. The function is explicitly given as an infinite product in Ahlfors' book [2].

**A.6. Quasiconformal mappings.** Quasiconformal mappings are a generalization of conformal mappings that play an important role in modern analysis and a central role in the current paper. There are (at least) three equivalent definitions of a  $K$ -quasiconformal mapping between planar domains. Suppose  $f : \Omega \rightarrow \Omega'$  is a homeomorphism. We say  $f$  is  $K$ -quasiconformal if any of the following equivalent conditions holds:

**Geometric definition:** for any generalized quadrilateral  $Q \subset \Omega$ ,  $\text{Mod}(Q)/K \leq \text{Mod}(f(Q)) \leq K\text{Mod}(Q)$ .

**Analytic definition:**  $f$  is absolutely continuous on almost every vertical and horizontal line and the partial derivatives of  $f$  satisfy  $|f_{\bar{z}}| \leq k|f_z|$  where  $k = (K - 1)/(K + 1)$ .

**Metric definition:** For every  $x \in \Omega$

$$\limsup_{r \rightarrow 0} \frac{\max_{y:|x-y|=r} |f(x) - f(y)|}{\min_{y:|x-y|=r} |f(x) - f(y)|} \leq K.$$

For a proof of the equivalence of the first two, see [2] and for a discussion of the third and a generalization to metric spaces see [74] and its references. In Euclidean space the equivalence of the three definitions is due to Gehring [66], [67], [67]. A composition of a  $K_1$ -quasiconformal map with a  $K_2$ -quasiconformal map is  $(K_1K_2)$ -quasiconformal. Thus the distance used in Theorem 2 satisfies the triangle inequality.

A closed curve in the plane is called a  $K$ -quasicircle if it is the image of a circle under a  $K$ -quasiconformal homeomorphism of the plane and is called a quasicircle if it is a  $K$ -quasicircle for some  $K < \infty$ . Quasicircles have a geometric characterization in terms of Ahlfors' three point condition: a curve  $\gamma$  is a quasicircle iff for any two points  $x, y \in \gamma$  one of the two arcs with endpoints  $x, y$  has diameter  $\leq M|x - y|$ . Quasicircles need not be differentiable; a famous example of a non-differentiable quasicircle is the von Koch snowflake.

Recall that  $\partial f = f_z = \frac{1}{2}(f_x - if_y)$  and  $\bar{\partial} f = f_{\bar{z}} = \frac{1}{2}(f_x + if_y)$ . For a  $K$ -quasiconformal map the ratio  $\mu_f = f_{\bar{z}}/f_z$  is a well defined complex function almost everywhere and satisfies  $\|\mu_f\|_\infty \leq k = (K - 1)/(K + 1)$ . The function  $\mu = \mu_f$  is

called the Beltrami coefficient of  $f$  and satisfies the following composition laws:

$$\begin{aligned} \mu_{f^{-1}} \circ f &= -(f_z/\bar{f}_z)^2 \mu_f, \\ \mu_{g \circ f}(z) &= (f_z(z)/\bar{f}_z(z)) \frac{\mu_g(f(z)) - \mu_f(z)}{1 - \mu_g(f(z))\mu_f(z)}. \end{aligned}$$

If a conformal map of the plane to itself fixes two points, it must be the identity. A  $(1 + \epsilon)$ -quasiconformal map of fixing two points must be close to the identity in the following sense.

**Lemma 44.** *There is a  $0 < k < 1$  and a  $C < \infty$  so that the following holds. Suppose that  $f$  is a quasiconformal mapping of the plane to itself that preserves  $\mathbb{H}$ , fixing  $0, 1$  and  $\infty$  and the Beltrami coefficient of  $f$  is  $\mu$  with  $\|\mu\|_\infty \leq k$ . Then*

$$|f(w) - [w - \frac{1}{\pi} \int_{\mathbb{R}^2} \mu(z) R(z, w) dx dy]| \leq C \|\mu\|_\infty^2,$$

for all  $|w| \leq 1$ , where

$$R(z, w) = \frac{1}{z-w} - \frac{w}{z-1} + \frac{w-1}{z} = \frac{w(w-1)}{z(z-1)(z-w)}.$$

This precise statement Lemma 2.6 [12] but is based on a similar result in [2], Section V.C. If  $|\mu|$  is bounded by  $\epsilon$  then since  $R$  is integrable, this says  $|f(w) - w| = O(\epsilon)$  as long as  $|w|$  is bounded. From this one can deduce

**Lemma 45.** *Suppose  $f : \mathbb{D} \rightarrow \mathbb{D}$  is  $(1 + \epsilon)$ -quasiconformal and that it fixes the boundary points  $1, -1, i$ . Then  $\sup_{x \in \mathbb{T}} |f(x) - x| = O(\epsilon)$ .*

This justifies our claim in the introduction that if we can approximate the prevertices in the QC-sense, then we have also approximated them in the uniform sense. We will also use the estimate:

**Lemma 46.** *Suppose  $f$  is a conformal mapping on  $\mathbb{D}$  such that  $f(0) = 0, f'(0) = 1$  and  $f$  has a  $(1 + \epsilon)$ -quasiconformal extension to the plane fixing  $\infty$ . Then for  $0 \leq r < 1$ ,  $\sup_{|z| \leq r} |f'(z) - 1| = O(\frac{\epsilon}{1-r})$ .*

To prove this, we use equation (10) of Section V.B, [2], which implies that for a  $(1 + \epsilon)$ -QC map  $f$  fixing  $0$  and  $\infty$  we have

$$|f(z)| \leq O(\epsilon) + |z|,$$



if  $|z| \leq 2$ . The same estimate applied to the inverse of  $f$  gives  $\geq |z| - O(\epsilon)$ , so we deduce  $|f(z) - z| \leq O(\epsilon)$  on the closed unit disk. The Cauchy estimates then imply  $|f'(z) - 1| = O(\epsilon/(1 - |z|))$ , which implies the lemma.

The following lemma from [14] is used in this paper to show that certain boundaries can be “flattened” with small quasiconformal distortion.

**Lemma 47.** *Suppose  $G : (x, y) \rightarrow (x, g(x, y))$  is differentiable. Let*

$$L_1(G, z) = \liminf_{w \rightarrow z} \frac{|G(z) - G(w)|}{|z - w|},$$

$$L_2(G, z) = \limsup_{w \rightarrow z} \frac{|G(z) - G(w)|}{|z - w|}.$$

Then

$$(16) \quad \frac{1}{2}(\sqrt{Y} - \sqrt{X}) = L_1(G, z) \leq L_2(G, z) = \frac{1}{2}(\sqrt{Y} + \sqrt{X}),$$

where

$$X = 1 + (g_x)^2 + (g_y)^2 - 2|g_y|, \quad Y = 1 + (g_x)^2 + (g_y)^2 + 2|g_y|.$$

Thus the quasiconformal dilatation of  $G$  is

$$K(z) = \limsup_{r \rightarrow 0} \frac{\max_{|z-w|=r} |G(z) - G(w)|}{\min_{|z-w|=r} |G(z) - G(w)|} = \frac{(\sqrt{Y} + \sqrt{X})}{(\sqrt{Y} - \sqrt{X})},$$

and  $\mu = \frac{K-1}{K+1} = \sqrt{X}/\sqrt{Y}$ . For a map of the form  $(x, y) \rightarrow (x + y + g(x, y))$  this becomes  $\mu = \sqrt{g_x^2 + g_y^2}/\sqrt{g_x^2 + (2 + g_y)^2}$ .

The following, which we also use, follows immediately from the above.

**Lemma 48.** *Suppose  $W \subset \mathbb{D}$  is a domain defined by  $\{z = re^{i\theta} : r < g(\theta)\}$ , where  $1 - \delta \leq g \leq 1$  and  $|g'| \leq \delta$  for all  $\theta$ . Then the map  $z \rightarrow z/g(\arg(z))$  is a  $1 + O(\delta)$  quasiconformal map of  $W$  to the disk.*

As noted earlier, any quasiconformal map has a dilatation  $\mu$  so that  $\|\mu\|_\infty < 1$ . Conversely, the “measurable Riemann Mapping theorem” says that given any such  $\mu$ , there is a  $K$ -quasiconformal map  $f$  with  $\mu = \bar{\partial}f/\partial f$ . The Beltrami equation  $\bar{\partial}f = \mu\partial f$  can be solved using a power series in  $\mu$  by setting

$$f = P[\mu(h + 1)] + z,$$

and

$$h = T\mu + T\mu T\mu + T\mu T\mu T\mu + \dots,$$

where  $T$  is the Beurling transform

$$Th(w) = \lim_{r \rightarrow 0} \frac{1}{\pi} \iint_{|z-w|>r} \frac{h(z)}{(z-w)^2} dx dy,$$

and  $P$  is the Cauchy integral

$$Ph(w) = -\frac{1}{\pi} \iint h(z) \left( \frac{1}{z-w} - \frac{1}{z} \right) dx dy.$$

Formally,  $\bar{\partial}P$  is the identity and  $\partial P = T$ . So if we choose  $f$  as above, then

$$\bar{\partial}f = \mu(h + 1),$$

$$\partial f = T\mu(h + 1) + 1 = h + 1.$$

Hence,  $\bar{\partial}f/\partial f = \mu(1 + h)/(1 + h) = \mu$ , as desired. To make the argument rigorous requires  $L^p$  estimates on these operators as described in [2], Chapter V.

Even though they don't have to be differentiable everywhere, Mori's theorem states that every  $K$ -quasiconformal map is Hölder continuous of order  $1/K$ , i.e.,

$$|f(x) - f(y)| \leq C|x - y|^{1/K}.$$

Moreover, any quasiconformal map of  $\mathbb{D}$  to itself extends continuously to the boundary. We shall discuss these boundary values in more detail below.

Numerical computation of quasiconformal maps with given dilatation is considered in [42], [43], [44].

**A.7. Quasi-isometries:** Quasiconformal maps are a generalization of biLipschitz maps, i.e., maps that satisfy

$$\frac{1}{K} \leq \frac{|f(x) - f(y)|}{|x - y|} \leq K.$$

From the metric definition it is clear that any  $K$ -biLipschitz map is  $K^2$ -quasiconformal.

For  $K$ -quasiconformal self-maps of the disk, there is almost a converse. Although a quasiconformal map  $f : \mathbb{D} \rightarrow \mathbb{D}$  need not be biLipschitz, it is a quasi-isometry of the disk with its hyperbolic metric  $\rho$ , i.e., there are constants  $A, B$  such that

$$\frac{1}{A}\rho(x, y) - B \leq \rho(f(x), f(y)) \leq A\rho(x, y) + B.$$

This says  $f$  is biLipschitz for the hyperbolic metric at large scales. A quasi-isometry is also called a rough isometry in some sources, e.g., [79], [133]. We will say  $f$  is a quasi-isometry with constant  $\epsilon$  if we can take  $A = 1 + \epsilon$  and  $B = \epsilon$ .

In [53] Epstein, Marden and Markovic show that any  $K$ -quasiconformal selfmap of the disk is a quasi-isometry respect to the hyperbolic metric with  $A = K$  and  $B = K \log 2$  if  $1 \leq K \leq 2$  and  $B = 2.37(K - 1)$  if  $K > 2$ . Note that small circles are asymptotically the same for the two metrics, so there is no difference between “hyperbolic-quasiconformal” and “Euclidean-quasiconformal” maps. There is a difference, however, between “hyperbolic biLipschitz” and “Euclidean biLipschitz”.

**Theorem 49.** *For a map  $f : \mathbb{D} \rightarrow \mathbb{D}$  we have (1)  $\Rightarrow$  (2)  $\Rightarrow$  (3)  $\Rightarrow$  (4) where*

- (1)  $f$  is biLipschitz with respect to the hyperbolic metric.
- (2)  $f$  is quasiconformal.
- (3)  $f$  is a quasi-isometry with respect to the hyperbolic metric.
- (4) There is a hyperbolic biLipschitz map  $g : \mathbb{D} \rightarrow \mathbb{D}$  so that  $g|_{\mathbb{T}} = f|_{\mathbb{T}}$ .

*In other words, the three classes of maps (hyperbolic biLipschitz, quasiconformal, hyperbolic quasi-isometry) all have the same set of boundary values.*

The boundary extension is a quasisymmetric homeomorphism, i.e., there is an  $k < \infty$  (depending only on  $K$ ) so that  $1/k \leq |f(I)|/|f(J)| \leq k$ , whenever  $I, J \subset \mathbb{T}$  are adjacent intervals of equal length. Conversely, any quasisymmetric homeomorphism of  $\mathbb{T}$  can be extended to a  $K$ -quasiconformal selfmap of the disk, where  $K$  depends only on  $k$ .

**A.8. Trees-of-intervals.** The dyadic intervals of generation  $n$  in  $\mathbb{R}$  are of the form  $[2^{-n}j, 2^{-n}(j + 1))$  and form the vertices of a infinite binary tree (we say  $I, J$  are adjacent if their lengths differ by a factor of 2 and one contains the other). This property is very useful and in this paper we make use of it through the following results.

**Lemma 50.** *Suppose  $\mathcal{D}$  is a disjoint, finite collection of dyadic intervals, ordered from left to right, and all with length  $\leq L$ . Let  $\mathcal{C}$  be the collection of all dyadic intervals of length  $\leq L$  which contain some element of  $\mathcal{D}$ . If  $\mathcal{C}$  has  $m$  elements, it can be enumerated in time  $O(m)$ .*

*Proof.* Start with the leftmost element  $I_1$  of  $\mathcal{D}$  and form the list  $\gamma_1$ , of nested increasing intervals until reaching size  $L$ . Then move the second element  $I_2$  of  $\mathcal{D}$ , and form the nested, increasing list until we hit an element of  $\gamma_1$ . Form  $\gamma_2$  by cutting  $\gamma_1$  at this point and replacing the bottom portion by the list starting at  $I_2$ . Continue moving to the right. When we have finished, all  $m$  elements of  $\mathcal{C}$  has been found and only  $O(m)$  work has been done.  $\square$

More generally, we define a tree-of-intervals as a collection of half-open intervals  $\mathcal{I}$  which contains a maximal element (an interval containing all the others) and say  $I$  is a child of  $J$  if  $I \subset J$  and  $I$  is maximal in  $\mathcal{I}$  with this property. The tree has degree  $d$  if every interval has at most  $d$  children. We will say such a tree is complete if each interval is either a leaf of the tree or is the union of its children.

**Lemma 51.** *Suppose  $\mathcal{I} = \{I_j\}_1^n$  is a tree-of-intervals of degree  $d$  and  $\mathcal{J} = \{J_j\}_1^m$  is a complete binary tree-of-intervals. Assume the root of  $\mathcal{J}$  contains the root of  $\mathcal{I}$ . Then for every element of  $\mathcal{I}$  we can find the minimum element of  $\mathcal{J}$  containing it in total time  $O(d \cdot n + m)$ .*

*Proof.* This is clearly true if either  $n = 1$  or  $m = 1$ . Consider the case  $n > 1$  and  $m > 1$  and suppose the lemma holds for all pairs where both coordinates are strictly smaller. Let  $I_0, J_0$  be the largest elements of  $\mathcal{I}$  and  $\mathcal{J}$  respectively. Clearly  $I_0 \subset J_0$ . Check the children of  $J_0$  to see if either contains  $I_0$ . Continue this way, creating a path in the  $\mathcal{J}$  tree until we either reach (1) a leaf  $J$  of  $\mathcal{J}$  containing  $I_0$  or (2) an interval  $J$  neither of whose children contain  $I_0$ . This takes work  $C_1 g$  if  $J$  is  $g$  levels below  $J_0$ , since we only have to do a bounded amount of work per level.

In case (1), we assign  $J$  to every element of  $\mathcal{I}$  and we are done. In case (2), we assign  $J$  to  $I_0$  and to every descendent of  $I_0$  which contains the dividing point of  $J$  (the common endpoint it's children  $J_1, J_2$ ). These descendent form a path  $\gamma$  in the  $\mathcal{I}$  tree and if there are  $p$  such descendants we can find them all in time  $C_2 dp$  since we only have to check  $d$  children at each stage.

Now remove  $\gamma$  from the tree  $\mathcal{I}$ . Each connected component of what remains has its intervals either all in  $J_1$  or all in  $J_2$ , and thus satisfies the hypothesis of the lemma with respect to the one of the subtrees  $\mathcal{J}_1, \mathcal{J}_2$  of  $\mathcal{J}$  rooted at these points. By induction the assignments can be done for each component  $\mathcal{I}_k$  in time  $C_3 d \cdot i_k \cdot j_k$

where  $i_k$  is the number of vertices in the  $\mathcal{I}_k$  and  $j_k$  is the number of vertices in the choice of  $\mathcal{J}_1$  or  $\mathcal{J}_2$  covering this component. Summing over all the components gives  $C_3(d(n-p) + (m-g))$ . Added to the  $C_1g + C_2dp$  already done, this proves the lemma.  $\square$

This seems closely related to merging heaps in computer science (a heap is a tree whose vertices are labeled by numbers so that the children's labels are less than the parents), although here the labels are intervals and the ordering is set inclusion.

In Section 14, following Lemma 29 we claimed that in linear time we could find gaps or crescents that were a bounded hyperbolic distance from the image of each Whitney box. Here we give a few more details. Associate to each Whitney square,  $Q_j$ , its base  $I_j \subset \mathbb{R}$ . Then map  $I_j$  to  $\partial\Omega_k$  by the map  $f$  and back to  $\mathbb{R}$  by  $\varphi_k$  (the iota map for  $\Omega_k$ ). Let  $W_j$  be the image of  $Q_j$  under these two maps. Since  $\varphi_k$  is a quasi-isometry,  $W_j$  is a bounded hyperbolic distance from the Whitney box corresponding to the image  $K_j$  of  $I_j$ . The  $\{K_j\}$  still form a tree-of-intervals which we denote  $\mathcal{K}$ . Let  $\mathcal{J}$  be the complete binary tree-of-intervals consisting of the bases of all the bending lamination geodesics. If  $J \in \mathcal{J}$  is the minimal element containing  $K \in \mathcal{K}$ , then the ideal triangle (or crescent if  $J$  is a leaf) bounded above by the geodesic corresponding to  $J$  must hit the Whitney box corresponding to  $K$  and thus is a bounded hyperbolic distance from  $W_j$ . This is what we wanted. Thus finding the claimed gaps/crescents, reduces to an application of Lemma 51.

#### APPENDIX B. FAST POWER SERIES MANIPULATIONS (OR, $O(n \log n)$ SUFFICES)

In order to prove Theorems 1 or 2 with  $C(\epsilon) = O(\log \frac{1}{\epsilon} \log \log \frac{1}{\epsilon})$  we can only use operations on power series of length  $p \sim \log \frac{1}{\epsilon}$  that take time at most  $O(p \log p)$ . In this section we review some basic results about power series manipulations and check that all the operations we need can be carried out this quickly. If one uses naive manipulations of power series, then one simply gets Theorem 2 with a larger constant, e.g.,  $C(\epsilon) = O(\log^c \frac{1}{\epsilon})$  for some  $c$ . To conform with the references, we replace  $p$  by  $n$ ; from this point on  $n$  will refer to the number of terms in a power series (rather than the number of vertices in a polygon, as it did in earlier sections). This summary is taken mostly from [122] and [128].

The Fourier matrix is given by

$$F_n = \begin{pmatrix} 1 & 1 & 1 & \dots & 1 \\ 1 & \omega & \omega^2 & \dots & \omega^{n-1} \\ 1 & \omega^2 & \omega^4 & \dots & \omega^{2(n-1)} \\ \vdots & \vdots & \vdots & \ddots & \vdots \\ 1 & \omega^{n-1} & \omega^{2(n-1)} & \dots & \omega^{(n-1)(n-2)} \end{pmatrix}$$

where  $\omega$  is an  $n$ th root of unity. The fast Fourier transform (FFT) applies  $F_n$  to an  $n$ -vector in time  $O(n \log n)$  [40].  $F_n$  is unitary (after rescaling) and its conjugate transpose,  $F_n^*$ , can also be applied in  $O(n \log n)$  time. The discrete Fourier transform (DFT) takes a  $n$ -long sequence of complex numbers  $\{a_k\}_0^{n-1}$  and a  $n$ -root of unity  $\omega$  and returns the values of the polynomial  $p(z) = a_0 + a_1z + \dots + a_{n-1}z^{n-1}$  at the points  $z = \{1, \omega, \omega^2, \dots, \omega^{n-1}\}$ . Composing DFT with its adjoint returns the original sequence times  $n$ .

Suppose  $f(z) = \sum_{k=0}^n a_k z^k$  and  $g(z) = \sum_{k=0}^n b_k z^k$ . How fast can we multiply, divide or compose these series? Let  $M(n)$  denote the number of field operations it takes to multiply two power series of length  $n$ . The usual process of convolving the coefficients shows  $M(n) = O(n^2)$ . A divide and conquer method of Karatsuba and Ofman [85] improves this to  $O(n^\alpha)$  with  $\alpha = \log 3 / \log 2$ , but the fastest known method uses the Fast Fourier Transform [40], which shows  $M(n) = O(n \log n)$  (two power series of length  $n$  can be multiplied by taking the DFT of each, multiplying the results term-by-term, taking the DFT of the result and finally dividing by  $n$ ).

Other operations on power series are generally estimated in terms of  $M(n)$ . For example, inversion (finding the reciprocal power series,  $1/f$ , given the series for  $f$ ) is  $O(M(n))$ . Like several other operations on power series, this is most easily proven using Newton's method (applied to series rather than numbers). For example,  $1/f$  is the solution of the equation  $\frac{1}{g} - f = 0$ . If  $g_k$  is an approximate solution with  $n > 0$  terms correct, then

$$g_{k+1} = g_k - \frac{\frac{1}{g_k} - f}{-1/g_k^2} = g_k - \frac{f g_k - 1}{z^n} g_k z^n,$$

has  $2n$  correct terms. The right side requires two multiplications and so the work to compute inversions is  $O(M(n)) + O(M(n/2)) + \dots + O(1) = O(M(n))$ .

Given inversion, one can divide power series (multiply  $f$  by  $1/g$ ) compute  $\log f$  (integrate  $f'/f$  term-by-term) or  $\exp(f)$  (solve  $\log g = f$  by Newton's method) all in time  $O(M(n))$ .

Composition of power series is a little harder. Brent and Kung showed that given power series  $f, g$  of order  $n$  and  $g_0 = 0$ , the composition  $f \circ g$  can be computed in time  $\text{Comp}(n) = O(\sqrt{n \log n} M(n))$ . Using FFT multiplication, this gives  $O(n^{3/2} \log^{3/2} n \log \log n)$ . They also showed that reversion (i.e., given  $f$  find  $g$  so  $f \circ g(z) = z$ ) can be solved using Newton's method with the iteration

$$g \rightarrow g - \frac{f \circ g}{f' \circ g},$$

which doubles the number of correct terms in  $g$  with every step. Thus  $\text{Rev}(n) = O(\text{Comp}(n)) = O(\sqrt{n \log n} M(n))$ .

Fortunately, there are some special cases when composition is faster. For example, if we want to post-compose with a linear fractional transformation  $\sigma(z) = (az + b)/(cz + d)$ , this is the same as adding and dividing series, so is only  $O(M(n))$ .

Pre-composing by  $\sigma$  is more complicated. A function  $f$  is called algebraic if it satisfies

$$P_d(z)f(z)^d + \cdots + P_0(z) = 0,$$

for some polynomials  $P_0, \dots, P_d$ . Clearly every rational function is algebraic with  $d = 1$ . The power series of algebraic functions satisfy linear recursions and  $n$  terms of the series can be computed in  $O(n)$ . Moreover, pre-composition by algebraic functions is fast; if  $f$  has  $p$  terms,  $g$  has  $q$  terms and is algebraic of degree  $d$  then the first  $n$  terms of  $f \circ g$  can be computed in time  $O(qd^2 \frac{p(q-v)}{n} M(n + pv) \log n)$  where  $v$  is the valuation of  $P_d$  (the largest power of  $z$  that divides  $P_d(z)$ ) and  $q$  is the maximum of the degrees of  $P_i$ , plus 1. For linear fractional transformations  $v = 0$  and  $q = 2$  so the time to pre-compose by such a map is  $O(M(n) \log n) = O(n \log^2 n)$ . (There is an extensive generalization of the algebraic case to fast manipulations of holonomic functions, as developed by van der Hoeven [127], although we do not need to use it here.)

This is too slow for our purposes. Fortunately, the only times we will have to pre-compose with a Möbius transformation correspond to various manipulations of power and Laurent series in the fast multipole method and all of these can be accomplished

in  $O(n \log n)$  by fast application of Toeplitz, Hankel and Pascal matrices as shown by Tang in [122] (the following discussion is based on [122]).

A matrix is called circulant if each column is a down-shift of the previous one, is called Toeplitz if it is constant on diagonals (slope  $-1$ ) and called Hankel if it is constant on antidiagonals (slope  $1$ ). The general forms of these three types are:

$$C(x) = \begin{pmatrix} x_1 & x_n & x_{n-1} & \dots & x_2 \\ x_2 & x_1 & x_n & \dots & x_3 \\ x_3 & x_2 & x_1 & \dots & x_4 \\ \vdots & \vdots & \vdots & \ddots & \vdots \\ x_n & x_{n-1} & x_{n-2} & \dots & x_1 \end{pmatrix},$$

$$T(x) = \begin{pmatrix} x_0 & x_1 & x_2 & \dots & x_{n-1} \\ x_{-1} & x_0 & x_1 & \dots & x_{n-2} \\ x_{-2} & x_{-1} & x_0 & \dots & x_{n-3} \\ \vdots & \vdots & \vdots & \ddots & \vdots \\ x_{-n+1} & x_{-n+2} & x_{-n+3} & \dots & x_0 \end{pmatrix},$$

$$H(x) = \begin{pmatrix} x_{-n+1} & x_{-n+2} & x_{-n+3} & \dots & x_0 \\ x_{-n+2} & x_{-n+3} & x_{-n+4} & \dots & x_1 \\ x_{-n+3} & x_{-n+4} & x_{-n+5} & \dots & x_2 \\ \vdots & \vdots & \vdots & \ddots & \vdots \\ x_0 & x_1 & x_2 & \dots & x_{n-1} \end{pmatrix}$$

A circulant matrix can be applied to a vector using three applications of FFT, i.e., because  $C_n(x)$  applied to a vector  $y$  is the same as  $\text{IFFT}(\text{FFT}(x) \cdot \text{FFT}(y))$ . A Toeplitz matrix can be embedded in a circulant matrix of the form

$$C_{2n} = \begin{pmatrix} T_n & S_n \\ S_n & T_n \end{pmatrix}$$

where

$$S_n = \begin{pmatrix} 0 & x_{-n+1} & x_{-n+2} & \dots & x_{-1} \\ x_{n-1} & 0 & x_{-n+1} & \dots & x_{-2} \\ x_{n-2} & & 0 & \dots & x_{-3} \\ \vdots & \vdots & \vdots & \ddots & \vdots \\ x_1 & x_2 & x_3 & \dots & 0 \end{pmatrix}$$

To apply  $T$  to an  $n$ -vector  $y$ , append  $n$  zeros to  $y$  to get a  $2n$ -vector, apply  $C_n$  and take the first  $n$  coordinates of the result. This takes  $O(n \log n)$  time. If  $H$  is a Hankel matrix then  $R \cdot H$  is a Toeplitz matrix where  $R$  is the permutation matrix that is 1's on the main anti-diagonal and 0 elsewhere, i.e., it reverses the order of the coordinates



of a vector. Thus  $H = R \cdot (R \cdot H)$ , is a Toeplitz matrix followed by a permutation and can clearly be applied in time  $O(n \log n)$  as well.

The Pascal matrix is lower triangular with its  $(j, k)$ th entry being the binomial coefficient  $C_i^j = \binom{i}{j}$ .

$$\begin{pmatrix} 1 & 0 & 0 & \dots & 0 \\ 1 & 1 & 0 & \dots & 0 \\ 1 & 2 & 1 & \dots & 0 \\ \vdots & \vdots & \vdots & \ddots & \vdots \\ C_{n-1}^0 & C_{n-1}^1 & C_{n-1}^2 & \dots & C_{n-1}^{n-1} \end{pmatrix}$$

This matrix can be written as  $P = \text{diag}(v_1) \cdot T \cdot \text{diag}(v_2)$  where

$$v_1 = (1, 1, 2!, 3!, \dots, (n-1)!),$$

$v_2 = \frac{1}{v_1}$  (term-wise) and  $T$  is the Toeplitz matrix

$$T = \begin{pmatrix} 1 & 0 & 0 & \dots & 0 \\ 1 & 1 & 0 & \dots & 0 \\ \frac{1}{2!} & 1 & 1 & \dots & 0 \\ \vdots & \vdots & \vdots & \ddots & \vdots \\ \frac{1}{(n-1)!} & \frac{1}{(n-2)!} & \frac{1}{(n-3)!} & \dots & 1 \end{pmatrix}$$

The diagonal matrices can be applied in  $O(n)$  and the Toeplitz in  $O(n \log n)$  and hence so can  $P$ . Similarly for the transpose of  $P$ .

Now for the applications to fast multipole translation operators. There are three types of conversions to consider. First, local to local translation

$$\sum_{k=0}^{n-1} a_k (z-a)^k \rightarrow \sum_{k=0}^{n-1} b_k (z-b)^k,$$

then multipole to local

$$\sum_{k=0}^n a_k (z-a)^{-k} \rightarrow \sum_{k=0}^n b_k (z-b)^k,$$

and finally, multipole to multipole,

$$\sum_{k=0}^n a_k (z-a)^{-k} \rightarrow \sum_{k=0}^n b_k (z-b)^{-k}.$$

Let  $c = b - a$  and consider the local-to-local translation. We have

$$\sum_{k=0}^{n-1} a_k (w - c)^k = \sum_{k=0}^{n-1} a_k \sum_{j=0}^k w^j (-c)^{k-j} \binom{k}{j},$$

so the matrix corresponding to local translation has  $k$ th column

$$((-c)^k, (-c)^{k-1} \binom{k}{1}, \dots, (-c)^0 \binom{k}{k}, 0, \dots, 0)^t$$

or

$$LL = \begin{pmatrix} 1 & -c & c^2 & \dots & (-c)^{n-1} \\ 0 & 1 & -2c & \dots & (-c)^{n-2} C_{n-1}^1 \\ 0 & 0 & 1 & \dots & (-c)^{n-3} C_{n-1}^2 \\ \vdots & \vdots & \vdots & \ddots & \vdots \\ 0 & 0 & 0 & \dots & 1 \end{pmatrix}$$

This matrix is equal to

$$\text{diag}(1, -c, \dots, (-c)^{n-1}) \cdot P' \cdot \text{diag}(1, -c^{-1}, \dots, (-c)^{-n+1}),$$

where  $P'$  is the transpose of  $P$ . The diagonal matrices can be applied in  $O(n)$  time and  $P'$  can be applied in  $O(n \log n)$ . Thus local-to-local translations can be done this fast.

Similarly, the multipole-to-multipole and multipole-to-local transformations correspond to applying the matrices

$$MM = \begin{pmatrix} 1 & 0 & 0 & \dots & 0 \\ \binom{1}{1}c & 1 & 0 & \dots & 0 \\ \binom{2}{2}c^2 & \binom{2}{1}c & 1 & \dots & \\ \vdots & \vdots & \vdots & \ddots & \vdots \\ \binom{n-1}{n-1}c^{n-1} & \binom{n-1}{n-2}c^{n-2} & \binom{n-1}{n-3}c^{n-3} & \dots & 1 \end{pmatrix}$$

$$ML = \begin{pmatrix} -c^{-1} & c^{-2} & c^{-3} & \dots & c^{-n+1} \\ -c^{-2} & 2c^{-3} & -3c^{-4} & \dots & \\ -c^{-3} & 3c^{-4} & -6c^{-5} & \dots & \\ \vdots & \vdots & \vdots & \ddots & \vdots \\ -c^{-n+1} & (n-1)c^{-n} & -\binom{n}{2}c^{-n-1} & \dots & (-1)^{n-1} \binom{2p-2, p-1}{c}^{-2n-1} \end{pmatrix}.$$

We can rewrite these matrices as

$$MM = \text{diag}(1, c, \dots, c^{n-1}) \cdot P \cdot \text{diag}(1, c^{-1}, \dots, c^{-n+1}),$$

$$ML = \text{diag}(1, c^{-1}, \dots, c^{1-n}) \cdot P \cdot P' \cdot \text{diag}(-c^{-1}, c^{-2}, \dots, (-c)^{-n}),$$

where  $P'$  is the transpose of  $P$ . As with local translations, these are compositions of diagonal matrices (which can be applied in  $O(n)$ ) and matrices that can be applied in  $O(n \log n)$  time.

We will also use structured matrices to compute expansions around  $\infty$  of functions of the form  $\int \frac{d\mu(z)}{(z-w)^k}$ ,  $k = 1, 2, 3$ . We will only consider the Cauchy transform ( $k = 1$ ) since the others can be obtained by term-by-term differentiation of that one. Suppose  $f(z) = \sum_{k=0}^n a_k z^k$  is a power series for an analytic function, bounded by one and defined on  $\mathbb{D}$  and  $\varphi(x, y)$  is a polynomial in  $x$  and  $y$  of uniformly bounded degree. Then the Cauchy transform

$$F(w) = \int_S \frac{f(z)\varphi(x, y)dx dy}{z - w},$$

is analytic in  $w$  outside  $S = [-\frac{1}{2}, \frac{1}{2}]^2$ , so has an expansion  $F(w) = \sum_{k=1}^{\infty} b_k w^{-k}$ . Given  $\{a_k\}_0^n$ , thinking of  $\varphi$  as fixed, we want to compute  $\{b_k\}_1^n$ . For each monomial of the form  $z^k x^a y^b$  we can precompute the expansion using explicit formulas ( $O(n)$  for each of  $O(n)$  monomials) and then we simply apply the resulting matrix to the vector  $\{a_k\}$ . Naively, we can do this in time  $O(n^2)$ .

Actually we can compute the expansion in only  $O(n \log n)$ . Let  $d\mu = x^a y^b dx dy$  restricted to  $Q = [0, 1]^2$ . We want to compute the expansion at  $\infty$  of

$$\begin{aligned} F(w) &= \iint \frac{z^n}{w - z} d\mu(z) = \iint z^n \frac{1}{w} \left(1 + \frac{z}{w} + \left(\frac{z}{w}\right)^2 + \dots\right) d\mu(z) \\ &= \sum_{k=0}^{\infty} w^{-k-1} \iint z^{n+k} d\mu(z) \\ &= \sum_{k=1}^{\infty} a_{k,n} w^{-k}, \end{aligned}$$

where

$$a_{k,n} = c(n + k + 1, a, b) = \iint_Q (x + iy)^{n+k-1} x^a y^b dx dy.$$

Since  $a_{k,n}$  only depends on  $k + n$ ,  $A$  is a Hankel matrix. As noted above, a  $n \times n$  Hankel matrix can be applied to a  $n$ -vector using FFT in time  $O(n \log n)$ .

The individual coefficients have explicit formulas involving Euler's Beta function. Evaluations for a few small values of  $a, b$  (as given by *Mathematica* are)

$$c(n, 0, 0) = \frac{i - i^{n+1} + 2(1 + i)^n}{2 + 3n + n^2},$$

$$c(n, 1, 0) = \frac{2i - i^n + in + 2(1+i)^n((2-i) + n)}{(1+n)(2+n)(3+n)},$$

$$c(n, 2, 0) = \frac{i(6 + 2i^n + 5n + n^2) + 2(1+i)^n((4-4i) + n((5-2i) + n))}{(1+n)(2+n)(3+n)(4+n)}$$

$$c(n, 1, 1) = -\frac{1 + i^n - 2(1+i)^n(2+n)}{(1+n)(2+n)(4+n)},$$

$$c(n, 2, 1) = \frac{-3(2i)i^n - n + 2(1+i)^n(1+n)((4-i) + n)}{(1+n)(2+n)(3+n)(5+n)},$$

$$c(n, 0, 1) = \frac{-1 - i^{n+1}(2+n) + 2(1+i)^n((2+i) + n)}{(1+n)(2+n)(3+n)}.$$

Thus  $n$ -term Laurent expansions for Beurling transforms of the appropriate degree  $n$  polynomials can be computed in time  $O(n \log n)$ .

In Section 11 we claimed that  $\epsilon$ -representations and partial representations could be computed from each other quickly. We can now see why this is true. Given a  $O(n)$ -term Laurent expansion on an annulus we can clearly create  $O(n)$ -term power series expansions that approximate it on disks contained in the annulus in time  $O(n \log n)$ , just as with the multipole to local conversions discussed before. If the double of the disk is contained in the annulus where the function is bounded by 1, then the convergence of the power series is geometric and  $O(n)$  terms give accuracy of order  $\lambda^n$  for some  $\lambda < 1$ . Thus we can do the conversion from representations to partial representations.

To go the other direction, we need to compute the coefficients of a Laurent expansion for  $f$  from knowing power series approximations for  $f$  on disks that cover a contour  $\gamma$  around the origin. The coefficients can be computed exactly as integrals of the form  $\int_{\gamma} f(z)z^k dz$ . This integral can be broken into pieces  $\int_{\gamma_n}$  where  $\gamma = \cup_n \gamma_n$  is a decomposition of  $\gamma$  into pieces, where each piece stays inside one of the disks where we have a power series approximation for  $f$ . If this approximation is of the form  $\sum_j a_j(z-a)^j$ , then we wish to evaluate integrals of the form

$$\int_{\gamma_n} \left( \sum_j a_j(z-a)^j \right) z^k dz.$$

We can convert  $z^k$  to a series with center  $a$ , e.g.,  $z^k = \sum_q b_{q,k}(z-a)^q$  just as before with Pascal matrices and then we have to evaluate

$$\begin{aligned} \int_{\gamma_n} \left( \sum_j a_j (z-a)^j \right) \left( \sum_q b_{q,k} (z-a)^q \right) dz &= \sum_q \sum_j a_j b_{q,k} \int_{\gamma_n} (z-a)^{j+q} dz \\ &= \sum_q I_{j,k} \sum_j b_{q,k} a_j \end{aligned}$$

where  $b_{q,k}$  is a Pascal matrix and  $I_{j,q} = \int_{\gamma_n} (z-a)^{j+q} dz$  is an explicit Hankel matrix. We have seen above that both types of matrix can be applied in  $O(n \log n)$ . So that the contour integral using the power series on each piece of the contour can be evaluated this fast. If the power series approximations agree with the Laurent series to within  $\epsilon$  then resulting coefficients will be accurate up to an error of  $\int_{\gamma} \epsilon |dz| = O(|\gamma| \epsilon)$ . Normalizing so that  $\gamma$  and its image both have length about 1, we see that the coefficients are accurate to  $O(\epsilon)$  and so the reconstructed Laurent series agrees with the original to within  $\sum_k \epsilon = O(n\epsilon) = O(\epsilon \log \epsilon) = O(\epsilon^{1-\beta})$  with  $\beta$  as close to 0 as we wish (taking a larger constant in front).

The compositions of power series considered earlier were exact computations in the sense that given two  $n$ -term power series,  $f$  and  $g$ , we are computing the exact first  $n$  coefficients of  $f \circ g$ . However, they are inexact in the sense that we are truncating up to  $n^2 - n$  terms of the full composition. We will be most interested in the case when  $f$  and  $g$  are conformal maps whose power series coefficients decay exponentially. Then the  $n$ -term truncation of  $f \circ g$  equals  $f \circ g$  up to an error of  $e^{-cn}$ . Since the truncation introduces an error anyway, we may as well tolerate an error of the same size coming from an inexact computation of the first  $n$  terms that we keep. Can we approximate the first  $n$  terms of  $f \circ g$  faster than we can compute them exactly (i.e., faster than  $O(n^{3/2} \log^{3/2} n \log \log n)$ )? The answer is yes, at least in the special case that we care about.

**Lemma 52.** *Suppose  $f$  and  $g$  are conformal maps of  $D(0, R)$ ,  $R \geq 2$  such that  $f$  has a  $(1 + \epsilon)$ -quasiconformal extension to  $\mathbb{R}^2$  that fixes  $\infty$ . Assume also that  $f(0) = g(0)$  and  $f'(0) = g'(0) = 1$ . Then given the first  $n$  terms of the power series for  $f$  and  $g$  we can compute in time  $O(n \log n)$ , an  $O(n)$  term power series  $h$  so that  $|h - g \circ f^{-1}| \leq O(\epsilon^{2(1-\beta)})$  on  $D(0, 1)$ .*

*Proof.* Let  $\{\omega_j\}_0^{n-1}$  denote the  $n$ th roots of unity. Using the FFT we can compute the images of all these points under either  $f$  or  $g$  in time  $O(n \log n)$ . By Lemma 46,  $|f' - 1| = O(\epsilon)$  on  $D(0, 2)$  and hence if  $|z - \omega_j| = O(\epsilon)$ ,

$$f(z) = f(\omega_j) + (1 + O(\epsilon))(z - \omega_j) + O(|z - \omega_j|^2).$$

In particular, if  $w = f(z)$ ,

$$\begin{aligned} f^{-1}(w) &= w + (\omega_j - f(\omega_j)) + O(\epsilon|z - \omega_j|) + O(|z - \omega_j|^2) \\ &= w + (\omega_j - f(\omega_j)) + O(\epsilon^2). \end{aligned}$$

Thus taking  $w = \omega_j$ ,

$$f^{-1}(\omega_j) = \omega_j + (\omega_j - f(\omega_j)) + O(\epsilon^2).$$

Therefore, we get

$$\begin{aligned} g \circ f^{-1}(\omega_j) &= g(\omega_j) + g'(\omega_j)(\omega_j - f(\omega_j)) + O(|\omega_j - f(\omega_j)|^2) + O(\epsilon^2) \\ &= g(\omega_j) + g'(\omega_j)(\omega_j - f(\omega_j)) + O(\epsilon^2). \end{aligned}$$

So define a degree  $n$  polynomial by setting its values on the roots of unity using

$$h(\omega_j) = g(\omega_j) + g'(\omega_j)(\omega_j - f(\omega_j)).$$

Since we can compute and evaluate  $g$  and  $g'$  at the roots of unity in  $O(n \log n)$ , we can find the series expansion for  $h$  around 0 in time  $O(n \log n)$  using an FFT.

Clearly  $h$  is a good approximation to  $g \circ f^{-1}$  on the  $n$ th roots of unity (they differ by  $O(\epsilon^2)$  on these points). What about the rest of  $\mathbb{D}$ ? We shall show that the functions differ by at most  $O(\epsilon^2)$  on  $\mathbb{D}$  as well. Let

$$\sigma(z) = \prod_{j=0}^{n-1} (z - \omega_j) = z^n - 1.$$

Let

$$\psi(z) = \sum_{k=0}^{n-1} \frac{h(\omega_j)/(n\omega_j^{n-1})}{z - \omega_j}.$$

The zeros of  $\sigma$  cancel the simple poles of  $\psi$ , so  $P = \psi \cdot \sigma$  is entire and since  $|\sigma| \sim |z|^n$  and  $|\psi| \sim |z|^{-1}$  near  $\infty$ ,  $P$  must be a polynomial of degree  $n - 1$ . Moreover, by

l'Hopital's rule

$$\begin{aligned} \frac{h(\omega_j)}{n\omega_j^{n-1}} &= \lim_{z \rightarrow \omega_j} (z - \omega_j)\psi(z) \\ &= \lim_{z \rightarrow \omega_j} (z - \omega_j) \frac{P(z)}{\sigma(z)} \\ &= \frac{1 \cdot P(\omega_j) + (\omega_j - \omega_j)P'(\omega_j)}{\sigma'(\omega_j)} = \frac{P(\omega_j)}{\sigma'(\omega_j)}, \end{aligned}$$

which implies  $P(\omega_j) = h(\omega_j)$  for all  $j = 0, \dots, n-1$ , and this means  $P = h$  as polynomials. Thus

$$\begin{aligned} |h(z)| = |P(z)| &\leq |\psi(z)| \cdot |\sigma(z)| \\ &\leq (\max_j |h(\omega_j)|) \sum_{j=0}^{n-1} \frac{1/n}{|z - \omega_j|} \cdot (|z^n| + 1) \\ &\leq 4M, \end{aligned}$$

if  $|z| \leq 1/2$  and  $M = \max_j |h(\omega_j)|$ .

Suppose  $1 < r < R/2$ . The map  $g \circ f^{-1}$  is conformal on  $D(0, R/2)$  (if  $\epsilon$  is small enough), so its power series at 0 has terms that decay like  $(2/R)^k$ . If  $H$  is the  $m$ -term truncation of this power series and we choose  $m \sim n$  large enough, then  $|H - g \circ f^{-1}| \leq O((2/R)^m) = O(\epsilon^2)$  on  $\mathbb{D}$ . Since  $H$  is a degree  $n-1$  polynomial that interpolates its own values on the roots of unity,  $H - h$  is a degree  $n-1$  polynomial with values  $= O((2/R)^n)$  on the  $n$ th roots of unity and hence, by our calculation above applied to  $H - h$ , is bounded by  $O(\epsilon^2)$  on  $\mathbb{D}$ . By Lemma 21, this means that a truncation  $h_t$  of  $h$  satisfies

$$|h_t(z) - g \circ f^{-1}(z)| = O(\epsilon^{2(1-\beta)}),$$

on  $D(0, r)$  where  $r = R^\beta$ . □

Exact evaluation of a degree  $n$  polynomial at  $m$  points takes  $O((n+m) \log^2(n+m))$  [3] and recovering a degree  $n-1$  polynomial from its values at  $n$  points takes  $O(n \log^2 n)$ , so our approximate method is faster for the cases we consider. Multipole methods can also be used to give faster approximate evaluation and interpolation algorithms. See [51], [107]. These are  $O(n \log \frac{1}{\epsilon})$  where  $n$  is the degree and  $\epsilon$  is the desired accuracy. In our case, however,  $n \sim \log \frac{1}{\epsilon}$ , so this is not faster than exact calculation.

## REFERENCES

- [1] A. Aggarwal, L. J. Guibas, J. Saxe, and P. W. Shor. A linear-time algorithm for computing the Voronoi diagram of a convex polygon. *Discrete Comput. Geom.*, 4(6):591–604, 1989.
- [2] L. V. Ahlfors. *Lectures on quasiconformal mappings*. The Wadsworth & Brooks/Cole Mathematics Series. Wadsworth & Brooks/Cole Advanced Books & Software, Monterey, CA, 1987. With the assistance of Clifford J. Earle, Jr., Reprint of the 1966 original.
- [3] A. V. Aho, K. Steiglitz, and J. D. Ullman. Evaluating polynomials at fixed sets of points. *SIAM J. Comput.*, 4(4):533–539, 1975.
- [4] F. Aurenhammer. Voronoi diagrams - a survey of a fundamental geometric data structure. *ACM Comp. Surveys*, 23:345–405, 1991.
- [5] F. Aurenhammer and R. Klein. Voronoi diagrams. In *Handbook of computational geometry*, pages 201–290. North-Holland, Amsterdam, 2000.
- [6] T. F. Banchoff and P. J. Giblin. Global theorems for symmetry sets of smooth curves and polygons in the plane. *Proc. Roy. Soc. Edinburgh Sect. A*, 106(3-4):221–231, 1987.
- [7] L. Banjai and L. N. Trefethen. A multipole method for Schwarz-Christoffel mapping of polygons with thousands of sides. *SIAM J. Sci. Comput.*, 25(3):1042–1065 (electronic), 2003.
- [8] M. Bern and D. Eppstein. Mesh generation and optimal triangulation. In *Computing in Euclidean geometry*, volume 1 of *Lecture Notes Ser. Comput.*, pages 23–90. World Sci. Publishing, River Edge, NJ, 1992.
- [9] A. Beurling and L. Ahlfors. The boundary correspondence under quasiconformal mappings. *Acta Math.*, 96:125–142, 1956.
- [10] I. Binder, M. Braverman, and M. Yampolsky. On the computational complexity of the Riemann mapping. *Ark. Mat.*, 45(2):221–239, 2007.
- [11] C. J. Bishop. Divergence groups have the Bowen property. *Ann. of Math. (2)*, 154(1):205–217, 2001.
- [12] C. J. Bishop. BiLipschitz approximations of quasiconformal maps. *Ann. Acad. Sci. Fenn. Math.*, 27(1):97–108, 2002.
- [13] C. J. Bishop. Quasiconformal Lipschitz maps, Sullivan’s convex hull theorem and Brennan’s conjecture. *Ark. Mat.*, 40(1):1–26, 2002.
- [14] C. J. Bishop. An explicit constant for Sullivan’s convex hull theorem. In *In the tradition of Ahlfors and Bers, III*, volume 355 of *Contemp. Math.*, pages 41–69. Amer. Math. Soc., Providence, RI, 2004.
- [15] C. J. Bishop and H. Hakobyan. A central set of dimension 2. *Proc. Amer. Math. Soc.*, 136(7):2453–2461, 2008.
- [16] C.J. Bishop. Bounds for the CRDT algorithm. To appear in *Computational Methods in Function Theory*.
- [17] C.J. Bishop. A fast QC-mapping theorem for polygons. 2009. Preprint.
- [18] E. Bishop and D. Bridges. *Constructive analysis*, volume 279 of *Grundlehren der Mathematischen Wissenschaften [Fundamental Principles of Mathematical Sciences]*. Springer-Verlag, Berlin, 1985.
- [19] H. Blum. A transformation for extracting new descriptors of shape. In W.W. Dunn, editor, *Proc. Symp. Models for the perception of speech and visual form*, pages 362–380, Cambridge, 1967. MIT Press.
- [20] H. Blum. Biological shape and visual science. *Journal of Theoretical Biology*, 38:205–287, 1973.
- [21] H. Blum and R.N. Nagel. Shape descriptors using weighted symmetric axis functions. *Pattern Recognition*, 10(3):167–180, 1978.
- [22] M. Bridgeman. Average bending of convex pleated planes in hyperbolic three-space. *Invent. Math.*, 132(2):381–391, 1998.



- [23] M. Bridgeman. Average curvature of convex curves in  $H^2$ . *Proc. Amer. Math. Soc.*, 126(1):221–224, 1998.
- [24] M. Bridgeman and R. D. Canary. From the boundary of the convex core to the conformal boundary. *Geom. Dedicata*, 96:211–240, 2003.
- [25] J. W. Bruce, P. J. Giblin, and C. G. Gibson. Symmetry sets. *Proc. Roy. Soc. Edinburgh Sect. A*, 101(1-2):163–186, 1985.
- [26] R. D. Canary. The conformal boundary and the boundary of the convex core. *Duke Math. J.*, 106(1):193–207, 2001.
- [27] L. Carleson. Interpolations by bounded analytic functions and the corona problem. *Ann. of Math. (2)*, 76:547–559, 1962.
- [28] F. Chazal and A. Lieutier. Stability and homotopy of a subset of the medial axis. *Proc. 9th ACM Sympos. Solid Modeling Appl.*, 2004.
- [29] F. Chazal and R. Soufflet. Stability and finiteness properties of medial axis and skeleton. *J. Dynam. Control Systems*, 10(2):149–170, 2004.
- [30] B. Chazelle. Triangulating a simple polygon in linear time. *Discrete Comput. Geom.*, 6(5):485–524, 1991.
- [31] H. Cheng. A constructive Riemann mapping theorem. *Pacific J. Math.*, 44:435–454, 1973.
- [32] C.-S. Chiang and C.M. Hoffmann. The medial axis transform for 2d regions. *ACM Transactions on graphics*, 1982.
- [33] F. Chin, J. Snoeyink, and C. A. Wang. Finding the medial axis of a simple polygon in linear time. *Discrete Comput. Geom.*, 21(3):405–420, 1999.
- [34] H. I. Choi, S. W. Choi, and H. P. Moon. Mathematical theory of medial axis transform. *Pacific J. Math.*, 181(1):57–88, 1997.
- [35] S. W. Choi and H.-P. Seidel. Hyperbolic Hausdorff distance for medial axis transformation. *Graphical Models*, 63:369–384, 2001.
- [36] S. W. Choi and H.-P. Seidel. Linear one-sided stability of MAT for weakly injective domain. *J. Math. Imaging Vision*, 17(3):237–247, 2002.
- [37] S.W. Choi and S.-W. Lee. Stability analysis of medial axis transform. In *Proc. 15th ICPR Brcelona, Spain*, volume 3, pages 139–142, 2000.
- [38] E.B. Christoffle. Sul problema della temperature stazonaire e la rappresetazione di una data superficie. *Ann. Mat. Pura Appl. Serie II*, pages 89–103, 1867.
- [39] B. Cipra. The best of the 20th century: Editors name top 10 algorithms. *SIAM News*, 33(4):1, May 2000.
- [40] J. W. Cooley and J. W. Tukey. An algorithm for the machine calculation of complex Fourier series. *Math. Comp.*, 19:297–301, 1965.
- [41] T. Culver, J. Keyser, and D. Manocha. Accurate computation of the medial axis of a polyhedron. In *Proceedings of the fifth ACM symposium on Solid modeling and applications, June 8-11, 1999, Ann Arbor, MI USA*, pages 179–190, 1999.
- [42] P. Daripa. A fast algorithm to solve nonhomogeneous Cauchy-Riemann equations in the complex plane. *SIAM J. Sci. Statist. Comput.*, 13(6):1418–1432, 1992.
- [43] P. Daripa. A fast algorithm to solve the Beltrami equation with applications to quasiconformal mappings. *J. Comput. Phys.*, 106(2):355–365, 1993.
- [44] P. Daripa and D. Mashat. An efficient and novel numerical method for quasiconformal mappings of doubly connected domains. *Numer. Algorithms*, 18(2):159–175, 1998.
- [45] R.T. Davis. Numerical methods for coordinate generation based on Schwarz-Christoffel transformations. In *4th AIAA Comput. FLuid Dynamics Conf., Williamsburg VA*, pages 1–15, 1979.

- [46] T. K. DeLillo. The accuracy of numerical conformal mapping methods: a survey of examples and results. *SIAM J. Numer. Anal.*, 31(3):788–812, 1994.
- [47] G.L. Dirichlet. Über die reduction der positiven quadratischen formen mit drei unbestimmten ganzen zahlen. *J. Reine Angew. Math.*, 40:209–227, 1850.
- [48] T. A. Driscoll and L. N. Trefethen. *Schwarz-Christoffel mapping*, volume 8 of *Cambridge Monographs on Applied and Computational Mathematics*. Cambridge University Press, Cambridge, 2002.
- [49] T. A. Driscoll and S. A. Vavasis. Numerical conformal mapping using cross-ratios and Delaunay triangulation. *SIAM J. Sci. Comput.*, 19(6):1783–1803 (electronic), 1998.
- [50] H. B. Duan and E. Rees. The existence of bitangent spheres. *Proc. Roy. Soc. Edinburgh Sect. A*, 111(1-2):85–87, 1989.
- [51] A. Dutt, M. Gu, and V. Rokhlin. Fast algorithms for polynomial interpolation, integration, and differentiation. *SIAM J. Numer. Anal.*, 33(5):1689–1711, 1996.
- [52] D. B. A. Epstein and A. Marden. Convex hulls in hyperbolic space, a theorem of Sullivan, and measured pleated surfaces. In *Analytical and geometric aspects of hyperbolic space (Coventry/Durham, 1984)*, volume 111 of *London Math. Soc. Lecture Note Ser.*, pages 113–253. Cambridge Univ. Press, Cambridge, 1987.
- [53] D. B. A. Epstein, A. Marden, and V. Markovic. Quasiconformal homeomorphisms and the convex hull boundary. *Ann. of Math. (2)*, 159(1):305–336, 2004.
- [54] D. B. A. Epstein, A. Marden, and V. Markovic. Complex earthquakes and deformations of the unit disk. *J. Differential Geom.*, 73(1):119–166, 2006.
- [55] D. B. A. Epstein, A. Marden, and V. Markovic. Convex regions in the plane and their domes. *Proc. London Math. Soc. (3)*, 92(3):624–654, 2006.
- [56] D. B. A. Epstein and V. Markovic. The logarithmic spiral: a counterexample to the  $K = 2$  conjecture. *Ann. of Math. (2)*, 161(2):925–957, 2005.
- [57] P. Erdős. On the Hausdorff dimension of some sets in Euclidean space. *Bull. Amer. Math. Soc.*, 52:107–109, 1946.
- [58] G. Evans, A. Middleditch, and N. Miles. Stable computation of the 2D medial axis transform. *Internat. J. Comput. Geom. Appl.*, 8(5-6):577–598, 1998.
- [59] W. D. Evans and D. J. Harris. Sobolev embeddings for generalized ridged domains. *Proc. London Math. Soc. (3)*, 54(1):141–175, 1987.
- [60] S. Fortune. Voronoï diagrams and Delaunay triangulations. In *Computing in Euclidean geometry*, volume 1 of *Lecture Notes Ser. Comput.*, pages 193–233. World Sci. Publishing, River Edge, NJ, 1992.
- [61] S. Fortune. Voronoi diagrams and Delaunay triangulations. In *Handbook of discrete and computational geometry*, CRC Press Ser. Discrete Math. Appl., pages 377–388. CRC, Boca Raton, FL, 1997.
- [62] D. H. Fremlin. Skeletons and central sets. *Proc. London Math. Soc. (3)*, 74(3):701–720, 1997.
- [63] D. Gaier. *Konstruktive Methoden der konformen Abbildung*. Springer Tracts in Natural Philosophy, Vol. 3. Springer-Verlag, Berlin, 1964.
- [64] J. B. Garnett. *Bounded analytic functions*, volume 96 of *Pure and Applied Mathematics*. Academic Press Inc. [Harcourt Brace Jovanovich Publishers], New York, 1981.
- [65] C. Gaudeau, M. Boiron, and J. Thouvenot. Squelettisation et anamorphose dans l'étude de la dynamique des déformations des structures: application à l'analyse de la motricité gastrique. In *Recognition of shapes and artificial intelligence (Second AFCET-IRIA Cong., Toulouse, 1979)*, Vol. III (French), pages 57–63. IRIA, Rocquencourt, 1979.
- [66] F. W. Gehring. The definitions and exceptional sets for quasiconformal mappings. *Ann. Acad. Sci. Fenn. Ser. A I No.*, 281:28, 1960.

- [67] F. W. Gehring. Symmetrization of rings in space. *Trans. Amer. Math. Soc.*, 101:499–519, 1961.
- [68] P. Giblin. Symmetry sets and medial axes in two and three dimensions. In *The mathematics of surfaces, IX (Cambridge, 2000)*, pages 306–321. Springer, London, 2000.
- [69] P. J. Giblin and D. B. O’Shea. The bitangent sphere problem. *Amer. Math. Monthly*, 97(1):5–23, 1990.
- [70] L. Greengard and V. Rokhlin. A fast algorithm for particle simulations. *J. Comput. Phys.*, 73(2):325–348, 1987.
- [71] H. N. Gursoy and N. M. Patrikalakis. Automated interrogation and adaptive subdivision of shape using medial axis transform. *Advances in Engineering Software and Workstations*, 13(5/6):287–302, 1991.
- [72] Z.-X. He and O. Schramm. On the convergence of circle packings to the Riemann map. *Invent. Math.*, 125(2):285–305, 1996.
- [73] Z.-X. He and O. Schramm. The  $C^\infty$ -convergence of hexagonal disk packings to the Riemann map. *Acta Math.*, 180(2):219–245, 1998.
- [74] J. Heinonen and P. Koskela. Quasiconformal maps in metric spaces with controlled geometry. *Acta Math.*, 181(1):1–61, 1998.
- [75] P. Henrici. *Applied and computational complex analysis. Vol. 3.* Pure and Applied Mathematics. John Wiley & Sons Inc., New York, 1986. Discrete Fourier analysis—Cauchy integrals—construction of conformal maps—univalent functions, A Wiley-Interscience Publication.
- [76] P. Hertling. An effective Riemann mapping theorem. *Theoret. Comput. Sci.*, 219(1-2):225–265, 1999. Computability and complexity in analysis (Castle Dagstuhl, 1997).
- [77] C.M. Hoffmann. Computer vision, descriptive geometry and classical mechanics. In *Computer Graphics and Mathematics*, pages 229–244. Springer Verlag, Eurographics Series, 1992.
- [78] C.M. Hoffmann and D. Dutta. On the skeleton of simple CSG objects. *Trans. ASME*, 115:87–94, 1993.
- [79] I. Holopainen. Rough isometries and  $p$ -harmonic functions with finite Dirichlet integral. *Rev. Mat. Iberoamericana*, 10(1):143–176, 1994.
- [80] L. Hörmander. *The analysis of linear partial differential operators. I*, volume 256 of *Grundlehren der Mathematischen Wissenschaften [Fundamental Principles of Mathematical Sciences]*. Springer-Verlag, Berlin, second edition, 1990. Distribution theory and Fourier analysis.
- [81] L. H. Howell. Numerical conformal mapping of circular arc polygons. *J. Comput. Appl. Math.*, 46(1-2):7–28, 1993.
- [82] C. Hu. Algorithm 785: a software package for computing schwarz-christoffel conformal transformation for doubly connected polygonal regions. *ACM Transactions on Mathematical Software*, 24(3):317–333, 1998.
- [83] V. I. Ivanov and M. K. Trubetskov. *Handbook of conformal mapping with computer-aided visualization*. CRC Press, Boca Raton, FL, 1995. With 1 IBM-PC floppy disk (5.25 inch; HD).
- [84] R. A. Jinkerson, S. L. Abrams, L. Bardis, C. Chryssostomidis, A. Clement, N. M. Patrikalakis, and F. E. Wolter. Inspection and feature extraction of marine propellers. *Journal of Ship Production*, 9(2):88–106, 1993.
- [85] A. Karatsuba and Yu. Ofman. Multiplication of many-digit numbers by automatic computers. *Doklady Akad. Nauk SSSR*, 145:293–294, 1962.
- [86] R. Klein and A. Lingas. A linear-time randomized algorithm for the bounded Voronoi diagram of a simple polygon. *Internat. J. Comput. Geom. Appl.*, 6(3):263–278, 1996. ACM Symposium on Computational Geometry (San Diego, CA, 1993).
- [87] P. K. Kythe. *Computational conformal mapping*. Birkhäuser Boston Inc., Boston, MA, 1998.

- [88] D.-T. Lee. The medial axis transform of a planar shape. *IEEE Transactions on pattern analysis and machine intelligence*, 4(4):363–369, 1982.
- [89] D. T. Lee and R. L. Drysdale, III. Generalization of Voronoï diagrams in the plane. *SIAM J. Comput.*, 10(1):73–87, 1981.
- [90] Y.-H. Lee and S.-J. Horng. The equivalence of the chessboard distance transform and the medial axis transform. *Int. J. Comput. Math.*, 65(3-4):165–177, 1997.
- [91] T. Maekawa and N. M. Patrikalakis. Computation of singularities and intersections of offsets of planar curves. *Computer Aided Geometric Design*, 10(5):407–429, 1993.
- [92] T. Maekawa and N. M. Patrikalakis. Interrogation of differential geometry properties for design and manufacture. *The Visual Computer*, 10(4):216–237, 1994.
- [93] D. E. Marshall and S. Rohde. Convergence of a variant of the zipper algorithm for conformal mapping. *SIAM J. Numer. Anal.*, 45(6):2577–2609 (electronic), 2007.
- [94] D. Milman. The central function of the boundary of a domain and its differentiable properties. *J. Geom.*, 14(2):182–202, 1980.
- [95] D. Milman and Z. Waksman. On topological properties of the central set of a bounded domain in  $\mathbf{R}^m$ . *J. Geom.*, 15(1):1–7, 1981.
- [96] B. Mohar. A polynomial time circle packing algorithm. *Discrete Math.*, 117(1-3):257–263, 1993.
- [97] B. Mohar. Circle packings of maps in polynomial time. *European J. Combin.*, 18(7):785–805, 1997.
- [98] Z. Nehari. *Conformal mapping*. Dover Publications Inc., New York, 1975. Reprinting of the 1952 edition.
- [99] S. T. O’Donnell and V. Rokhlin. A fast algorithm for the numerical evaluation of conformal mappings. *SIAM J. Sci. Statist. Comput.*, 10(3):475–487, 1989.
- [100] J. O’Rourke. *Computational geometry in C*. Cambridge University Press, Cambridge, second edition, 1998.
- [101] N. Papamichael and E. B. Saff, editors. *Computational complex analysis*. North-Holland Publishing Co., Amsterdam, 1993. *J. Comput. Appl. Math.* **46** (1993), no. 1-2.
- [102] N. M. Patrikalakis and T. Maekawa. *Shape Interrogation for Computer Aided Design and Manufacturing*. Springer Verlag, 2002.
- [103] H. Pottmann and J. Wallner. *Computational line geometry*. Mathematics+Visualization. Springer-Verlag, Berlin, 2001.
- [104] F. P. Preparata. The medial axis of a simple polygon. In *Mathematical foundations of computer science (Proc. Sixth Sympos., Tatranská Lomnica, 1977)*, pages 443–450. Lecture Notes in Comput. Sci., Vol. 53. Springer, Berlin, 1977.
- [105] F. P. Preparata and M. I. Shamos. *Computational geometry*. Texts and Monographs in Computer Science. Springer-Verlag, New York, 1985. An introduction.
- [106] V. T. Rajan. Optimality of the Delaunay triangulation in  $\mathbf{R}^d$ . *Discrete Comput. Geom.*, 12(2):189–202, 1994.
- [107] J. H. Reif. Approximate complex polynomial evaluation in near constant work per point. *SIAM J. Comput.*, 28(6):2059–2089 (electronic), 1999.
- [108] B. Rodin and D. Sullivan. The convergence of circle packings to the Riemann mapping. *J. Differential Geom.*, 26(2):349–360, 1987.
- [109] H.A. Schwarz. Conforme abbildung der oberfläche eines tetraeders auf die oberfläche einer kugel. *J. Reine Ange. Math.*, pages 121–136, 1869. Also in collected works, [110], pp. 84-101.
- [110] H.A. Schwarz. *Gesammelte Mathematische Abhandlungen*. Springer, Berlin, 1890.

- [111] M. I. Shamos and D. Hoey. Closest-point problems. In *16th Annual Symposium on Foundations of Computer Science (Berkeley, Calif., 1975)*, pages 151–162. IEEE Computer Society, Long Beach, Calif., 1975.
- [112] E. C. Sherbrooke, N. M. Patrikalakis, and E. Brisson. Computation of the medial axis transform of 3-d. *Symposium on Solid Modeling and Applications*, pages 187–200, 1995.
- [113] E.C. Sherbrooke, N. M. Patrikalakis, and E. Brisson. An algorithm for the medial axis transform of 3d polyhedral solids. *IEEE Transactions on Visualization and Computer Graphics*, 2(1):44–61, 1996.
- [114] E.C. Sherbrooke, N. M. Patrikalakis, and F.-E. Wolter. Differential and topological properties of medial axis transforms. *CVGIP: Graphical Model and Image Processing*, 58(6):574–592, 1996.
- [115] W. D. Smith. Accurate circle configurations and numerical conformal mapping in polynomial time. 1991. unpublished technical memorandum, NEC Research Institute, Princeton, NJ.
- [116] K. Stephenson. Circlepack. software available from <http://www.math.utk.edu/~kens/>.
- [117] K. Stephenson. The approximation of conformal structures via circle packing. In *Computational methods and function theory 1997 (Nicosia)*, volume 11 of *Ser. Approx. Decompos.*, pages 551–582. World Sci. Publishing, River Edge, NJ, 1999.
- [118] K. Stephenson. Circle packing and discrete analytic function theory. In *Handbook of complex analysis: geometric function theory, Vol. 1*, pages 333–370. North-Holland, Amsterdam, 2002.
- [119] K. Stephenson. Circle packing: a mathematical tale. *Notices Amer. Math. Soc.*, 50(11):1376–1388, 2003.
- [120] K. Strebel. On the existence of extremal Teichmüller mappings. *J. Analyse Math.*, 30:464–480, 1976.
- [121] D. Sullivan. Travaux de Thurston sur les groupes quasi-fuchsien et les variétés hyperboliques de dimension 3 fibrées sur  $S^1$ . In *Bourbaki Seminar, Vol. 1979/80*, pages 196–214. Springer, Berlin, 1981.
- [122] Z. Tang. *Fast transformations based on structured matrices with applications to the fast multipole method*. PhD thesis, University of Maryland, College Park, Maryland, 2004.
- [123] R. Thom. Sur le cut-locus d’une variété plongée. *J. Differential Geometry*, 6:577–586, 1972. Collection of articles dedicated to S. S. Chern and D. C. Spencer on their sixtieth birthdays.
- [124] W.P. Thurston. *The geometry and topology of 3-manifolds*. The Geometry Center, University of Minnesota, 1979.
- [125] L. N. Trefethen, editor. *Numerical conformal mapping*. North-Holland Publishing Co., Amsterdam, 1986. Reprint of *J. Comput. Appl. Math.* **14** (1986), no. 1-2.
- [126] L. N. Trefethen and T. A. Driscoll. Schwarz-Christoffel mapping in the computer era. In *Proceedings of the International Congress of Mathematicians, Vol. III (Berlin, 1998)*, pages 533–542 (electronic), 1998.
- [127] Joris van der Hoeven. Fast evaluation of holonomic functions. *Theoret. Comput. Sci.*, 210(1):199–215, 1999.
- [128] Joris van der Hoeven. Relax, but don’t be too lazy. *J. Symbolic Comput.*, 34(6):479–542, 2002.
- [129] W. von Koppenfels and F. Stallmann. *Praxis der konformen Abbildung*. Die Grundlehren der mathematischen Wissenschaften, Bd. 100. Springer-Verlag, Berlin, 1959.
- [130] G.M. Voronoi. Nouvelles applications des paramètres continus à la théorie des formes quadratiques. recherches sur les paralléloèdres primitifs. *J. Reine Angew. Math.*, 134:198–287, 1908.
- [131] J. Wang. Medial axis and optimal locations for min-max sphere packing. *J. Comb. Optim.*, 4(4):487–503, 2000.
- [132] R. Wegmann. Methods for numerical conformal mapping. In *Handbook of complex analysis: geometric function theory. Vol. 2*, pages 351–477. Elsevier, Amsterdam, 2005.

- [133] W. Woess. *Random walks on infinite graphs and groups*, volume 138 of *Cambridge Tracts in Mathematics*. Cambridge University Press, Cambridge, 2000.
- [134] E.-F. Wolter. Cut locus and the medial axis in global shape interrogation and representation. 1993. MIT, Dept. of Ocean Engineering, Design Laboratory Memorandum 92-2.
- [135] Q. J. Wu. Sphere packing using morphological analysis. In *Discrete mathematical problems with medical applications (New Brunswick, NJ, 1999)*, volume 55 of *DIMACS Ser. Discrete Math. Theoret. Comput. Sci.*, pages 45–54. Amer. Math. Soc., Providence, RI, 2000.
- [136] C. Yao and J.G. Rokne. A straightforward algorithm for computing the medial axis of a simple polygon. *Internat. J. Comput. Math.*, 39:51–60, 1991.
- [137] C.-K. Yap. An  $O(n \log n)$  algorithm for the Voronoï diagram of a set of simple curve segments. *Discrete Comput. Geom.*, 2(4):365–393, 1987.
- [138] Q. Zhou. Computable real-valued functions on recursive open and closed subsets of Euclidean space. *Math. Logic Quart.*, 42(3):379–409, 1996.

C.J. BISHOP, MATHEMATICS DEPARTMENT, SUNY AT STONY BROOK, STONY BROOK, NY  
11794-3651

*E-mail address:* bishop@math.sunysb.edu